PAN AFRICAN UNIVERSITY
INSTITUTE FOR BASIC SCIENCES,
TECHNOLOGY AND INNOVATION
(PAUISTI)

Signal Transmission and Detection Scheme for Energy and Spectrally Efficient Indoor Optical Wireless Communications

Zelalem Hailu Gebeyehu

A Thesis submitted to the department of Electrical Engineering of Pan African University Institute of Science, Technology and Innovation in partial fulfillment of the requirements for the award of the Degree of Doctor of Philosophy in Electrical Engineering (Telecommunication Engineering) of Pan African University.

2018

Declaration

This thesis is my original work, except where due acknowledgement is made in the text, and to the best of my knowledge has not been previously submitted to Pan African University or any other institution for the award of degree or diploma.

NAME: Zelalem Hailu

REG. NO. EE-400-0003/15

SIGNATURE _____ DATE: _____

TITLE OF THESIS: SIGNAL TRANSMISSION AND DETECTION SCHEME FOR ENERGY AND SPECTRALLY EFFICIENT INDOOR OPTICAL WIRELESS COMMUNICATIONS

PROGRAMME: DOCTOR OF PHILOSOPHY IN ELECTRICAL ENGINEERING

SUPERVISOR CONFIRMATION:

This thesis has been submitted to Department of Electrical Engineering of Pan African University Institute of Science, Technology and Innovation with our approval as supervisors.

1. Name Dr. Kibet Langat Signature _____ Date_____
2. Name Dr. Ciira Maina Signature _____ Date_____

Acknowledgements

First of all, I am thankful to the God for the good health and wellbeing that were necessary to complete this work.

Secondly, I would like to express my heartfelt gratitude to my supervisors, Dr. Kibet Langat and Dr. Ciira Maina of Dedan Kimathi University of Technology for their continuous support and motivation. I am grateful to African Union (AU) for the scholarship and the research fund grants. My sincere thanks also go to the Pan African University's staffs, JICA, and Department of Electrical Engineering, for providing me with all the necessary facilities for the research.

Finally, I would like to express my deep gratitude to my family, colleagues, friends and others whom directly or indirectly supported me in many ways for successful accomplishment of this research work.

Abstract

The tremendous growth of wireless data traffic and exhaustive utilization of conventional radio frequency (RF) spectrum have motivated the telecom industry and researchers in the field to investigate the potential of alternative spectrum bands for wireless communication. In response to the looming conventional RF spectrum crisis, a lot of attention is given to utilize the spectrum in the range of optical domain for wireless communication. Optical wireless communication (OWC) is widely considered and believed to be the best complement of the conventional RF based wireless communication. In optical spectrum, a huge unregulated frequency resource is available for OWC which is many more times higher than that of the conventional RF spectrum. Intensity modulation and direct detection (IM/DD) type of communication has been confirmed as the most cost effective candidate for OWC. In IM/DD based OWC systems, the information signal has to be real and non-negative. Therefore, further signal processing needs to be carried on the complex bipolar orthogonal frequency division multiplexing (OFDM) signal to generate a real positive unipolar OFDM signal. Orthogonal frequency divisions multiplexing (OFDM) is a widely accepted multicarrier transmission schemes for high speed OWC due to its efficacy of combating inter symbol interference (ISI) and its efficiency of delivering a more efficient communication capacity. Among proposed OFDM schemes for OWC in literatures, asymmetrically clipped optical OFDM (ACO-OFDM) and direct-current-biased optical OFDM (DCO-OFDM) have got a wide acceptance. In spite of their wide acceptance, DCO-OFDM scheme has energy inefficiency issues and the spectral efficiency of ACO-OFDM is not attractive for high speed OWC.

In this research work, a stratified asymmetrically clipped optical OFDM (STACO-OFDM) is proposed and investigated for IM/DD based OWC. STACO-OFDM utilizes both even and odd subcarriers for transmission of information bits in stratified fashion. STACO-OFDM follows an optimal design strategy and architecture to improve both spectral and energy efficiency of the system at the same time. Detailed theoretical framework of STACO-OFDM over both linear additive white Gaussian noise (AWGN) and frequency selective multipath channels is given on this thesis. The performance of STACO-OFDM is investigated and compared with both ACO-OFDM and DCO-OFDM schemes with the aid of theoretical and simulation analysis. For equal data rate systems, the theoretical and simulation results have shown that STACO-OFDM scheme can offer better energy efficiency compared to both ACO-OFDM and DCO-OFDM schemes over

linear AWGN and frequency selective multipath channels. Furthermore, for the same used QAM modulations, the spectral efficiency of STACO-OFDM is equivalent to the spectral efficiency offered DCO-OFDM and better than the spectral efficiency of ACO-OFDM scheme.

In this thesis, the potential of adaptive optical OFDM to enhance the spectral efficiency of OWC on frequency selective optical wireless channel is also investigated. In particular, the performance of frequency selective rate adaptive M-QAM ACO-OFDM scheme is evaluated using theoretical and simulation analysis. In comparison to fixed M-QAM ACO-OFDM schemes, rate adaptive M-QAM ACO-OFDM scheme has shown better spectral efficiency performances for non-outage OWC systems over frequency selective channels.

List of publications

Part of the thesis is published as research articles in peer reviewed journals indexed in (Scopus, EBSCOhost, and J-Gate etc.) and ranked in Scimago journal and country rank database as follows.

1. Zelalem Hailu, Kibet Langat, and Ciira Maina, "Stratified ACO-OFDM Modulation for Simultaneous Transmission of Multiple Frames Both on Even and Odd Subcarriers," Journal of Communications, vol. 12, no. 5, pp. 261-270, 2017.
2. Zelalem Hailu, P. Kibet Langat, and Ciira Wa Maina, "Rate Adaptive ACO-OFDM on Multipath Channels for Enhancing Spectral Efficency," International Journal of Applied Engineering Research, vol. 12, no. 21, pp. 11029-11034, 2017.
3. Zelalem Gebeyehu, Philip Kibet Langat and Ciira Maina, "BER performance of stratified ACO-OFDM for optical wireless communications over multipath channel," Journal of Computer Networks and Communications, vol. 2018, April 2018.

Contents

List of figures

List of tables

Abbreviations

ACO-OFDM	asymmetrically clipped optical orthogonal frequency division multiplexing
ADC	analog to digital converter
ADO-OFDM	asymmetrically clipped direct current biased optical OFDM
AWGN	additive white Gaussian noise
BER	bit error rate
CIR	channel impulse response
CP	cyclic prefix
CSI	channel state information
DAC	digital to analog converter
DCO-OFDM	direct current biased optical OFDM
DD	direct detection
EU-OFDM	enhanced unipolar orthogonal frequency division multiplexing
FDM	frequency division multiplexing
FEC	forward error check
FFT	Fast Fourier Transform
FOV	field of view
IBI	inter block interference
ICI	inter carrier interference
IFFT	inverse Fast Fourier Transform
IM	intensity modulation
IM/DD	intensity modulation/ direct detection
IR	infrared
ISI	inter symbol interference
LAN	local area networks
LED	light emitting diode
LD	laser diode
LOS	line of sight
LTI	linear time invariant
M-PAM	multi-level pulse amplitude modulation

M-PPM	multi-level pulse position modulation
M-QAM	multi-level quadrature amplitude modulation
OFDM	orthogonal frequency division multiplexing
O-OFDM	optical orthogonal frequency division multiplexing
OOK	on-off keying
OP-OFDM	optical polar orthogonal frequency division multiplexing
OW	optical wireless
OWC	optical wireless communication
PAD	personal digital assistant
PAPR	peak- to- average power ratio
PD	photo detector
PPM	pulse position modulation
PWM	pulse width modulation
RF	radio frequency
SE	spectral efficiency
SNR	signal- to-noise ratio
U-OFDM	unipolar orthogonal frequency division multiplexing
VLC	visible light communication

Chapter 1

Introduction

The overutilization of the radio frequency (RF) spectrum, which is conventionally used for wireless communications, leaves a significant threat in the field of telecommunication. The growing number of user subscriptions in wireless network and the continuous emergence of bandwidth greedy multimedia services have aggravated the problem of RF spectrum depletion. Apart from the conventional RF spectrum, it is a great relief that the electromagnetic wave in millimeter and optical range can be utilized for wireless communications [1-4]. Starting from recent years, extensive research works are undergoing on both regions of millimeter and optical spectrum. According to previous theoretical and experimental investigations, Optical wireless communication (OWC) has shown amazing promises to be a good complement of the conventional RF based wireless communications.

The modern form of OWC involves the transmission of information bits using light wave both on infrared and visible light range [5-6]. Utilizing light (optical domain) for wireless communication has added up a number of advantages in the field of telecommunication. Wide unregulated bandwidth, good security features, and good immunity to electromagnetic interference are among the major advantages provided by OWC. In addition, the capability of visible light to be used for both communication and lighting purpose at the same time makes OWC more attractive.

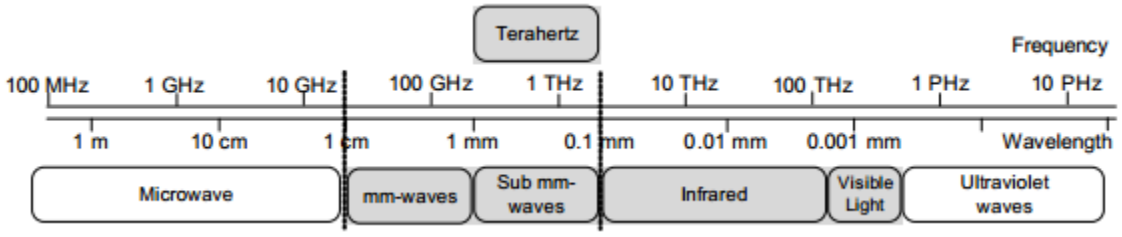

Figure 1. 1: Optional bands for high-speed wireless communications [7]

In spite of extensive undergoing researches and efforts, there are still gaps and challenges which are still open for research in OWC. Improving the spectral and energy efficiency of optical

modulations to achieve high speed OWC is still one major challenge which needs to be investigated. This research work presents optimal design strategies to improve the spectral and energy efficiency of optical modulation schemes for OWC.

1.1. Research Background

Due to its inherent ability of combating inter symbol interference (ISI) [8-9]; there has been a growing interest towards orthogonal frequency division multiplexing (OFDM) in the last couple of decades. The conventional complex bipolar OFDM is not directly applicable to OWC in the way it is applicable for RF based wireless communication [10-11]. Intensity modulation and direct detection (IM/DD) has been found to be best suited for cost effective OWC. Due to the requirement of the IM/DD system in OWC, the conventional complex bipolar OFDM signal should be modified in to positive unipolar OFDM signal before it modulates the intensity of the light from the light emitting diode (LED). This requirement of IM/DD system puts a significant challenge on the modulation schemes to achieve good spectral and energy efficiency. Therefore, developing an improved and efficient strategy to enhance the spectral and energy efficiency of unipolar OFDM is vital to realize high speed OWC.

1.2. Motivations

The wireless data traffic in telecommunication networks is growing in significant and continuous rate year by year. According to CISCO global wireless data traffic forecast [12], the amount of wireless data traffic will reach to 49 Exabyte by the year 2021 which is too much to be supported by the conventional RF spectrum alone. The RF spectrum below 10 GHz is overcrowded by different applications; hence, this conventional RF spectrum is already over utilized and exhausted. Therefore, migrating to new technological advancement and new electromagnetic spectrum is inevitable to satisfy this huge demand of wireless data traffic.

In counteracting to this spectrum crisis, significant attention and efforts have been done to utilize the spectrum in millimeter and optical wave range for wireless communication. The optical domain from the range of infrared to visible light region can offer a huge unregulated bandwidth approximately equals to 630 THz. Therefore, there is a great deal of motivation to utilize this

unregulated huge bandwidth for wireless communication in optical domain to solve the problem of bandwidth scarcity in today's wireless network. Moreover, advantages such as excellent security features and good immunity to electromagnetic interference, creates a wide attention and motivation towards OWC.

In the last decade, a significant number of research works have been conducted on OWC and impressive progresses and research outcomes have been achieved. In spite of amazing research progresses in the field of OWC, there are still many gaps and questions which are open to research. Among those gaps, the challenges of developing an efficient modulation scheme, which can offer good spectral and power/energy efficiencies at the same time for IM/DD based OWC, is an interesting one. Different single carrier based modulations such as on-off keying (OOK), pulse width modulation (PWM), pulse amplitude modulation (PAM), and pulse position modulation (PPM) are propose for IM/DD based OWC in different literatures [3, 13-14]. Even if they are efficient for low data rate communications, single carrier modulation schemes are highly vulnerable to ISI for high data rate OWC. On contrary, multi carrier communication such as OFDM in particular, has high immunity to ISI during high data rate communication. In addition, less complex single tap frequency domain equalization can be easily implemented for OFDM based communications. Therefore, OFDM based OWC is becoming more attractive compared to single carrier modulation based OWC. Regardless of different optical OFDM schemes proposed for OWC in literatures [11, 15-19], this area (optical OFDM) is still open to research. This work investigates and proposes a strategy of developing both spectral and power/energy efficient optical OFDM for OWC over IM/DD.

1.3. Challenges of unipolar optical OFDM in OWC

Unipolar optical OFDMs have the following major challenges:

I. **Spectral efficiency reduction:** compared to conventional complex bipolar OFDM, unipolar OFDMs are spectrally inefficient. Most unipolar optical OFDM offers less than 50% of spectral efficiency compared to the conventional bipolar OFDM. Due to the limited modulation bandwidth of the LED in frontend device, spectrally efficient modulation scheme is needed to realize a high speed OWC.

II. **Power and energy inefficiency:** certain unipolar OFDM schemes involve adding of DC bias in the process of altering the bipolar OFDM signal into a unipolar OFDM signal. The added DC bias increases the power dissipation and reduces the power and energy efficiency of the system. Good value of signal to noise ratio (SNR) is needed to achieve a good bit error ratio (BER) performance in high bitrate OWC. Because of the eye and skin safety regulation [12, 7] and limited dynamic range of LED, there is a constraint on the transmitted signal power to achieve good SNR without limitation. Hence, power/energy efficient modulation schemes are needed to achieve good communication performance in OWC.

1.4. Statement of problem

Different unipolar optical OFDM schemes have been proposed for OWC in different literatures [11, 15-19]. Apart from the spectral efficiency loss due to implementation of Hermatian symmetry in the process of generating real valued OFDM, the need of the OFDM signal to be strictly positive poses additional constraints in OWC. These constraints manifest themselves as either reduction on spectral efficiency or power efficiency of the system.

Among previously proposed unipolar optical OFDM schemes, DC-biased optical OFDM (DCO-OFDM) [11, 15] and asymmetry clipped optical OFDM (ACO-OFDM) [16-17] are the most widely accepted ones. DCO-OFDM is realized by adding a positive DC bias on the bipolar OFDM signal to generate positive unipolar OFDM signal. DCO-OFDM offers good spectral efficiency which is equals to 50% of the spectral efficiency of the conventional bipolar OFDM. On the other hand, DCO-OFDM is not attractive scheme in terms of power efficiency due to the added DC bias on the information signal in the process of generating positive unipolar OFDM. Due to the large peak-to-average power ratio (PAPR) of OFDM, some negative peaks of the signal will be clipped even after adding positive DC bias. Therefore, the clipping of those negative peaks introduce distortion which causes a limitation on the system performance. On contrary, ACO-OFDM is able to generate a positive unipolar OFDM signal without a need of any DC biasing. Hence, ACO-OFDM has better power/energy efficiency compared to DCO-OFDM. In ACO-OFDM, only odd subcarriers are modulated with the information bits while the even indexed subcarriers are left vacant and wasted. These sacrifices approximately half the spectral efficiency compared to DCO-

OFDM, which means the spectral efficiency of ACO-OFDM is even less than 25% of the spectral efficiency offered by the conventional bipolar OFDM. Hence, there is a gap in both ACO-OFDM and DCO-OFDM since good spectral and power efficiencies are needed at the same time to realize high bit rate OWC.

The other practical challenge in OWC is the channel state dynamism of optical wireless channel. Adaptive OFDM is a well-known proposed solution but enough work has not been done yet in OWC in this regard. Therefore, investigating the performance of adaptive OFDM to enhance the performance of OWC in frequency selective multipath channel is an apparent and important task.

1.5. Main objective of the research

The main objective of the research is to develop signal transmission and detection scheme for energy and spectrally efficient indoor optical wireless communication.

1.5.1. Specific objectives of the research

The research has the following specific objectives:

1. To design a multi-carrier transmission/detection scheme based on M-QAM OFDM with improved power and spectral efficiency.
2. To evaluate the performances of the developed M-QAM OFDM modulation scheme over AWGN channel environment using Monte Carlo simulation.
3. To evaluate and analyze the performance of the developed M-QAM OFDM modulation scheme over multipath fading channel.
4. To investigate the potential of adaptive optical OFDM scheme for performance improvement in frequency selective multipath optical wireless channel environment.

1.6. Contributions of the study

The major contributions of this research work are listed as follows.

- Different types of unipolar optical OFDM schemes are investigated for IM/DD based OWC. Existing concepts of OWC are reviewed in relatively detailed manner compared to

what is given in published articles. Performances of major existing unipolar optical OFDMs are analyzed for different channel conditions and their weakness are identified.

- In response to the weakness observed on existing modulation schemes, a new enhanced type of unipolar OFDM called **stratified ACO-OFDM (STACO-OFDM)** is proposed with the objective of improving spectral and power/energy efficiencies of OWC system. The theoretical and the simulation analysis of STACO-OFDM are given in this thesis in a detailed manner. The performance of STACO-OFDM is also analyzed both on linear AWGN and multipath diffused optical wireless channels. In addition, the performance of the proposed STACO-OFDM scheme is compared with the performance of the widely accepted conventional state-of-the-art DCO-OFDM and ACO-OFDM schemes over AWGN and multipath channels. Using similar QAM modulations on the three schemes, it is confirmed that STACO-OFDM can offer equivalent spectral efficiency with DCO-OFDM and better spectral efficiency (two times the spectral efficiency of ACO-OFDM) compared to ACO-OFDM. For similar spectral efficiency or bit rate OWC systems, the power/energy efficiency of STACO-OFDM outsmarts the power/energy efficiency performances of both ACO-OFDM and DCO-OFDM schemes over both linear AWGN and multipath channels.
- The potential of rate adaptive optical OFDM to enhance the performance of OWC is investigated and compared to the performance of optical OFDM with fixed QAM modulation schemes. In particular, the performance of rate adaptive ACO-OFDM scheme is compared to fixed QAM ACO-OFDM scheme over frequency selective optical wireless channel in terms of spectral efficiency enhancement. As the result, rate adaptive ACO-OFDM has shown better performance in terms of spectral efficiency compared to fixed QAM ACO-OFDM.

1.7. Organization of the thesis

The rest of this thesis is organized as follows.

- **Chapter 2:** This Chapter reviews different concepts of OWC system given on different research literatures and books. The fundamental concepts and the conventional state-of-the art OFDM schemes of OWC such as ACO-OFDM and DCO-OFDM are also explained on

this chapter. Element of OWC, physical link configurations, noise sources, and OFDM modulation schemes in OWC are given in different sections of chapter 2.

- **Chapter 3:** Chapter 3 introduces the methodology, concept, and theoretical analysis of STACO-OFDM scheme. The signal models of STACO-OFDM scheme at transmitter and receiver are also given for both linear AWGN and multipath channels. The theoretical analysis of spectral efficiency and BER performance of STACO-OFDM are also given on this chapter. Moreover, the performance of rated adaptive ACO-OFDM from the perspective of spectral efficiency is analyzed in the last section of chapter 3.
- **Chapter 4:** In this Chapter, the simulation results of STACO-OFDM, ACO-OFDM and DCO-OFDM are presented. The performance of STACO-OFDM is evaluated and compared with the performance of ACO-OFDM and DCO-OFDM schemes with the aid of simulation results. Furthermore, the performance of rate adaptive M-QAM ACO-OFDM is compared with the performance of fixed M-QAMs ACO-OFDM schemes in terms of spectral efficiency using simulation results.
- **Chapter 5:** Summarizes the key contribution of this thesis and gives concluding remarks from the presented results. Recommendations and future work highlights are also given on this particular area of research.
- **References:** The list of literatures which have been cited in this study is given in this part of the thesis document.
- **Appendices:** The phase graph of frequency domain diffused optical channel impulse response and the MATLAB code used for simulations are given on appendices.

Chapter 2

Literature Review

The growing number of research literatures on optical wireless communications show that the huge motivations towards utilization of optical domain for wireless communications. In the last decade, significant numbers of research literatures have been published in the area of optical wireless communications. The objective of this chapter is to provide literature review on advancement and development of research in the area of indoor optical wireless communications.

2.1. Introduction

The first and ancient forms of optical wireless communications were used by humans thousands years ago during ancient era of human beings. In the ancient times, it is believed that the ancient Greeks and Chinese were using fires flames to signal the incoming of enemies and threats. The photo-phone invented by Graham Bell in 19^{th} century is the first modern form of optical wireless communication in history [20]. The modern form of optical wireless communication is based on transmission of digital information signals using light wave in visible, ultra violet, and infrared range. The invention of laser diode in 1962 has created huge interest towards optical wireless communication [21-22].

Optical wireless communication is intended to be used in indoor and outdoor scenario for long, medium, and short distance communications depend on the application needed. In the outdoor case, it can be used for long distance satellite to satellite, satellite to ground station and vice-versa, and for medium distance it can also be used in building to building, vehicular, and mobile back haul communications. In the indoor situation, it can be used in wireless home area network, in automated industries, in hospitals, in aviation and in personal area network.

2.2. Indoor optical wireless communication

Most of the RF based wireless LANs operating at 2.4 GHz and 5 GHz provide a data rate below 10 Gbit/s. The speed provided by these wireless LANs will not be enough in the future due to numerous emerging multimedia services. Moreover, since these bands are unlicensed, there are still incompatibility issues between different brands. Interference is also another major challenge to put in consideration. Such challenges have provided a motivation to look for a solution for high speed data connectivity in indoor environment. Indoor optical wireless communication is the most promising technology to be the complement to those RF based communications. The optical spectrum intended for this application is unregulated, has huge bandwidth and high immunity for electromagnetic interference. In addition, since optical signals cannot penetrate walls, it cannot create an interference with the same system in adjacent rooms. Indoor optical wireless systems can be developed by using either infrared light or visible light spectrum. Visible light communication which uses visible range of optical spectrum becomes the center of interest from time to time for the dual purpose of lighting and communication as the same time.

Infrared has similar characteristics to that of visible light in many ways. It can pass through glass but not through walls [14]. So that, it is secured from interference since it can be confined in a room. For IR based OWC, peak wavelengths between 780 nm and 950 nm can be used. These peak wavelengths coincide with the peak sensitivity of silicon photodetectors [23]. The majority of IR systems use the near infrared IR band mainly due to the availability of effective, low-cost sources and detectors. OWC in near infrared regime offers much higher bandwidth compared to visible light spectrum. But in Indoor scenario it is difficult to achieve wider field of view (FOV) for gigabit IR communication. In IR regime, there is also a constraint in transmitted power level to secure eye safety. With directed line of sight (LOS) links, high data rates in the order of Gbit/s can be achieved [24].

2.3. Elements of optical wireless communications

Basically, OWC comprises of two main components, namely a transmitter which contains light source and receiver which contains light detectors. In OWC, the electrical signal to optical signal conversion is performed with the aid of LEDs or laser diodes (LDs). LEDs emitting in visible light

range appear to be the most potential candidates for transmitter front-end elements due to their increasing popularity in illumination applications [25]. In recent years, solid state lightings based on white LEDs for illumination purpose to light homes, cars, streets, stadiums, airplanes, and others are becoming more popular from time to time. This creates a great motivation towards visible light to realize energy efficient high speed communication along with the illumination purpose at the same time. In optical wireless (OW) visible light communication (VLC) [25], the primary purpose is illumination or lighting while high speed communication is the secondary function. Generally, those white LEDs are classified into two types, namely trichromatic and blue-chip LEDs [26]. The most common one is a blue-chip LED which has a phosphor layer on top of a single blue chip. Blue-chip LEDs are commonly found in most white LED bulbs which are easily available in the market. Trichromatic LEDs are fabricated by mixing light of the three primary colors (red, green, and blue) obtained using three different LED chips. This type of LED is mainly used for architectural design purposes and is more expensive compared to blue-chip LEDs. As shown in Fig. 2.1, the LED which is more common to realize low cost OWC has limited modulation bandwidth which is the main source of challenges in high speed OWC. Limited dynamic range of LED is also another challenge which has an effect of nonlinear distortion.

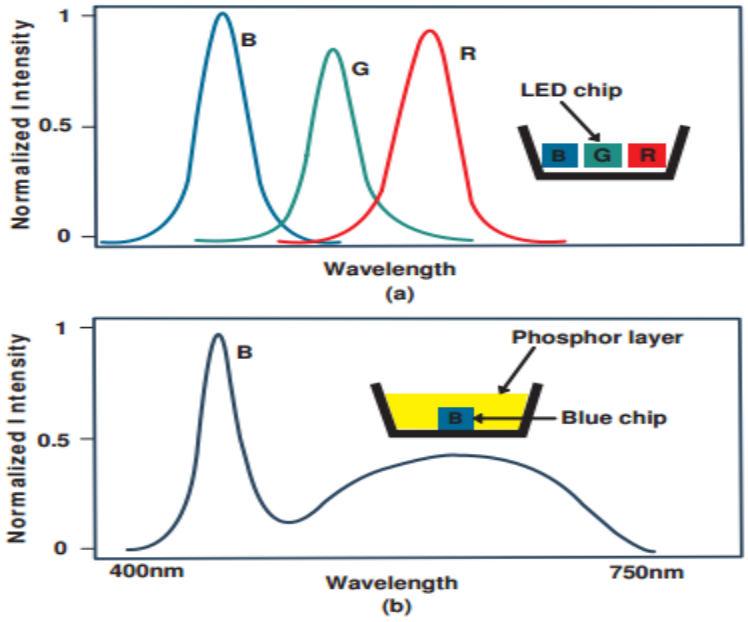

Figure 2. 1: Spectrum of (a). Trichromatic LED. (b). Blue-chip LED [26].

A number of photo-detectors can be used for light detection at the receiver side. Among them, imaging sensors [27-28], solar panels [29], and even LEDs [30-31] are commonly used in different applications. However, these devices generally have a slow frequency response and are rather unsuitable for high-speed communication. The best potential candidates for receiver front-end elements in high data rate OWC systems are photodiodes (PDs) [3, 32-33].

2.4. Optical wireless link configuration

There are different ways of making physical configuration of optical wireless links between transmitter and receiver in indoor OWC [34]. The most common and major physical link configurations are shown in Fig. 2.2 and explained as follows.

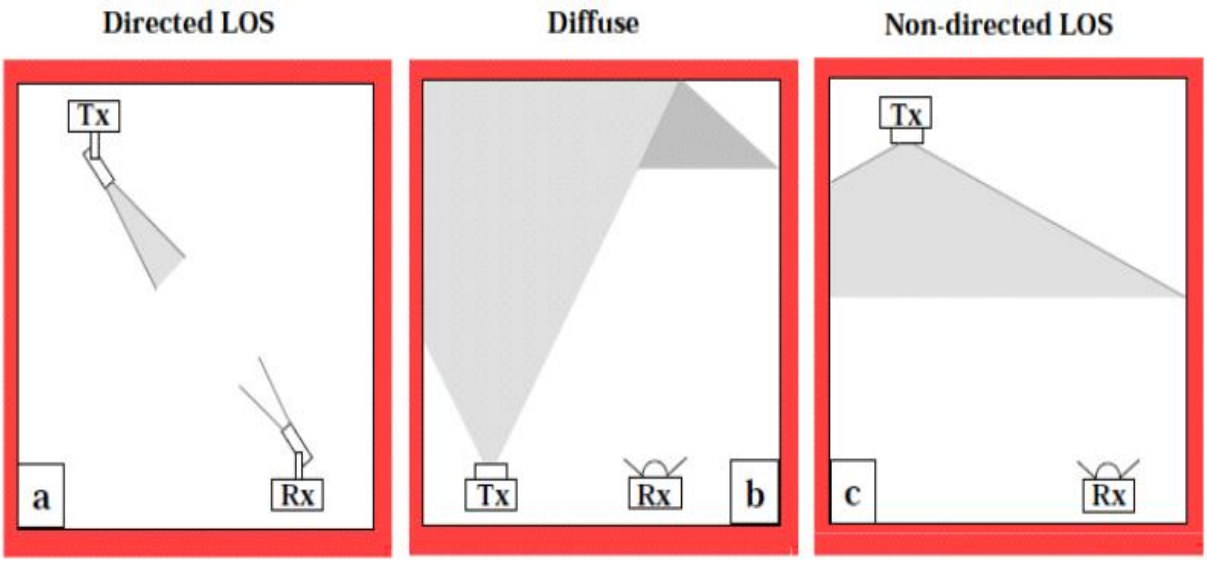

Figure 2. 2: Optical wireless link configurations [2].

a. **Directed LOS:** Directed line of sight (LOS) is mostly used in outdoor communication situations but it is also used in indoor OWC in some point to point communication cases. This link configuration mostly uses highly directed transmitter and narrow field of view (FOV) receiver to implement uninterrupted narrow optical link between transmitter and receiver. Since the optical power is concentrated in narrow optical beam, Directed LOS configuration is able to achieve long distance and high data rate communication compared

to other link configurations. Moreover, it is less affected by the distortion comes out of multipath dispersion. Therefore, the data rate performance is mainly affected by optical path loss rather than multipath depression. On the other hand, directed LOS configuration has a difficulty in supporting mobility and large communication coverage area. Different tracking techniques can be used to enable mobility but the system complexity will grow and become non cost effective link configuration. Furthermore, this link configuration is easily affected by optical beam blocking since the beam is narrow and easily intercepted.

b. **Diffused Link:** the transmitter (optical source) in this link configuration is set to point upward to the celling to emit wide optical beam. Diffused link is the most appropriate configuration for wireless LAN since it avoids the requirement of precise alignment of transmitter and receiver. In addition, it has good immunity for optical beam blocking since it is not relied on single concentrated narrow beam. It is also able to support mobility capabilities and relatively large coverage areas. The receiver in this link configuration has basically wide FOV; hence, the received optical signal is the integral of multiple diffusely reflected light beams from the ceiling and walls. Diffused link is more susceptible to optical path loss and multipath dispersion. Therefore, relatively high transmitted optical power is needed to reduce the bit error rate (BER) of the system.

c. **Non-directed LOS link:** this type of link configuration comprises both directed LOS and diffused optical signal components at the receiver. Therefore, this link configuration provides the advantages of both directed LOS and diffused link configurations. It also supports mobility of users with reliable service delivery and connectivity.

2.5. Signal propagation in indoor optical wireless channel

The optical waves follow different path while propagating from the transmitter to the receiver through the optical wireless channel. This introduces a situation that waves in different paths experience different loss and propagation delays, as well as different angle of incidence to the receiver surface. Because of this multipath propagation effect, the received signal is the aggregation of those signals with different delays and attenuation which undergo destructive and constructive interference while arriving at the surface of the receiver. The amplitude variation

because of the destructive and constructive interference is termed the multipath fading whereas the spreading of signal over time is known as multipath dispersion.

Unlike radio communication, in OWC the multipath fading is averaged out and has negligible effect because of spatial diversity effect introduced by the large area of the photo detector compared with the wave length of the signal [14]. However, the multipath dispersion is a serious problem which causes inter-symbol interference (ISI) in OWC. The effect of ISI in time domain is quantified by the delay spread or rms-delay, D, as:

$$D = \left[\frac{\int_{-\infty}^{\infty}(\tau-\mu)^2 A_c(\tau)d\tau}{\int_{-\infty}^{\infty} A_c(\tau)d\tau}\right]^{\frac{1}{2}} \quad (2.1)$$

Where: τ is multipath delay, $A_c(\tau)$ is power delay profile, μ is average delay spread. To avoid ISI, the rms-delay, D, should be short enough compared to the symbol period T_{sym}, i.e. $D \ll T_{sym}$ .The multipath dispersion will have a significant ISI effect for signal transmission at or above 10 Mbit/s. Alternatively, it is possible to express the multipath dispersion in frequency domain in terms of the channel coherence bandwidth (B_c) [23-24]. B_c is the frequency range over which the channel has equal and similar response on adjacent frequency component. It is related to the D as:

$$B_c = \frac{1}{kD} \quad (2.2)$$

In equation (2.2), k is a constant factor. In order to avoid ISI the signal bandwidth, B, should be significantly less than the coherence bandwidth, B_c, i.e. $B \ll B_c$. Holding this condition, in this scenario, all the signal frequency components are affected by the channel in similar manner and magnitude, which is known as *flat fading*. If $B > B_c$, some frequency components of the signal are affected differently and the channel shows frequency selective characteristics which is referred to as *frequency selective fading*. Frequency selective fading results in ISI which has an effect drastically degrade the quality of the communication.

Considering that the Doppler effect is insignificant due to the relatively slow speed of the user in indoor environment, OW channel can be described as linear time invariant (LTI) system within a short time scale. The effect of the channel on the transmitted signal can be represented by the linear convolution of the transmitted signal, x (t), and, the channel impulse response, h (t), as:

$$y(t) = x(t) * h(t) = \int_{-\infty}^{\infty} x(\tau)h(t-\tau)d\tau \quad (2.3)$$

2.6. Channel model in OWC

The impulse response of indoor optical wireless channel can be modeled as a standalone LOS link, diffused link, or the combination of LOS and diffused link depend on the link configuration. Delta dirac functions, $\delta(t)$, are used as base function to model the CIR of LOS links whereas unit step functions are used to model diffused links since the reflected optical signal has a diffused nature. The CIR of LOS link, $h_{LOS}(t)$, can be modeled as [35]:

$$h_{LOS}(t) = g_{los}\delta(t) \quad (2.4)$$

g_{los} is the optical path gain of the directed LOS link.

For the diffused link, $h'_{Dif}(t)$, which is the joint effect of the CIR of the diffused link, $h_{Dif}(t)$, and diffused link optical path gain, g_{Dif} , can be written as [35]:

$$h'_{Dif}(t) = g_{Dif}\, h_{Dif}(t) \quad (2.5)$$

Exponential decay and ceiling bounce models are the two well-known and widely used techniques to model CIR of the diffused links with good accuracy [35]. Exponential decay model is most appropriate when the transmitted optical waves have experienced multiple reflections before it reaches at the receiver. Therefore, $h_{Exp}(t)$, the CIR of diffused link from exponential decay model can be written as [18, 35-38]:

$$h_{Exp}(t) = H(0)\frac{1}{D}\, e^{\frac{-t}{D}}\, u(t) \quad (2.6)$$

Where $H(0),\ D,\ and\ u(t)$ are the DC optical path gain, the rms delay of the channel, and the unit step base function respectively. Ceiling bounce model is more accurate when most of the received optical waves experience single reflection. Therefore, $h_{Cell}(t)$, the CIR of diffused link from celling bonce model [18, 35-38]:

$$h_{Cell}(t) = H(0)\frac{6\, a^6}{(t+a)^7}\, u(t),\ and, a = 12\sqrt{\frac{11}{13}}\, D \quad (2.7)$$

The optical path gain $H(0)$ in equation (2.7) which accounts the optical path loss of reflected optical signals can be written in the form [35]:

$$H(0) \approx \int_0^{\infty} |h_{Cell}(t)|dt \tag{2.8}$$

The $h_{Dif}(t)$ term in equation (2.6) is equivalent to $e^{-t/D}/D$ and $6a^6/(t+a)^7$ for exponential decay and ceiling bounce models respectively. The g_{Dif} term in equation (2.6) is also equivalent to $H(0)$ for both ceiling bounce and exponential decay models. For the case of non-directed LOS link configuration having both LOS and diffuse components, the CIR, $h_{Nlos}(t)$, is given by:

$$h_{Nlos}(t) = h_{LOS}(t) + h'_{Dif}(t) = g_{los}\delta(t) + g_{Dif}h_{Dif}(t - \Delta T) \tag{2.9}$$

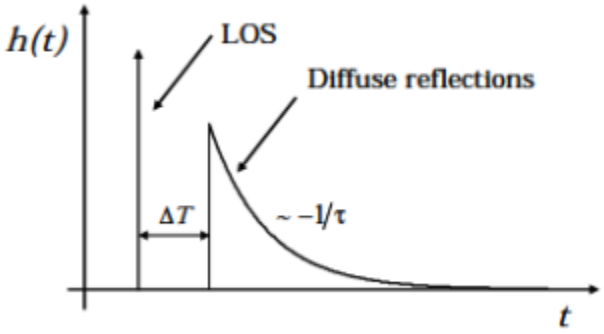

Figure 2. 3: Sample channel impulse response (CIR) of indoor optical wireless communication [33].

2.7. Noise sources and noise model in OWC

There are natural and various artificial noise sources which can cause performance degradation in OWC. Unlike optical fiber and RF wireless communications, the main source of noise in OWC is the background light from various sources. The background light is composed of radiations from natural sources (sun) and artificial sources such as fluorescent and incandescent lamps. The background light noise is available in a wide wavelength range. The normalized power spectral density of the background light along with the normalized sensitivity of silicon photodetector is given on Fig.2.4 [13, 39]. As shown in Fig.2.4, the normalized responsivity of silicon photodetector is in the range of 0.2-1 A/W [13, 39]. The background light from natural and artificial sources is the known causes for the generation of random electrons at random time on the

PD at the receiver front end. This generated random electron of photo current is known as shot noise. The photo current $I(t)$ generated at the PD is given by:

$$I(t) = \eta P_R^O + i(t)$$

$$= I_{PC} + i(t) \ \text{[A]} \tag{2.10}$$

Where,

η : Responsivity of PD

P_R^O : The constant optical power of the arriving light at PD

$i(t)$: The current fluctuation because of shot noise

I_{PC} : Average photocurrent

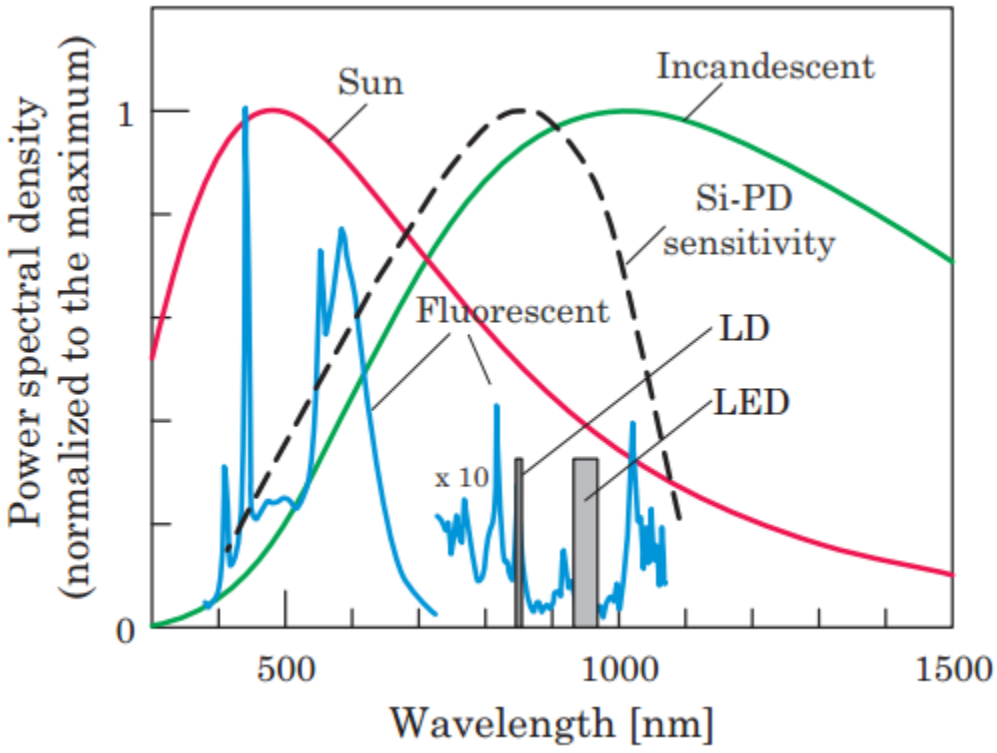

Figure 2. 4: Power spectral density of background noise [2, 38].

As shown in equation (2.10), the photocurrent $I(t)$ has DC component (I_{PC}) and AC component ($i(t)$). Even if the DC component can be removed using a DC blocker, the AC component still contributes noise to the system. The fluctuation introduced by the AC component is under the category of stationary random process [40]. Shot noise is in the category of white noise and its spectral density is equivalent to the average photo current I_{PC}. If the light intensity of the information signal is weaker than the light intensity of the background light, the shot noise can be modeled as random AWGN process. Therefore, the power spectral density N_o^{shot} of shot noise can be given as:

$$N_o^{shot} = 2qI_{PC} \quad [\mathrm{A}^2/\mathrm{Hz}] \tag{2.11}$$

Where, q is the charge of electron with a magnitude of $1.602 \times 10^{-19}\ C$ in coulombs. The shot noise variance δ_z^2 for receiver having effective noise bandwidth of B is also given by:

$$\delta_{shot}^2 = BN_o^{shot} = 2qBI_{PC} \tag{2.12}$$

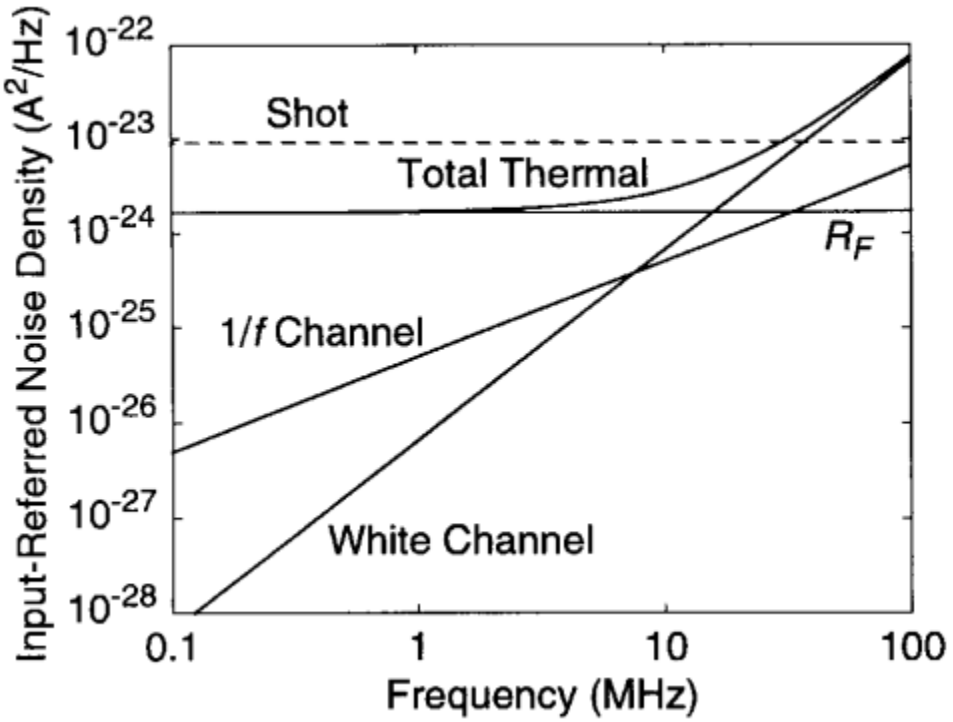

Figure 2. 5: Power spectral density of AWGN components [2, 38].

As shown in Fig.2.5, the shot noise of typical indoor optical wireless communication is in the order of 10^{-23} [3] and it is the most dominant noise source in OWC.

The second larger contribution of noise comes from the thermal noise produced at the Trans impedance amplifier (TIA) of the receiver. The noise contribution of thermal noise can be modeled with Gaussian statistics [41-42]. The PSD N_o^{ther} of thermal noise can be calculated using the following formula.

$$N_o^{ther} = \frac{4k_B T}{R} \quad [\frac{\mathrm{A}^2}{\mathrm{Hz}}] \tag{2.13}$$

Where:

$k_B = 1.381 \times 10^{-23}\ J/K$ is the Boltzmann constant

T is the temperature of the TIA in unit of kelvin

R is the value of the resistance of the TIA resistor in ohms

The magnitude of the thermal noise for typical indoor OWC is in the order of 10^{-24} as shown in Fig.2.5.

The shot noise and the thermal noise components generated at the receiver of OWC are uncorrelated. Hence, the PSD N_o of the overall AWGN available on the system is given by [3, 42]:

$$N_o = N_o^{shot} + N_o^{ther} \quad [\mathrm{A}^2/\mathrm{Hz}] \tag{2.14}$$

From Fig.2.5, the PSD of the AWGN in typical indoor OWC has an approximate magnitude of around $3.05\times10^{-23}\ A^2/Hz$ [37-38] where A refers to Ampere.

2.8. Intensity modulation and direct detection (IM/DD) in OWC

The incoherent light emission property of LED imposes significant challenges on choosing the type of modulation scheme in OWC. The incoherent light waves emitted from LED possess

different frequency and phase. Therefore, it is difficult to obtain a stable carrier with fixed phase and frequency for coherent phase and frequency modulation [14, 33]. The only efficient and cost effective type of communication in OWC is the one which incorporates intensity modulation and direct detection (IM/DD). In intensity modulation, the optical power emitted from the LED is varied in accordance with the electrical amplitude of the information signal. The IM/DD type of communication needs the information signal to be real valued and positive unipolar type. In OWC, modulation takes place in two phases. First the information to be transmitted is coded in to waveforms and then these waveforms modulate the light intensity emitted from the light source. The block diagram of IM/DD based OWC is shown on Fig.2.6.

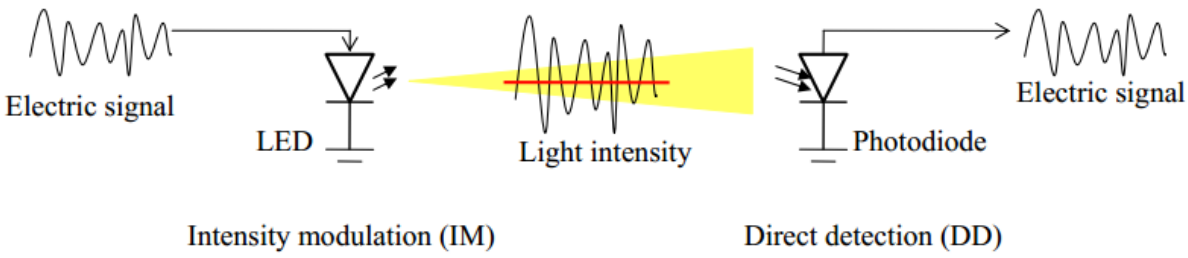

Figure 2. 6: Intensity modulation and direct detection (IM/DD) in OWC [7].

2.9. Transmission schemes in OWC

In practice, single-carrier and multi-carrier transmission are the two variant transmission schemes popularly used in OWC. The most widely used single-carrier modulation techniques include multi-level pulse position modulation (M-PPM) and multi-level pulse amplitude modulation (M-PAM). Multi-carrier modulation such as multi-level quadrature amplitude modulation optical orthogonal frequency division multiplexing (M-QAM-O-OFDM) is the most common modulation type used in most practical scenarios.

2.9.1. Single carrier transmission scheme

Single carrier modulation can be realized easily in OWC by adapting the RF communication single-carrier modulation strategy using PPM, PWM, on-off keying (OOK), and unipolar M - PAM. Single carrier modulation is the best candidate in flat fading channel since its

implementation complexity is less compared to multi-carrier modulation. In addition, in single carrier modulation, the signal can be easily shaped to constraint it in the linear range of LED; hence, in relative to multi-carrier modulation, it is less prone to nonlinear distortion.

During high speed or data rate applications, the optical wireless channel is frequency selective in nature. These frequency selectivity characteristics introduce inter-symbol interference (ISI) on the transmitted signal which reduces the performance of the system in terms of bit error rate (BER). So that, single-carrier modulation is more challenging for the realization of high speed OWC communication.

2.9.2. Multicarrier transmission schemes

The basic principle of multi-carrier transmission is to allocate multiple sub-channels with uniformly spaced center frequencies for conveying a number of bits in parallel. For a given bandwidth, the signaling rate on each sub-channel is much lower and the signaling intervals are by the same factor longer than for a corresponding single carrier transmission. Therefore, multi-carrier transmission is a good remedy to cope with the effect of frequency selective fading in high speed communication. A common and widely accepted form of multi-carrier modulation with overlapping sub-channel spectra is orthogonal frequency division multiplexing (OFDM) in which cyclic signal extensions in guard periods preserve the orthogonality of the information bearing signal pulses, making the data detection in the receivers a particularly straightforward and simple task [43]. The conventional complex bi-polar OFDM is not directly applicable for OWC since the input signal to the LED needs to be real and positive unipolar due to the use of the IM/DD scheme. To generate real unipolar OFDM signal, different types of optical OFDM schemes have been proposed for OWC in research literatures [11-17].

2.10. OFDM in OWC

At high data rate, OWC channel has limited coherent bandwidth less than the symbol rate of the signal. This can lead to a serious ISI on the received signal which degrades the quality of communication significantly. The main reason for the ISI is multi-path dispersion which comes from multiple reflection of the optical signal from different reflectors and scatters. In contrast to single-carrier transmission, multi-carrier transmission is the best candidate to cope up with inter-

symbol interference. Multi-carrier modulation such as M-QAM O-OFDM has better robustness to ISI because the symbol duration of each symbol on subcarriers is long enough compared to the rms delay spread of the optical wireless channel. Therefore, M-QAM O-OFDM is the best candidate to realize high data rates [44-46]. The OFDM scheme use cyclic prefix (CP), so that the channel can be considered as flat fading over the subcarrier bandwidth [8, 47]. Thus, the inter sub-carrier interference (ICI) can be effectively migrated by adding cyclic prefix (CP) on the information signal. Moreover, In O-OFDM, it is possible to use less complex single tap equalization in frequency domain to mitigate the effect of channel impulse response on the received information.

The basic concept of O-OFDM relies on using a large number of parallel narrow-band sub-carriers instead of a single wide-band carrier to transport information. Data is transmitted in parallel fashion over a number of orthogonal frequencies. OFDM uses longer symbol period on each subcarrier compared to single carrier system with the same capacity [8]. The use of longer duration symbols in OFDM helps the system to reduce the effect of ISI. In addition, residual ISI is mitigated by guard interval introduced by cyclic prefix [8].

In O-OFDM, modulation is achieved through inverse fast Fourier transform (IFFT) at the transmitter side. The resulting discrete time domain OFDM signal is changed in to analogue waveform by using digital to analogue converter. The time-domain analogue signal is used to modulate the emitted light intensity from the light source. The modulating analog signal needs to be real-valued and non-negative. Hermitian symmetry is introduced on the subcarriers to generate real-valued signal [8, 11, 15]. Unipolar O-OFDM schemes are the modification of the conventional bipolar OFDM transmission technique in which the input electrical signal to the LED is real and positive since information signal is encoded on the intensity of the optical carrier wave. Photo detectors (PD) are used at the receiver to convert the directly detected optical signal intensity into electrical domain.

A widely accepted system model of unipolar optical OFDM systems is depicted in Fig. 2.7 and 2.8. The information stream T_x is first arranged into a block of complex data symbols denoted by X_k. The complex symbols are drawn from M-QAM constellations and mapped on vector X as follows.

$$X = [0\ X_k\ \ 0\ X_k^*],\ \ k = 1, 2, ..., \tfrac{N}{2} - 1 \tag{2.15}$$

The OFDM modulator applies an N -point inverse fast Fourier transform (IFFT) on the vector X and adds a cyclic prefix creating the real time signal. The CP is used to mitigate the effect of both inter-carrier interference (ICI) and inter-block interference (IBI) by converting the linear convolution into a circular convolution. However, the resulting bi-polar time domain OFDM signal should be converted to positive unipolar one prior to the process of intensity modulation [48].

There are two widely accepted approaches to obtain a non-negative unipolar signal in M-QAM O-OFDM. The first one is direct-current-biased O-OFDM (DCO-OFDM), it involves injection of DC bias on the OFDM symbol [15-16, 49]. The second technique, proposed by Armstrong and Lowery [11] includes design O-OFDM unipolar half-Gaussian signals which are known as asymmetrically clipped O-OFDM (ACO-OFDM) [11, 17, 50-51]. It is realized by using only the odd subcarriers for data transmission while the even ones are vacant. In ACO-OFDM, the negative part of the resulting signal after IFFT is clipped at the transmitter.

2.10.1. DCO-OFDM

DCO-OFDM is realized by adding a positive DC bias on the bi-polar OFDM signal. This is the easiest and straight forward technique for turning a bipolar signal into a unipolar positive signal. The OFDM signal has an inherent characteristic of having large peak- to-average power ratio (PAPR) in which some of the signals can be in negative region even after introducing a large DC bias. Therefore, those negative peaks will be clipped and resulting a non-linear distortion which limits the system performance [8].

For DCO-OFDM scheme having a total of N subcarriers, the input QAM symbols X_k are mapped to subcarriers in the form of vector X^{DCO} as follows.

$$X^{DCO} = [X_k],\ k = 0, 1, 2, ..., N - 1 \tag{2.16}$$

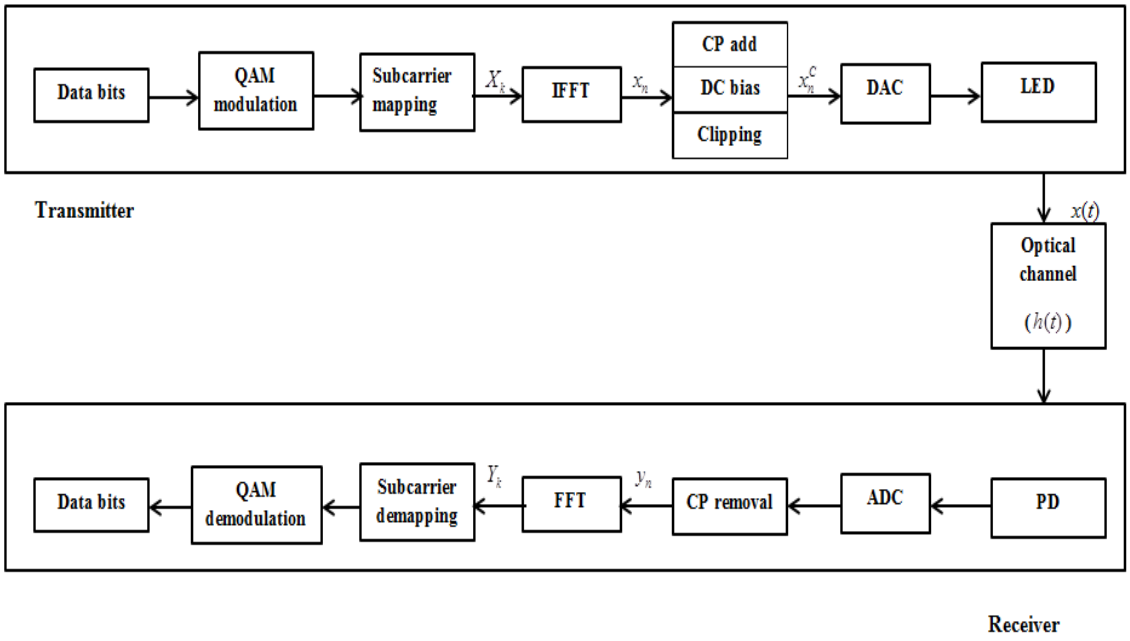

Figure 2. 7: Block diagram of DCO-OFDM scheme.

Hermitian symmetry is employed by loading the first and the $(N/2)^{th}$ subcarriers with zero QAM symbols and conjugate symmetry of the information QAM symbol on subcarriers in the second half. Therefore,

$$X_k = X_{N-k}^* \tag{2.17}$$

And

$$X_0 = X_{\frac{N}{2}} = 0 \tag{2.18}$$

The discrete time OFDM symbol x_n generated by taking the IFFT operation on vector X^{DCO} is given by:

$$x_n = \frac{1}{\sqrt{N}} \sum_{k=0}^{N-1} X_k e^{j\frac{2\pi kn}{N}},\ n = 0,1,2,...,N-1 \tag{2.19}$$

x_n is real and bipolar since it can have positive or negative value. To modify the bipolar signal to unipolar x_n^{DC}, a DC bias of k_{DC} is added on x_n as follows:

$$x_n^{DC} = x_n + k_{DC} \tag{2.20}$$

OFDM signal has well known characteristics of having high peak to average power (PAPR) ratio. So that, some samples will still be in the negative region even after adding the DC bias. The clipping of those negative samples which are left in the negative region introduce a distortion on the information. The optimum DC bias is different for different level M-QAM modulation and it is the multiple of the standard deviation of the signal at the output of IFFT module. DCO-OFDM is energy inefficient scheme due to the additional power dissipation incurred by the added DC bias. Compared to bipolar OFDM signal, the increment of the dissipated electrical power B_{DC} in DCO-OFDM due to the added DC bias can be written as [17]:

$$B_{DC} = 10\log_{10}(k_{DC}^2 + 1) \tag{2.21}$$

On the other hand, the DCO-OFDM scheme is known for offering better spectral efficiency since half of the available odd and even subcarriers are utilized for carrying information bits. The spectral efficiency Se_{DCO} of DCO-OFDM for N available subcarriers is given by [17]:

$$Se_{DCO} = \frac{(\log_2 M)(N-2)}{2(N+N_{CP})} \tag{2.22}$$

Where, M and N_{CP} are the level of QAM modulation used and the number of cyclic prefix respectively.

2.10.2. ACO-OFDM scheme

The DC bias in DCO-OFDM has a significant effect of increasing the dissipated electrical energy and the required optical power at the transmitter [52]. The power efficiency of DCO-OFDM is not satisfactory and promising. Unlike the DCO-OFDM, the ACO-OFDM scheme, avoids the DC biasing and generate a positive unipolar OFDM signal [11]. In ACO-OFDM, only odd-indexed frequency subcarriers are modulated with the valuable information. This creates a symmetry property among the bipolar time domain OFDM samples. As shown on Fig.2.8, X_k is the complex representation of the QAM symbol loaded on k^{th} sub-carrier.

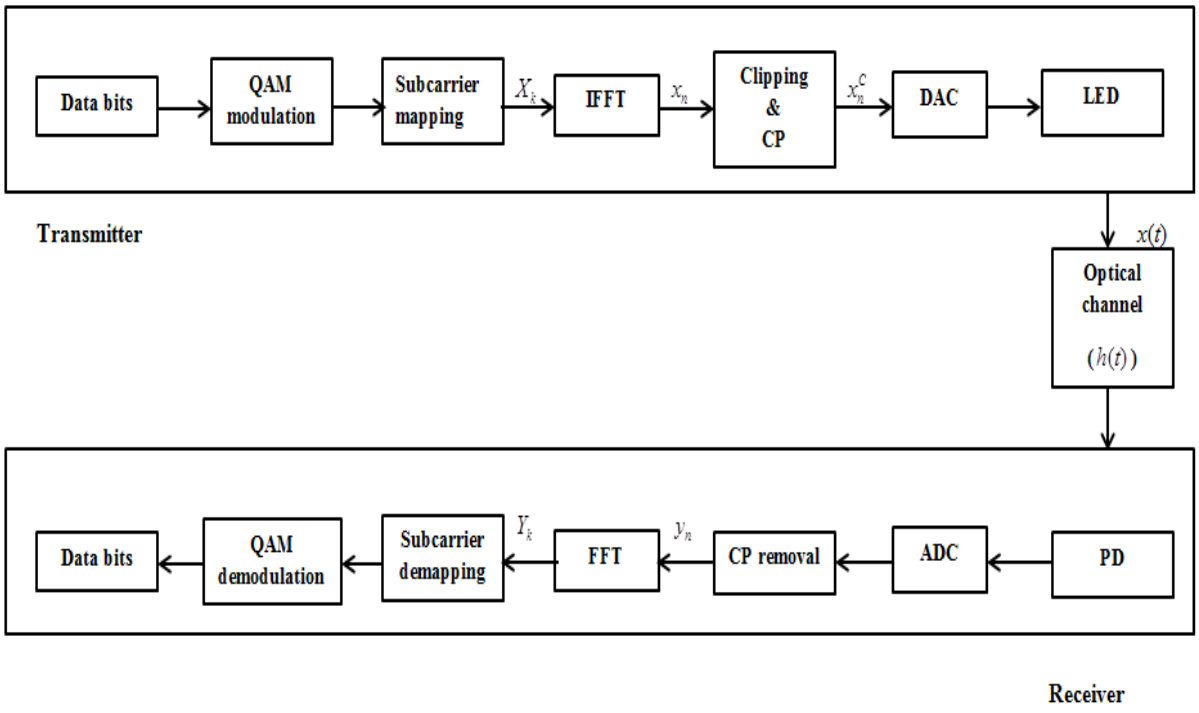

Figure 2. 8: Block diagram of ACO-OFDM scheme.

The vector of the QAM symbol X^{ACO} which is mapped on the available subcarriers can be written as:

$$X^{ACO} = [X_k],\ k = 0,1,2,...,N-1 \tag{2.23}$$

Where:

$$X_k = X_{N-k}^* \tag{2.24}$$

And

$$X_k = 0,\ k = 0,2,4,...,N-2 \tag{2.25}$$

Therefore, the even indexed subcarriers are not utilized for transmitting the information bits since they are loaded with zero QAM symbols. The frequency domain QAM symbol X_k and the discrete time domain OFDM signal sample x_n are related with IFFT/FFT operations as:

$$x_n = \frac{1}{\sqrt{N}} \sum_{k=0}^{N-1} X_k e^{j\frac{2\pi kn}{N}},\ n = 0,1,2,...,N-1 \tag{2.26}$$

$$X_k = \frac{1}{\sqrt{N}} \sum_{n=0}^{N-1} x_n e^{-j\frac{2\pi kn}{N}},\ k = 0,1,2,...,N-1 \tag{2.27}$$

In ACO-OFDM, the contribution of k^{th} subcarrier to the samples $x_{n,k}$ and $x_{n+\frac{N}{2},k}$ at n^{th} and $(n+\frac{N}{2})^{th}$ time instants respectively are related as follows:

$$x_{n,k} = \frac{1}{\sqrt{N}} X_k e^{j\frac{2\pi nk}{N}} \tag{2.28}$$

And

$$x_{n+\frac{N}{2},k} = \frac{1}{\sqrt{N}} X_k e^{j\frac{2\pi (n+\frac{N}{2})k}{N}}$$

$$= \frac{1}{\sqrt{N}} X_k e^{j\frac{2\pi nk}{N}} e^{j\pi k} \tag{2.29}$$

The even subcarriers have no contribution on the samples at any time instant due to the zero QAM symbol loaded on them. Therefore, for odd k; the relation given on (2.28) becomes:

$$x_{n+\frac{N}{2},k} = -\frac{1}{\sqrt{N}} X_k e^{j\frac{2\pi nk}{N}} \tag{2.30}$$

Therefore, from (2.28) and (2.30):

$$x_{n,k} = -x_{n+\frac{N}{2},k} \tag{2.31}$$

The contribution of all subcarriers to the samples at n^{th} and $(n+\frac{N}{2})^{th}$ time instants can also be related as:

$$x_n = -x_{n+N/2} \tag{2.32}$$

Since x_n is a real bipolar signal, it has to be modified into positive unipolar signal by clipping the negative valued samples in to zero. The positive unipolar OFDM signal x_n^{ACO} after clipping the negative samples is given by:

$$x_n^{ACO} = \begin{cases} 0, & x_n \le 0 \\ x_n, & x_n \ge 0 \end{cases} \tag{2.33}$$

The clipping of negative samples will have two consequences on the received signal at subcarriers on receiver side. The amplitude of the received QAM symbol will be reduced by half compared to the transmitted QAM symbols because of the clipping. In addition, the clipping noise with half the power of transmitted signal will fall on the even subcarriers at the receiver end. These two effects of clipping can be clearly seen from the frequency domain of the OFDM signal. The frequency domain OFDM signal X_k can be obtained from the time domain signal x_n using FFT operation as follows.

$$\begin{aligned} X_k &= \frac{1}{\sqrt{N}} \sum_{n=0}^{N-1} x_n e^{-j\frac{2\pi kn}{N}} \\ &= \frac{1}{\sqrt{N}} \sum_{n=0}^{\frac{N}{2}-1} x_n e^{-j\frac{2\pi kn}{N}} + x_{n+N/2} e^{-j\frac{2\pi(n+N/2)k}{N}} \\ &= \frac{1}{\sqrt{N}} \sum_{\substack{n=0 \\ x_n>0}}^{\frac{N}{2}-1} x_n e^{-j\frac{2\pi nk}{N}} + x_{n+N/2} e^{-j\frac{2\pi(n+N/2)}{N}} + \frac{1}{\sqrt{N}} \sum_{\substack{n=0 \\ x_n<0}}^{\frac{N}{2}-1} x_n e^{-j\frac{2\pi nk}{N}} + x_{n+N/2} e^{-j\frac{2\pi(n+N/2)}{N}} \\ &= \frac{1}{\sqrt{N}} \sum_{\substack{n=0 \\ x_n>0}}^{\frac{N}{2}-1} x_n e^{-j\frac{2\pi nk}{N}} + x_{n+N/2} e^{-j\frac{2\pi nk}{N}} e^{-j\pi k} + \frac{1}{\sqrt{N}} \sum_{\substack{n=0 \\ x_n<0}}^{\frac{N}{2}-1} x_n e^{-j\frac{2\pi nk}{N}} + x_{n+N/2} e^{-j\frac{2\pi nk}{N}} e^{-j\pi k} \end{aligned} \tag{2.34}$$

Since only odd subcarriers are non-zero in ACO-ODM scheme, the above equation will reduce to:

$$X_k = \frac{1}{\sqrt{N}} \sum_{\substack{n=0 \\ x_n>0}}^{\frac{N}{2}-1} x_n e^{-j\frac{2\pi nk}{N}} + (-x_{n+N/2}) e^{-j\frac{2\pi nk}{N}} + \frac{1}{\sqrt{N}} \sum_{\substack{n=0 \\ x_n<0}}^{\frac{N}{2}-1} x_n e^{-j\frac{2\pi nk}{N}} + (-x_{n+N/2}) e^{-j\frac{2\pi nk}{N}} \qquad (2.35)$$

But according to equation (2.32), the first and the second terms of each summation on the above equation (2.35) are similar and equal in values. Therefore, the equation can be further reduced to:

$$X_k = \frac{2}{\sqrt{N}} \sum_{\substack{n=0 \\ x_n>0}}^{\frac{N}{2}-1} x_n e^{-j\frac{2\pi nk}{N}} + \frac{2}{\sqrt{N}} \sum_{\substack{n=0 \\ x_n<0}}^{\frac{N}{2}-1} x_n e^{-j\frac{2\pi nk}{N}} \qquad (2.36)$$

The above equation can be modified in to the following form.

$$\frac{X_k}{2} = \frac{1}{\sqrt{N}} \sum_{\substack{n=0 \\ x_n>0}}^{\frac{N}{2}-1} x_n e^{-j\frac{2\pi nk}{N}} + \frac{1}{\sqrt{N}} \sum_{\substack{n=0 \\ x_n<0}}^{\frac{N}{2}-1} x_n e^{-j\frac{2\pi nk}{N}} \qquad (2.37)$$

But from the term:

$$X_k = \frac{1}{\sqrt{N}} \sum_{\substack{n=0 \\ x_n>0}}^{\frac{N}{2}-1} x_n e^{-j\frac{2\pi nk}{N}} + x_{n+N/2} e^{-j\frac{2\pi (n+N/2)}{N}} + \frac{1}{\sqrt{N}} \sum_{\substack{n=0 \\ x_n<0}}^{\frac{N}{2}-1} x_n e^{-j\frac{2\pi nk}{N}} + x_{n+N/2} e^{-j\frac{2\pi (n+N/2)}{N}} \qquad (2.38)$$

In the above equation, the second term of the first summation and the first term of the second summation are negative and clipped to zero at the transmitter. Hence, the received QAM symbol on the odd subcarriers are given by:

$$X_k^c = \frac{1}{\sqrt{N}} \sum_{n=0}^{N-1} x_n^{ACO} e^{-j\frac{2\pi nk}{N}}$$

$$= \frac{1}{\sqrt{N}} \sum_{\substack{n=0 \\ x_n>0}}^{\frac{N}{2}-1} x_n e^{-j\frac{2\pi nk}{N}} + \frac{1}{\sqrt{N}} \sum_{\substack{n=0 \\ x_n<0}}^{\frac{N}{2}-1} x_{n+N/2} e^{-j\frac{2\pi (n+N/2)}{N}}$$

$$= \frac{1}{\sqrt{N}} \sum_{\substack{n=0 \\ x_n>0}}^{\frac{N}{2}-1} x_n e^{-j\frac{2\pi nk}{N}} + \frac{1}{\sqrt{N}} \sum_{\substack{n=0 \\ x_n<0}}^{\frac{N}{2}-1} x_n e^{-j\frac{2\pi nk}{N}}$$

$$= \frac{X_k}{2} \tag{2.39}$$

As the above equation on (2.39) confirms, the clipping of negative samples at the transmitter reduce the amplitude of the received QAM symbols on odd subcarriers by half compared to the transmitted QAM symbols on the same subcarrier. The information signal can be demodulated and the data can be recovered from the odd subcarriers by discarding the even indexed subcarriers [11]. ACO-OFDM scheme wastes even-indexed subcarriers since only the odd-indexed subcarriers are utilized for carrying information bits. This makes ACO–OFDM scheme energy inefficient by sacrificing approximately half of the spectral efficiency in comparison to DCO-OFDM. The spectral efficiency Se_{ACO} of ACO-OFDM can be calculated as [17, 53]:

$$Se_{ACO} = \frac{(\log_2 M)(N)}{4(N + N_{CP})} \tag{2.40}$$

As we can see from equation (2.40), the spectral efficiency of ACO-OFDM is almost half that of DCO-OFDM and ACO-OFDM almost wasted 75% of the total available bandwidth offered by all subcarriers.

2.11. Related works on performance enhancements

Significant efforts have been made to enhance the performance of different variants of OFDM for OWC. In [18, 54], a unipolar type of OFDM, Flip OFDM, has been proposed. Flip OFDM transmits the positive and negative parts of the signal in two consecutive positive valued blocks by flipping the negative values to positive before transmission. Even if Flip OFDM uses both even and subcarrier, it offer similar spectral efficiency to ACO-OFDM due to its usage of double symbols for positive and negative parts successively. So its spectral efficiency is not attractive. The other type of unipolar OFDM is U-OFDM proposed in the literature [19]. U-OFDM is almost the same as Flip OFDM but proposed by another group independently at the same time. It uses the

same principle of successive transmission of positive and negative part of bipolar OFDM as Flip OFDM. It has the same spectral efficiency with ACO-OFDM which is not satisfactory. U-OFDM uses absolute value to change the negative part to positive before transmission. Therefore, this non-linear transformation changes the characteristics of the frequency domain of the signal which introduce a difficulty for frequency domain equalization.

There are also different models which propose layered architecture to enhance performance of optical OFDM. A layered architecture which superimposes ACO-OFDM on odd subcarriers and DCO-OFDM on even subcarriers is known as asymmetrically clipped DC-biased optical OFDM (ADO-OFDM) has been proposed in [55]. ADO-OFDM offers better spectral efficiency compared to ACO-OFDM but it has still the issue of power inefficiency due to the DC bias on the even subcarriers. The other model which uses layered architecture is called Enhanced Unipolar OFDM, eU-OFDM [56-57]. eU-OFDM is proposed to improve the spectral efficiency of U-OFDM by combining multiple U-OFDM frames in to a single unipolar time domain OFDM frames and developing frame work of separating them at the receiver by using successive demodulation. eU-OFDM has better spectral efficiency compared to ACO-OFDM but it needs time domain equalization and it has issue of latency for real time communication. Since it uses U-OFDM, due to the nonlinear transformation nature, frequency domain equalization is difficult.

2.12. Adaptive optical OFDM

The limited modulation bandwidth of LED at the transmitter device puts a major challenge in realization of high speed OWC. Therefore, enhancing the spectral efficiency of optical OFDM modulation schemes is of major concern. In practical situation, the optical wireless channel has a time dispersive nature which introduces ISI and frequency selectivity behaviour in frequency domain [34]. The effect of frequency selectivity of multipath optical wireless channel on transmitted baseband signal which occupies a bandwidth B is presented on Fig.2.9.

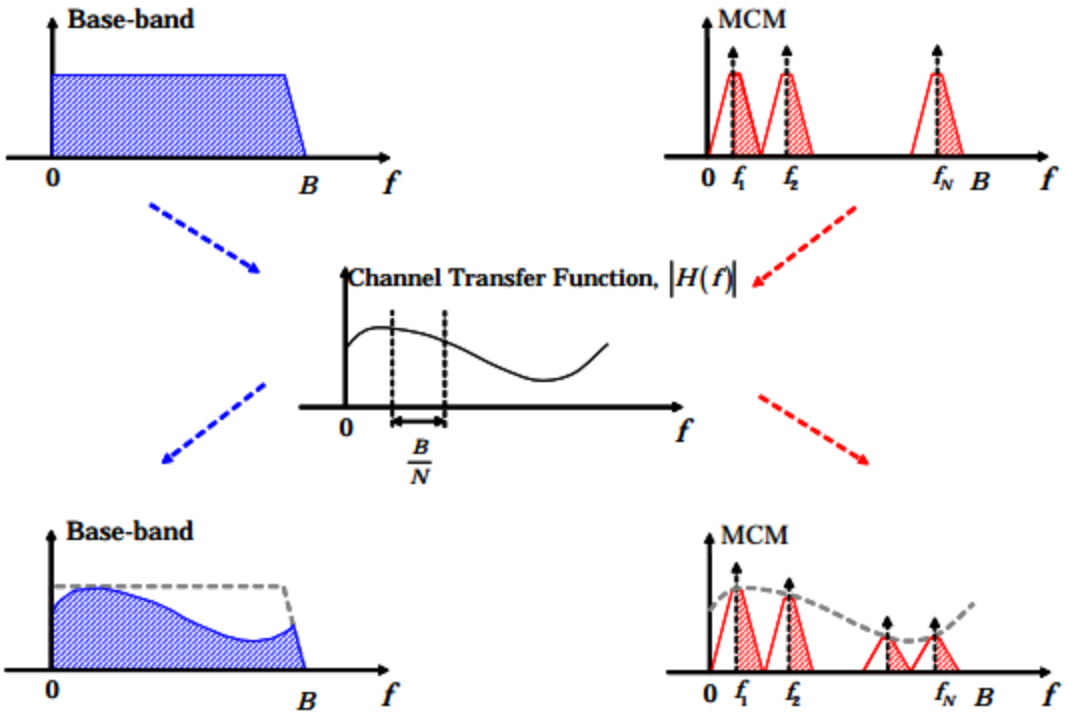

Figure 2. 9: Multicarrier and single carrier modulations on frequency selective channel [33].

As shown in Fig.2.9, the transmitted signal at different frequencies (subcarriers) is affected at different levels due to the frequency selectivity nature of the channel. During multicarrier modulation (MCM) such as OFDM scheme, the signal distortion or ISI introduced by the frequency selective channel can be mitigated by using frequency domain equalization. Nevertheless, the transmitted symbols on different subcarriers are affected with different value of loss (attenuation) factors due to the frequency selective channel. Hence, there will be significant degradation of SNR on some of the subcarriers to achieve acceptable BER with fixed modulation scheme for power constrained communication system. While using a fixed modulation scheme, there will be a reduction of spectral efficiency since the subcarriers with low SNR that cannot achieve the accepted BER will be left vacant. The well-known effective remedy for such challenge is incorporating rate adaptive capabilities in the OFDM modulation scheme. In rate adaptive OFDM scheme, variable numbers of bits are transmitted on different subcarriers based on the achieved SNR values on subcarriers while achieving acceptable BER.

Adaptive modulation techniques are well studied in the conventional RF based wireless communication to enhance the spectral efficiency of the communication system. On contrary, the

potential of adaptive modulation schemes to enhance the spectral efficiency of OWC is not yet studied in satisfactory level. In particular, the performance of rate adaptive optical OFDM to enhance the spectral efficiency of OWC with purely diffused optical wireless channel link configuration is not well studied. Different types of adaptive OFDM techniques, such as bit and power loading [58-61], were studied and proposed for conventional RF based wired and wireless communications. In OWC, adaptive DCO-OFDM scheme is studied on some literatures for NLOS/LOS optical wireless physical link configurations [34, 62-64].

Chapter 3

Research Methodology and Design

As presented in the previous chapter, ACO-OFDM and DCO-OFDM are widely accepted conventional state-of-the-art modulation schemes for IM/DD based OWC. Despite of their popularity, ACO-OFDM and DCO-OFDM schemes have either spectral or power inefficiency issues. To achieve high speed indoor OWC, the used modulation format needs to be both power and spectrally efficient. Therefore, exploring an optimized design strategy to develop both power and spectral efficient unipolar optical OFDM is vital and apparent. To address this challenge, a stratified asymmetrically clipped optical OFDM (STACO-OFDM) is proposed in this thesis. This chapter covers the system model and the analytical frame work of the proposed STACO-OFDM.

3.1. STACO-OFDM system model

STACO-OFDM is unipolar OFDM proposed for intensity modulation and direct detection (IM/DD) based indoor optical wireless communications. It utilizes a stratified architecture to use both odd and even subcarriers for information transmission. Even subcarriers are utilized on the 1^{st} stratum while the rest of the strata utilize odd subcarriers multiple times. The system architecture of STACO-OFDM is given with the aid of block diagram in Fig. 3.1.

As shown on Fig.3.1, the system model of STACO-OFDM comprises ACO-OFDM modulators at each stratum for simultaneous transmission of multiple OFDM frames at the same time. OFDM frames originating from each stratum are combined together to form single unified OFDM frame for transmission. To enable efficient inter-frame interference cancelation coming from multiple strata on the receiver end, the time domain signals from ACO-OFDM modulators at each stratum are further modified before combining them in to a single unified frame for transmission.

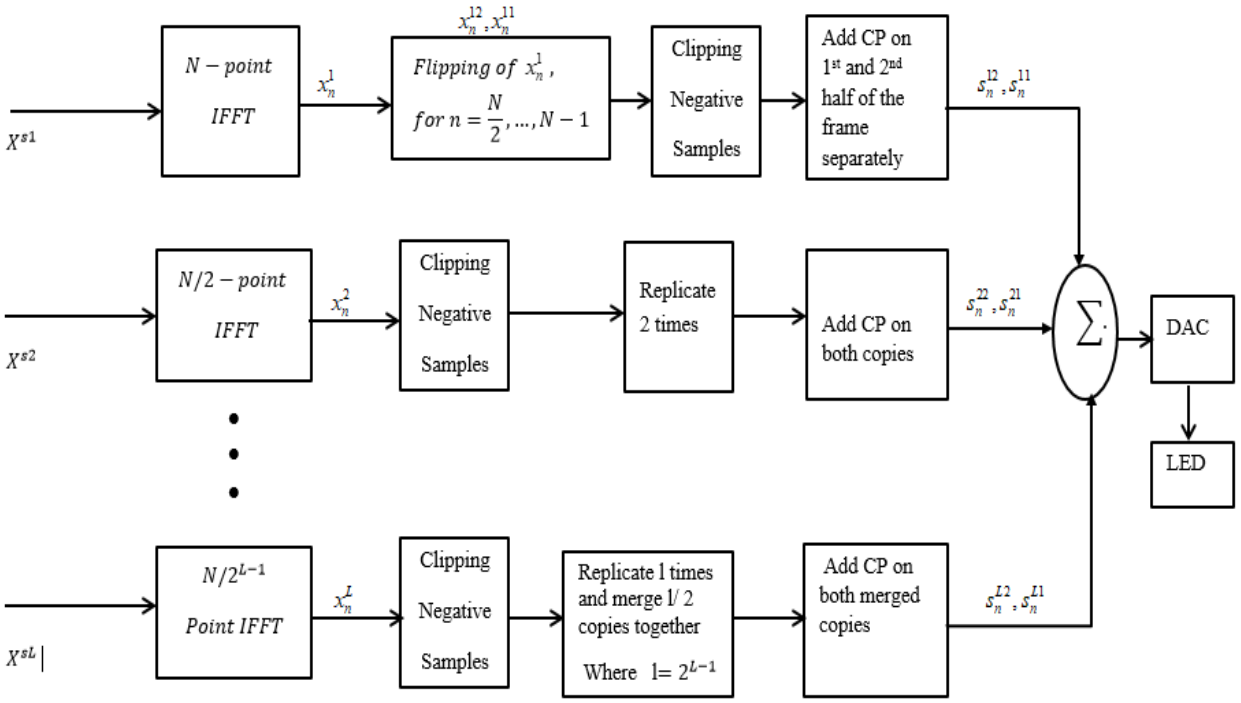

Figure 3. 1: Block diagram of STACO-OFDM scheme.

In the 1st stratum, subcarriers are loaded with input frequency domain QAM symbols X_k^1 represented by vector X^{s1} as:

$$X^{s1} = [X_k^1],\ k = 0,1,2,\ldots,N-1 \tag{3.1}$$

Only even indexed subcarriers are loaded with information QAM symbols and odd subcarriers are left vacant or loaded with zero QAM symbols on the 1st stratum of STACO-OFDM. In addition, Hermitian symmetry is employed on the second half of the total available subcarriers. Hence, the QAM symbol loaded on subcarriers will have the following relations to each other because of the employed Hermitian symmetry.

$$X_k^1 = (X_{N-k}^1)^* \tag{3.2}$$

$$X_0^1 = X_{N/2}^1 \tag{3.3}$$

In addition, the odd subcarriers at the 1st stratum are loaded with zero energy QAM symbols as:

$$X_k^1 = 0,\ k = 1,3,5,\ldots,N-1 \tag{3.4}$$

Therefore, the mapped QAM symbol vector X^{s1} on subcarriers will have the following form.

$$\begin{aligned} X^{s1} &= [X_k^1],\ k = 0,1,2,\ldots,N-1 \\ &= [0\ 0\ X_2^1\ 0\ X_4^1\ \ldots\ X_{N/2-2}^1\ 0\ 0\ 0\ X_{N/2+2}^1\ \ldots\ X_{N-4}^1\ 0\ X_{N-2}^1\ 0] \\ &= [0\ 0\ X_2^1\ 0\ X_4^1\ \ldots\ X_{N/2-2}^1\ 0\ 0\ 0\ (X_{N/2-2}^1)^*\ \ldots\ (X_4^1)^*\ 0\ (X_2^1)^*\ 0] \end{aligned} \tag{3.5}$$

On the 1st stratum, it is obvious that the Hermatian symmetry wastes half of the total available subcarriers similar to other unipolar OFDMs (ACO-OFDM & DCO-OFDM) which reduce the spectral efficiency by a factor of half compared to the conventional complex bipolar OFDM. As shown on Fig.3.1, the N-point IFFT module in ACO-OFDM modulator of 1st stratum transforms the input frequency domain QAM symbols in to real bipolar time domain samples. The time domain sample x_n^1 of the 1st stratum at n^{th} time instant is given by:

$$x_n^1 = \frac{1}{\sqrt{N}} \sum_{k=0}^{N-1} X_k^1 e^{j\frac{2\pi kn}{N}},\ n = 0,1,2,\ldots,N-1 \tag{3.6}$$

The real bipolar time domain signal x_n^1 has a symmetrical property at $N/2$ which can be clearly seen by comparing the contribution the k^{th} subcarrier to n^{th} and $(n+N/2)^{th}$ time domain samples. Let $x_{k,n}^1$ and $x_{k,n+N/2}^1$ are the contribution of the k^{th} subcarrier for samples at n^{th} and $(n+N/2)^{th}$ time instant respectively:

$$x_{k,n}^1 = \frac{1}{\sqrt{N}} X_k^1 e^{j\frac{2\pi nk}{N}} \tag{3.7}$$

And

$$x_{k,n+N/2}^1 = \frac{1}{\sqrt{N}} X_k^1 e^{j\frac{2\pi(n+\frac{N}{2})k}{N}}$$

$$= \frac{1}{\sqrt{N}} X_k^1 e^{j\frac{2\pi nk}{N}} e^{j\pi k}$$

$$= \frac{1}{\sqrt{N}} X_k^1 e^{j\frac{2\pi nk}{N}}, \text{ for even } k \quad (3.8)$$

Therefore, according to (3.7) and (3.8), the time domain signal samples at the first stratum have the following symmetrical relationships:

$$x_n^1 = x_{n+N/2}^1 \quad (3.9)$$

In the proposed STACO-OFDM, the combination of discrete time domain OFDM signal from all strata is done based on sub-frames. A sub-frame is the term used to refer half of the complete discrete time OFDM frame. Therefore, the frame having N discrete time samples could have two sub frames having $N/2$ samples each. The two sub-frames with length of $N/2$ samples are formed from the complete frame at 1st stratum. In this chapter, the following representations are used to represent the n^{th} sample of 1st and the 2nd sub-frames of l^{th} stratum.

x_n^{l1}: *the* 1^{st} *sub – frame of* l^{th} *stratum*
x_n^{l2}: *the* 2^{nd} *sub – frame of* l^{th} *stratum*

Therefore x_n^{11} and x_n^{12}, which are the 1st and 2nd sub-frames of the 1st stratum respectively, are given by:

$$x_n^{11} = x_n^1, \; n = 0,1,2,\ldots,\tfrac{N}{2}-1 \quad (3.10)$$

And

$$x_n^{12} = x_{n+N/2}^1, \; n = 0,1,2,\ldots,\tfrac{N}{2}-1 \quad (3.11)$$

But it is noted that x_n^{11} and x_n^{12} on (3.10) and (3.11) are real bipolar signals and need to be changed into positive unipolar signal to fulfill the requirement of IM/DD transmission system. Clipping of negative samples is strategy to obtain positive unipolar signal for the intensity modulation at the LED. But to enable successful information recovery by canceling inter-stratum inter-sub-frame

interference at the receiver end, the samples of the 2nd sub-frame of the 1st stratum are multiplied with -1 to obtain flipped samples with reversed polarity. The 2nd sub-frame of the 1st stratum after filliping, x_n^{flp}, can then be written as:

$$x_n^{flp} = -x_n^{12} = -x_{n+N/2}^{1},\ n = 0,1,2,...,\tfrac{N}{2}-1 \tag{3.12}$$

Then the negative samples are clipped from both sub-frames, x_n^{11} and x_n^{flp}, to generate positive unipolar signal. Let s_n^{11} and s_n^{12} are the two positive unipolar sub frames obtained after performing the clipping of negative samples on x_n^{11} and x_n^{flp} respectively, then they can be represented with the following equations.

$$s_n^{11} = \frac{1}{2}(x_n^{11} + |x_n^{11}|)$$

$$= \frac{1}{2}(x_n^{1} + |x_n^{1}|),\ n = 0,1,2,3,...,N/2-1 \tag{3.13}$$

And

$$s_n^{12} = \frac{1}{2}(x_n^{flp} + |x_n^{flp}|)$$

$$= \frac{1}{2}(-x_{n+N/2}^{1} + |-x_{n+N/2}^{1}|),\ n = 0,1,2,3,...,N/2-1 \tag{3.14}$$

The two sub-frames of the 1st stratum on (3.13) and (3.14) are now ready to combine with sub-frames of the other strata after adding cyclic prefix (CP) on them based on the length of the channel for the purpose of mitigating ISI.

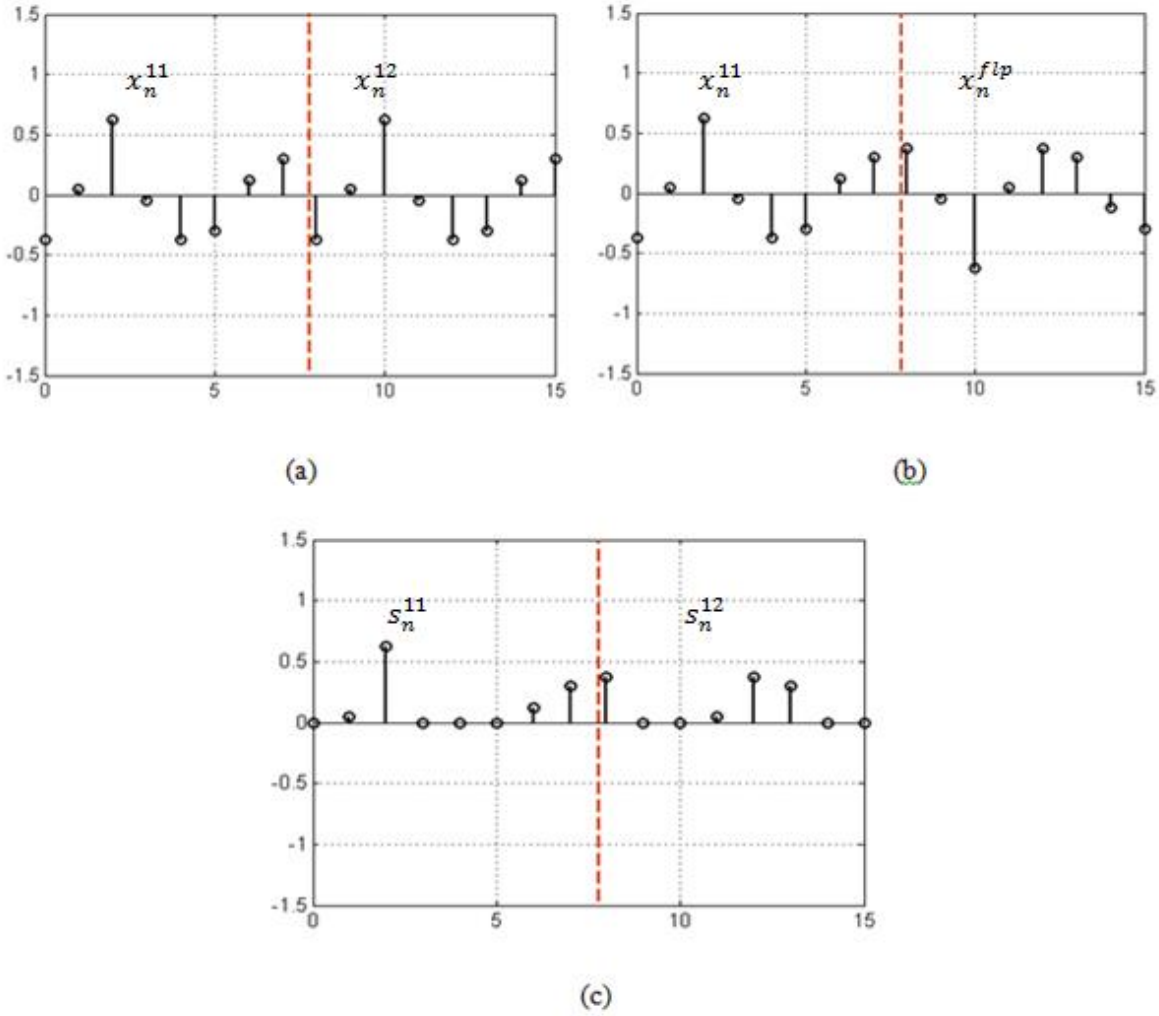

Figure 3. 2: signal processing at the 1st stratum (a) the bipolar time domain signal (b after the second sub-frame is flipped (c) after clipping of negative samples.

As presented in Fig.3.1, the lengths of IFFT points are decreasing by a factor of $1/2$ from one stratum to the next stratum in downward direction to higher level strata. This arrangement of IFFT module on STACO-OFDM is important to easily mitigate the inter stratum interference at the receiver while recovering the information carried on each stratum. If L, N_l and T_l are the total number of strata used in the system, the number of samples (IFFT/FFT points) at l^{th} stratum and OFDM symbol duration at l^{th} stratum respectively, then N_l and T_l can be written as:

$$N_l = \frac{N}{2^{l-1}},\ l = 1, 2, ..., L \tag{3.15}$$

And

$$T_l = \frac{T}{2^{l-1}},\ l = 1, 2, ..., L \tag{3.16}$$

Where,

N : is the number of IFFT/FFT points used on the 1st stratum

T : is the OFDM symbol duration at the 1st stratum

On (3.15) and (3.16), $l = 1, 2, 3, ..., L$ refers to the $1^{st}, 2^{nd}, 3^{rd}, ..., l^{th}$ stratum respectively. To combine discrete time OFDM frames coming from each stratum into one unified OFDM frame, the length of samples and frame durations from each stratum should be equal. Therefore, to equalize the length of samples and symbol durations of each stratum to N and T respectively, 2^{l-1} exact copies of time domain signal should be regenerated for stratum with index $l = 2, 3, ..., L$. Then, two $N/2$ samples long sub frames are constructed from the regenerated copies at each stratum. The signal generation technique is similar for the rest of strata (except the 1st stratum) which utilize odd subcarriers for transmission of information bits. Therefore, it will be adequate if the signal generations at the 2nd and the 3rd stratum are analyzed.

Let X_k^2 is the QAM symbol mapped to the k^{th} subcarrier of the 2nd stratum and X^{s2} is the vector representation for all mapped symbols on all subcarriers at the 2nd stratum, then X^{s2} can be represented as follows:

$$X^{s2} = [X_k^2],\ k = 0, 1, 2, 3, ..., N_2 - 1 \tag{3.17}$$

Where $N_2 = N/2$ from (3.15), therefore,

$$X^{s2} = [X_k^2],\ k = 0, 1, 2, 3, ..., N/2 - 1 \tag{3.18}$$

In the 2nd stratum, only odd subcarriers are utilized for carrying information signal while the even subcarriers are loaded with zero energy QAM symbols. Furthermore, Hermatian symmetry is employed on the second half of $N_2/2$ subcarriers. The QAM symbols X_k^2 loaded on subcarriers will satisfy the following equality relations:

$$X_k^2 = (X_{N_2-k}^2)^* \tag{3.19}$$

And

$$X_k^2 = 0,\ k = 0, 2, 4, ..., N_2 - 2 \tag{3.20}$$

Therefore, the vector of the QAM symbols loaded on 2nd stratum can be given by:

$$\begin{aligned} X^{s2} &= [X_k^2],\ k = 0,1,2,3,..., N_2 - 1 \\ &= [0\ X_1^2\ 0\ X_3^2\ ...\ X_{N_2/2-1}^2\ 0\ X_{N_2/2+1}^2\ 0\ ...\ X_{N_2-3}^2\ 0\ X_{N_2-1}^2] \\ &= [0\ X_1^2\ 0\ X_3^2\ ...\ X_{N_2/2-1}^2\ 0\ (X_{N_2/2-1}^2)^*\ 0\ ...\ (X_3^2)^*\ 0\ (X_1^2)^*] \end{aligned} \tag{3.21}$$

After taking N_2 points IFFT on X_k^2, the time domain sample x_n^2 at the n^{th} time instant is calculated as:

$$x_n^2 = \frac{1}{\sqrt{N_2}} \sum_{k=0}^{N_2-1} X_k^1 e^{j\frac{2\pi kn}{N_2}},\ n = 0,1,2,..., N_2 - 1 \tag{3.22}$$

The discrete samples of the 2nd stratum have the following symmetric relationship with each other:

$$x_n^2 = -x_{n+N_2/2}^2,\ n = 0,1,2,3,..., N_2/2 - 1 \tag{3.23}$$

But to equalize the length of samples on the 2nd stratum to N, exact copies of x_n^2 are generated by conserving the symbol energy. The two copies are set to be the two sub-frames x_n^{21} and x_n^{22} which are the 1st and the 2nd sub-frames of 2nd stratum respectively.

$$x_n^{21} = x_n^{22} = \frac{1}{\sqrt{2}} x_n^2,\ n = 0,1,2,..., N_2 - 1 \tag{3.24}$$

The factor $1/\sqrt{2}$ used in (3.24) for the purpose of symbol energy conservation before and after regeneration of copies of signal. The clipping of negative samples from both sub-frames is done as it has been done on the first stratum. The sub-frames, s_n^{21} and s_n^{22}, after clipping is done on x_n^{21} and x_n^{22} respectively, can be written as:

$$s_n^{21} = s_n^{22} = \frac{1}{2}(x_n^{21} + |x_n^{21}|]$$

$$= \frac{1}{2}(x_n^{22} + |x_n^{22}|]$$

$$= \frac{1}{2\sqrt{2}}(x_n^2 + |x_n^2|),\ n = 0,1,2,...,N_2 - 1 \quad (3.25)$$

After adding CP on s_n^{21} and s_n^{22} based on the channel length, the signal on the 2nd stratum becomes ready for combination with signal coming from other strata.

On the third stratum, the signal generation is similar to as that of the 2nd stratum. The QAM symbols X_k^3 loaded to the subcarriers at the 3rd stratum can be represented by vector X^{s3} as:

$$X^{s3} = [X_k^3],\ k = 0,1,2,3,...,N_3 - 1 \quad (3.26)$$

Where $N_3 = N/4$ from (3.15)

Hermatian symmetry is implemented on the second half of subcarriers to generate real bipolar signal. The odd subcarriers are loaded information QAM symbols while even subcarriers are loaded with zero QAM symbols. Therefore, the mapped symbols on all subcarriers are:

$$X^{s3} = [X_k^3],\ k = 0,1,2,3,...,N_3 - 1$$

$$= [0\ X_1^3\ 0\ X_3^3\ ...\ X_{N_3/2-1}^3\ 0\ X_{N_3/2+1}^3\ 0\ ...\ X_{N_3-3}^3\ 0\ X_{N_3-1}^3]$$

$$= [0\ X_1^3\ 0\ X_3^3\ ...\ X_{N_3/2-1}^3\ 0\ (X_{N_3/2-1}^3)^*\ 0\ ...\ (X_3^3)^*\ 0\ (X_1^3)^*] \quad (3.26)$$

The time domain signal is generated after taking N_3-point IFFT at the third stratum. The N_3 samples long time domain OFDM signal x_n^3 can be obtained from the following IFFT formula.

$$x_n^3 = \frac{1}{\sqrt{N_3}} \sum_{k=0}^{N_3-1} X_k^3 e^{j\frac{2\pi nk}{N_3}},\ n = 0,1,2,3,...,N_3 - 1 \quad (3.27)$$

Since the number of samples on the above equation is $N_3 = N/4$, four similar copies of x_n^3 are generated to make the length of samples equal to N. Scaling of signal amplitude with a factor of $1/2$ should be done on the regenerated copies to conserve the frame energy before and after regeneration. Then the two sub-frames, x_n^{31} and x_n^{32}, can be constructed by merging two copies together to form a signal with length of $N/2$ samples as:

$$x_n^{31} = x_n^{32} = \frac{1}{2}([x_n^3 \; x_n^3]) \tag{3.28}$$

Then after clipping to zero is performed on negative samples of x_n^{31} and x_n^{32}, the obtained positive unipolar sub-frames s_n^{31} and s_n^{32} can be represented as:

$$s_n^{31} = s_n^{32} = \frac{1}{2}(x_n^{31} + |x_n^{31}|]$$

$$= \frac{1}{2}(x_n^{32} + |x_n^{32}|], \; n = 0,1,2,3,...,N/2-1 \tag{3.29}$$

The two sub-frames at the rest of strata are also processed in similar manner as on the 2nd and the 3rd strata. The transmission of the entire information carried by all strata is carried out in two sessions. The first sub frames from all strata are combined together to form one combined sub frame to be transmitted in the first transmission sessions. Similarly the second sub- frames from all strata are combined together to form the 2nd combined sub-frame for the second transmission session. Let x_n^{t1} and x_n^{t2} are the first and the second combined sub-frames respectively, then the two combined sub-frames for the proposed STACO-OFDM scheme having L total number of strata can be written as:

$$x_n^{t1} = s_n^{11} + s_n^{21} + s_n^{31} + ... + s_n^{L1} \tag{3.30}$$

And

$$x_n^{t2} = s_n^{12} + s_n^{22} + s_n^{32} + ... + s_n^{L2} \tag{3.31}$$

As presented in Fig. 3.3, x_n^{t1} and x_n^{t2} will be transmitted in two consecutive transmission sessions separately after changed into analogue form. In the first transmission session, the information signals x_n^{t1} is transmitted through the optical wireless channel with CIR of $h(t)$ and corrupted by the zero mean AWGN noise $z_1(t)$ at the receiver. Therefore, the received signal $x^{r1}(t)$ from the 1st transmission can be represented as:

$$x^{r1}(t) = x^{t1}(t) * h(t) + z^1(t) \tag{3.32}$$

Where $x^{t1}(t)$ is the analogue version of x_n^{t1}, Similarly, the received signal $x^{r2}(t)$ from the 2nd transmission becomes:

$$x^{r2}(t) = x^{t2}(t) * h(t) + z^2(t) \tag{3.33}$$

Where:

$x^{t2}(t)$: The analog version of x_n^{t2}

$z^2(t)$: The AWGN

Since the received signal at the receiver will be changed in to discrete form by the ADC before the FFT operation takes place, it is possible to represent the received signals in discrete form as follows:

$$x_n^{r1} = x_n^{t1} * h_n + z_n^1 \tag{3.34}$$

And

$$x_n^{r2} = x_n^{t2} * h_n + z_n^2 \tag{3.35}$$

Where:

x_n^{r1} : The discrete form of $x^{r1}(t)$

x_n^{r2} : The discrete form of $x^{r2}(t)$

z_n^2 : The discrete form of $z^2(t)$

h_n : The discrete form of $h(t)$

z_n^1: The discrete form of $z^1(t)$

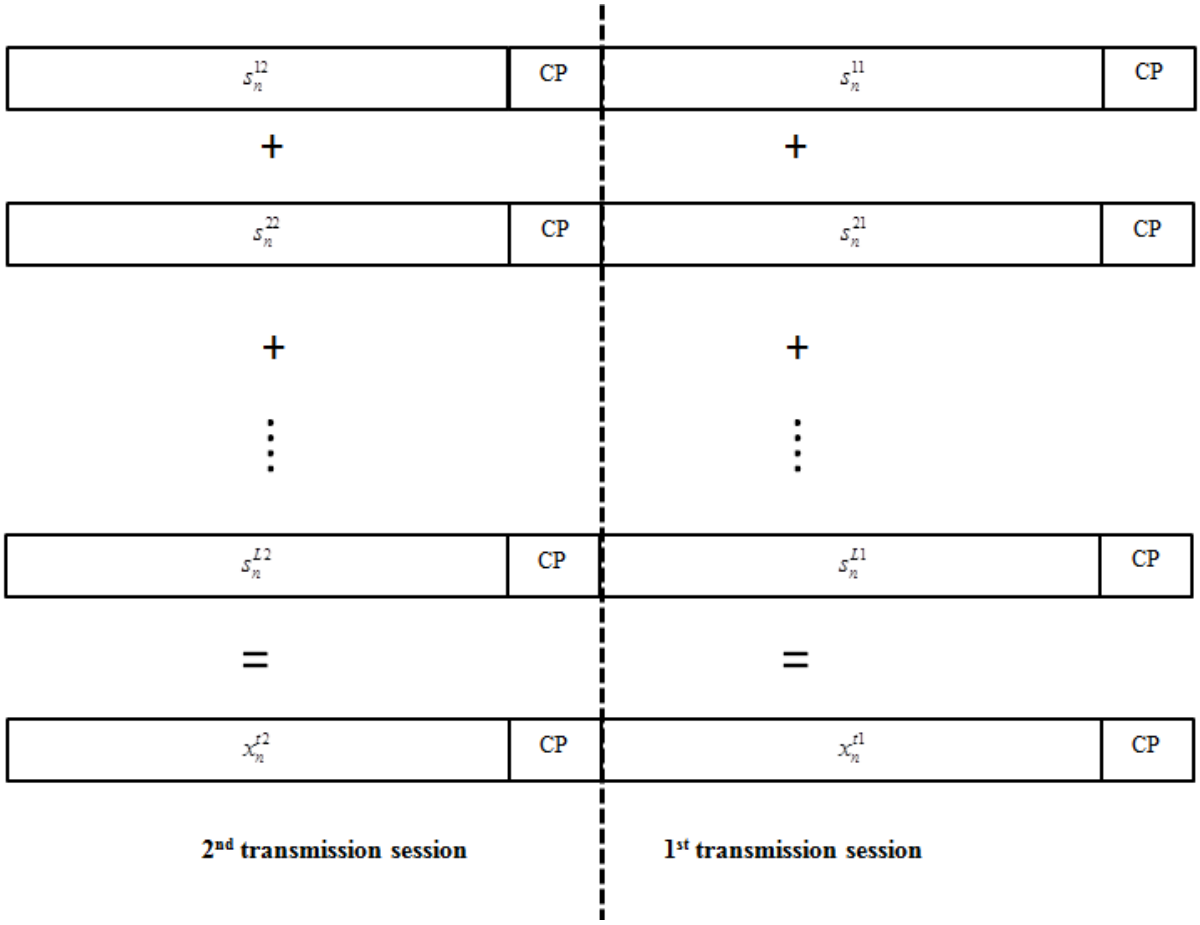

Figure 3. 3: Frame structure of STACO-OFDM scheme.

If we consider only pure AWGN channel environments by avoiding the effect of the channel, the received signals become:

$$x_n^{r1} = x_n^{t1} + z_n^1 \tag{3.36}$$

And

$$x_n^{r2} = x_n^{t2} + z_n^2 \tag{3.37}$$

The information signal recovery strategy at the receiver is adopted from successive demodulation [56-57] technique which recovers the information stratum by stratum successively. The recovery starts from the first stratum and continues towards the last stratum. To recover the information

carried by the 1st stratum, the demodulation starts by subtracting the signal received from the 2nd transmission (x_n^{r2}) from the signal received from the 1st transmission (x_n^{r1}). The output signal y_n^1 after subtraction can be written as:

$$\begin{aligned} y_n^1 &= x_n^{r1} - x_n^{r2} \\ &= (x_n^{t1} - x_n^{t2}) + (z_n^1 - z_n^2) \\ &= ((s_n^{11} + s_n^{21} + ... + s_n^{L1}) - (s_n^{12} + s_n^{22} + ... + s_n^{L2})) + z_n \end{aligned} \tag{3.38}$$

On (3.38), $z_n = z_n^1 - z_n^1$ is the AWGN having double sided power spectral density of N_o . Moreover z_n^1 and z_n^2 are statistically independent. In STACO-OFDM, the 1st and the 2nd sub-frames are similar for all strata except the first stratum. Hence, the first and the second sub-frames of all strata other than the 1st stratum will be vanished form (3.38) because of the subtraction operation. Therefore, y_n^1 becomes:

$$y_n^1 = s_n^{11} - s_n^{22} + z_n \tag{3.39}$$

But using (3.13) and (3.14), the above equation can be re-written as:

$$y_n^1 = \frac{1}{2}((x_n^1 + |x_n^1|) - (-x_{n+N/2}^1 + |-x_{n+N/2}^1|) + z_n,\ n = 0,1,2,3,...,N/2-1 \tag{3.40}$$

And using equation (3.9), the above equation can be reduced to the following form.

$$\begin{aligned} y_n^1 &= \frac{1}{2}((x_n^1 + |x_n^1|) - (-x_n^1 + |-x_n^1|) + z_n \\ &= \frac{1}{2}(x_n^1 + |x_n^1| + x_n^1 - |-x_n^1|) + z_n \\ &= \frac{1}{2}(2x_n^1) + z_n \\ &= x_n^1 + z_n,\ n = 0,1,2,3,...,N/2-1 \end{aligned} \tag{3.41}$$

The result on equation (3.41) is similar to 1st half of the bipolar OFDM signal from the output of IFFT module at the 1st stratum given on equation (3.6) with added AWGN noise samples. If we ignore z_n from (3.41) without loss of generality, the output signal y_n^1 is exactly similar to the first half of the bipolar signal at the 1st stratum as:

$$y_n^1 = x_n^1,\ n = 0,1,2,...,N/2-1 \tag{3.42}$$

But from equation (3.9) it is noted that the first and the second half of x_n^1 are equal and similar, Therefore it possible to recover the information carried by the 1st stratum by padding $N/2$ zeros at the end of y_n^1. This can be easier to comprehend if we observe the frequency domain representation of the received signal at the first stratum. Let Y_k^1 is the frequency domain signal received on k^{th} sub carrier at the first stratum, and then Y_k^1 can be written in terms of y_n^1 as follows.

$$Y_k^1 = \frac{1}{\sqrt{N}} \sum_{n=0}^{N-1} y_n^1 e^{-j\frac{2\pi nk}{N}}$$

$$= \frac{1}{\sqrt{N}} \sum_{n=0}^{N/2-1} y_n^1 e^{-j\frac{2\pi nk}{N}} + y_{n+N/2}^1 e^{-j\frac{2\pi (n+N/2)k}{N}} \tag{3.43}$$

In the above equation, the second term is equals to zero since the samples beyond index $N/2-1$ are zero valued. Therefore,

$$Y_k^1 = \frac{1}{\sqrt{N}} \sum_{n=0}^{N/2-1} y_n^1 e^{-j\frac{2\pi nk}{N}}$$

$$= \frac{1}{\sqrt{N}} \sum_{n=0}^{N/2-1} x_n^1 e^{-j\frac{2\pi nk}{N}} \tag{3.43}$$

It might also be important to relate the received frequency domain QAM symbol Y_k^1 at k^{th} subcarrier of the first stratum with the transmitted frequency domain QAM symbol X_k^1 at the first stratum. The frequency domain representation of the signal X_k^1 at the first stratum can be calculated in terms of the time domain signal x_n^1 as follows:

$$X_k^1 = \frac{1}{\sqrt{N}} \sum_{n=0}^{N-1} x_n^1 e^{-j\frac{2\pi nk}{N}}$$

$$= \frac{1}{\sqrt{N}} \sum_{n=0}^{N/2-1} x_n^1 e^{-j\frac{2\pi nk}{N}} + x_{n+N/2}^1 e^{-j\frac{2\pi(n+N/2)k}{N}}$$

$$= \frac{1}{\sqrt{N}} \sum_{n=0}^{N/2-1} x_n^1 e^{-j\frac{2\pi nk}{N}} + x_{n+N/2}^1 e^{-j\frac{2\pi nk}{N}} e^{-j\pi k} \quad (3.44)$$

But only even subcarriers are loaded with information bits at the first stratum. Hence, the term $e^{-j\pi k}$ in the above equation equals to 1 for even k and X_k^1 becomes:

$$X_k^1 = \frac{1}{\sqrt{N}} \sum_{n=0}^{N/2-1} x_n^1 e^{-j\frac{2\pi nk}{N}} + x_{n+N/2}^1 e^{-j\frac{2\pi nk}{N}}$$

$$= \frac{1}{\sqrt{N}} \sum_{n=0}^{N/2-1} x_n^1 e^{-j\frac{2\pi nk}{N}} + x_n^1 e^{-j\frac{2\pi nk}{N}}$$

$$= \frac{2}{\sqrt{N}} \sum_{n=0}^{N/2-1} x_n^1 e^{-j\frac{2\pi nk}{N}} \quad (3.45)$$

Therefore, (3.43) and (3.45) confirm that the QAM symbol received at the k^{th} even subcarrier of the first stratum is similar to the transmitted symbol at the same subcarrier with scaling factor of $1/2$. Hence, the amplitude of the received QAM symbol at the first stratum is equal to half of the amplitude of the QAM symbols transmitted at the same stratum as:

$$Y_k^1 = \frac{1}{2} X_k^1, \; k = 2, 4, 6, ..., N-2 \quad (3.46)$$

Hence, the information signal transmitted on the first stratum can be recovered from the even subcarriers by using conventional ACO-OFDM demodulator. The clipping noise due to the clipping of $N/2$ samples on the 2nd half of the time domain signal to zero falls on the odd subcarriers and does not affect the recovery of information bits from even subcarriers. Fig.3.4 presents the time domain signal y_n^1 of the 1st stratum before and after zero padding for the transmitted signal presented on Fig.3.2.

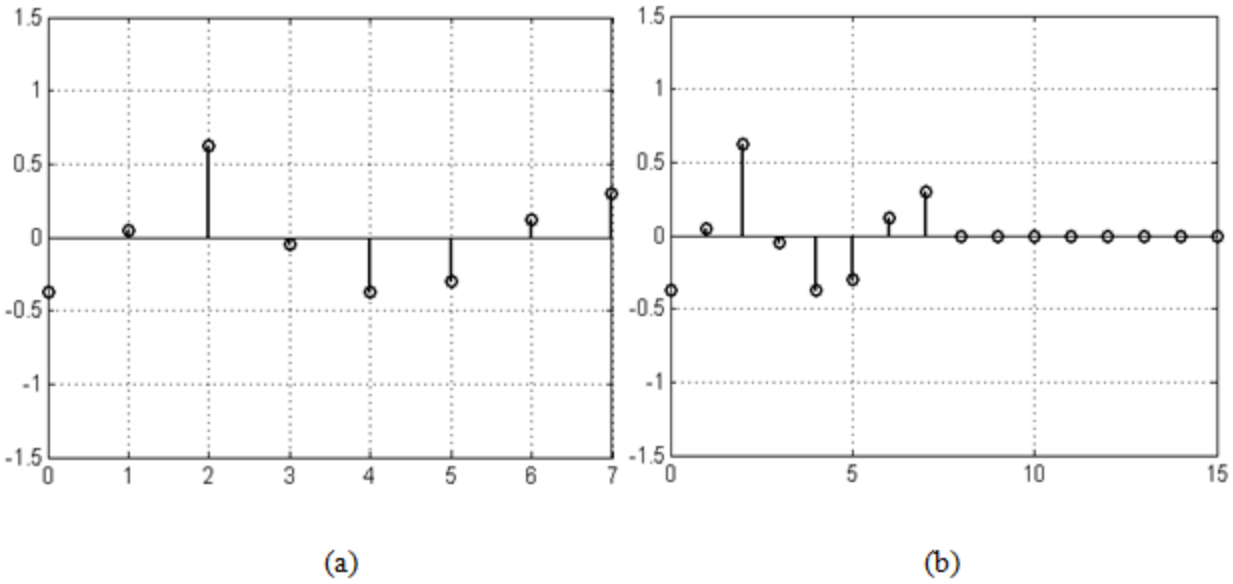

Figure 3. 4: The signal on 1st stratum at the receiver end: (a). Before padding zeros (b). After padding zeros.

The zero padding process is equivalent to performing zero level clipping on the second half of the time domain signal. The zero padding or clipping process has two main effects. The first effect is, it introduces amplitude reduction on the QAM symbols loaded on even subcarriers at the 1st stratum by a factor of $1/2$. The second effect is, all off the clipping noise due to the zero padding fall on the odd subcarriers. Therefore, the clipping noise needs to be removed from odd subcarriers before demodulation is done to recover information carried by other strata. After padding zeros and taking FFT operation on the zero padded signals, the complete information of the 1st stratum can be recovered from even sub carriers as confirmed on equation (3.46). To continue the demodulation process of the next stratum, the contribution of the first stratum should be removed from the received time domain signal. Therefore, the recovered information bits on the first stratum are re-modulated at the receiver and the output time domain signal is processed in the same way as the time domain signal is processed at the 1st stratum on the transmitter side. The first and the second sub frames of the re-modulated signal are subtracted from x_n^{r1} and x_n^{r2} respectively to remove the contribution of the 1st stratum's information from the combined signal. The clipping noise due to 1st stratum also removed from the odd sub carriers when the contribution of the 1st stratum is removed from the combined signal. After removing the contribution of the 1st stratum from the combined signal, the information carried by the 2nd stratum can be recovered from the odd

subcarriers by using ACO-OFDM demodulator. The interference coming from other strata (from 3rd to L^{th} stratum) has no effect on the demodulation of the signal at 2nd stratum. Ignoring the channel effects and AWGN, let x_n^{R1} and x_n^{R2} are the output signals after removing the contribution of the first stratum from x_n^{r1} and x_n^{r2} respectively. Hence,

$$x_n^{R1} = x_n^{r1} - s_n^{11} \tag{3.47}$$

And

$$x_n^{R2} = x_n^{r2} - s_n^{12} \tag{3.48}$$

But according to (3.30) and (3.31), the equations given on (3.47) and (3.48) can be written in the following forms.

$$x_n^{R1} = s_n^{21} + s_n^{31} + ... + s_n^{L1} \tag{3.49}$$

And

$$x_n^{R2} = s_n^{22} + s_n^{32} + ... + s_n^{L2} \tag{3.50}$$

Then by adding x_n^{R1} and x_n^{R2}, output signal y_n^{s2} having a length of N_2 samples is obtained as:

$$\begin{aligned} y_n^{s2} &= x_n^{R1} + x_n^{R2} \\ &= 2s_n^{21} + 2(s_n^{31} + ... + s_n^{L1}) \\ &= \frac{2}{\sqrt{2}}\left(\frac{1}{2}(x_n^2 + |x_n^2|)\right) + 2(s_n^{31} + ... + s_n^{L1}) \end{aligned} \tag{3.51}$$

But to conserve the same energy in the first stratum before and after adding the two signals, y_n^{s2} is scaled by a factor $\sqrt{2}/2$ to obtain a scaled signal y_n^2 as:

$$y_n^2 = \frac{\sqrt{2}}{2} y_n^{s2}$$

$$= \frac{1}{2}(x_n^2 + |x_n^2|) + \sqrt{2}(s_n^{31} + ... + s_n^{L1})$$

$$= \tilde{x}_n^2 + I_n^2,\ n = 0,1,2,..., N_2 - 1 \tag{3.52}$$

Where:

- $\tilde{x}_n^2 = \frac{1}{2}(x_n^2 + |x_n^2|)$ is the output signal after negative samples are clipped to zero from x_n^2
- $I_n^2 = \sqrt{2}(s_n^{31} + ... + s_n^{L1})$ is the interference on the second stratum and which is coming from higher level strata

The interference I_n^2 on the second stratum has a symmetric property around $N_2/2$, hence the samples of I_n^2 are related to each other in the following way.

$$I_n^2 = I_{n+N_2/2}^2,\ n = 0,1,2,..., N_2/2 - 1 \tag{3.53}$$

Since I_n^2 has symmetrical property, it does not affect the information recovery of the second stratum. This can be clearly observed by visualizing Y_k^2, which is the frequency domain representation of y_n^2.

$$Y_k^2 = \frac{1}{\sqrt{N_2}} \sum_{n=0}^{N_2-1} y_n^2 e^{-j\frac{2\pi nk}{N_2}}$$

$$= \frac{1}{\sqrt{N_2}} \sum_{n=0}^{N_2-1} (\tilde{x}_n^2 + I_n^2) e^{-j\frac{2\pi nk}{N_2}}$$

$$= \frac{1}{\sqrt{N_2}} \sum_{n=0}^{N_2-1} \tilde{x}_n^2 e^{-j\frac{2\pi nk}{N_2}} + \frac{1}{\sqrt{N_2}} \sum_{n=0}^{N_2/2-1} (I_n^2 e^{-j\frac{2\pi nk}{N_2}} + I_{n+N_2/2}^2 e^{-j\frac{2\pi (n+N_2/2)k}{N_2}})$$

$$= \frac{1}{\sqrt{N_2}} \sum_{n=0}^{N_2-1} \tilde{x}_n^2 e^{-j\frac{2\pi nk}{N_2}} + \frac{1}{\sqrt{N_2}} \sum_{n=0}^{N_2/2-1} (I_n^2 e^{-j\frac{2\pi nk}{N_2}} + I_{n+N_2/2}^2 e^{-j\frac{2\pi nk}{N_2}} e^{-j\pi k})$$

$$= \frac{1}{\sqrt{N_2}} \sum_{n=0}^{N_2-1} \tilde{x}_n^2 e^{-j\frac{2\pi nk}{N_2}} + \frac{1}{\sqrt{N_2}} \sum_{n=0}^{N_2/2-1} (I_n^2 e^{-j\frac{2\pi nk}{N_2}} + I_n^2 e^{-j\frac{2\pi nk}{N_2}} e^{-j\pi k}) \quad (3.54)$$

In the second stratum of STACO-OFDM, it is noted that only odd subcarriers are carrying information bits. For odd k, the $e^{-j\pi k}$ term on the second summation of (3.54) turns to be -1. Hence, the second summation of (3.54) become zero and Y_k^2 becomes:

$$Y_k^2 = \frac{1}{\sqrt{N_2}} \sum_{n=0}^{N_2-1} \tilde{x}_n^2 e^{-j\frac{2\pi nk}{N_2}} \quad (3.55)$$

Therefore, the received symbols at the odd subcarriers of the 2nd stratum only depends on $\tilde{x}_n^2$ and the interference coming from the higher level strata does not affect the information recovery. The clippings of negative samples only reduce the amplitudes of the received symbols by a factor of $1/2$ compared to the transmitted symbols at the same subcarriers. Therefore,

$$Y_k^2 = \frac{1}{2} X_k^2, \; k = 1, 3, 5, ..., N_2 - 1 \quad (3.56)$$

The clipping noise falls on even subcarriers. The clipping noise has no effect on the recovery of the information signal carried by the first stratum since it has been already recovered from even subcarriers. After 2nd stratum information bits are recovered, they are re-modulated and subtracted from x_n^{R1} and x_n^{R2} to remove the contribution of second stratum form the combined signal. The successive demodulation continues for the rest of strata in similar way as it is done in second stratum. Since the interference coming from higher layer stratum has no effect on the information recovery, information bits can be recovered from odd subcarriers successively stratum by stratum. The total information bits carried by all strata are fully recovered in the end of demodulation process at the last stratum. The demodulated information bits from all strata will be converted to a single serial bits stream for delivering to a user.

Latency and receiver complexities are two implementation issues in the realization of STACO-OFDM. Some delay is expected at the receiver due to the successive demodulation process. The issue of latency can be solved by reducing the number of strata and by using high speed digital signal processors in each stratum. The IFFT and FFT modules have dominant contributions for the

complexity of OFDM receiver [17]. The number of IFFT and FFT modules can be reduced by using fewer strata in the STACO-OFDM scheme.

3.2. Spectral efficiency

The spectral efficiency (SE) of the proposed STACO-OFDM scheme with a total of L strata is equal to the summation of spectral efficiencies provided by each stratum. For N available total sub carriers in the system, the spectral efficiency η_1 delivered by the 1st stratum is given by:

$$\eta_1 = \frac{(\log_2 M_1)(\mathrm{N}_1^{\mathrm{info}})}{(\mathrm{N}+\mathrm{N}_{CP})}$$

$$= \frac{(\log_2 M_1)(\mathrm{N}-4)}{4(\mathrm{N}+\mathrm{N}_{CP})} \qquad (3.57)$$

In equation (3.57), N_{CP} is the cyclic prefix added to combat ISI, M_1 is the level of QAM modulation used at the 1st stratum, and N_1^{info} is the number of information carrying subcarriers at the 1st stratum. The factor $\frac{1}{4}$ comes from the fact that 75 percent of the available sub carriers are wasted due to the vacant odd subcarriers and Hermitian symmetry at the 1st stratum. The spectral efficiency η_l of any of l^{th} stratum which utilizes only odd subcarrier is given by:

$$\eta_l = \frac{(\log_2 M_l)(\mathrm{N}_l^{\mathrm{info}})}{(\mathrm{N}+\mathrm{N}_{CP})}$$

$$= \frac{(\log_2 M_l)(\mathrm{N})}{2^{l+1}(\mathrm{N}+\mathrm{N}_{CP})}, l = 2,3,4,...,L \qquad (3.58)$$

Where M_l and N_l^{info} are the level of QAM modulation used and the number of information carrying subcarriers at l^{th} stratum. From (3.57) and (3.58), the spectral efficiency η_T of STACO-OFDM with a total of L strata can be written as:

$$\eta_T = \sum_l \eta_l,\ l = 1,2,...,L$$

$$= \frac{(\log_2 M_1)(\mathrm{N}-4)}{4(\mathrm{N}+\mathrm{N}_{CP})} + \sum_{l=2}^{L} \frac{(\log_2 M_l)(N)}{2^{l+1}(N+N_{CP})} \tag{3.59}$$

The spectral efficiency of the proposed STACO-OFDM is equivalent to the spectral efficiency of DCO-OFDM and two times the spectral efficiency of conventional ACO-OFDM for enough number of used strata.

3.3. Electrical signal power

It is well known that time domain OFDM signal can be treated as Gaussian distribution for enough number of IFFT/FFT points (greater than 64) [65]. If $x(t)$ is real bipolar time domain OFDM signal from the output of IFFT module, it can be defined as Gaussian distribution with standard deviation of σ_x, mean μ_x, and variance σ_x^2 for enough number of available sub carriers. The average electrical power of $x(t)$ is also equal to the variance of the distribution, i.e. σ_x^2. The probability distribution function (PDF), $f_x(m)$ of $x(t)$, is given by [64]:

$$f_x(m) = \frac{1}{\sqrt{2\pi}\sigma_x} e^{-\frac{(m-\mu_x)^2}{2\sigma_x^2}} \tag{3.60}$$

In the case of STACO-OFDM, the bipolar time domain OFDM signal at each stratum has also a property of Gaussian distribution for enough number of IFFT/FFT points. For the system having total strata of L, the time domain signal $x_l(t)$ at l^{th} stratum will follow Gaussian distribution with standard deviation σ_l,mean μ_l, and variance σ_l^2. Flipping of the second half of the time domain signal during the generation of unipolar signal on the first stratum provides equal negative and positive samples which results in zero mean Gaussian distribution. The mean is zero for the rest of strata since the negative and the positive samples are equal in magnitudes due to the symmetry property around $N_l/2$. Therefore, the PDF of the signal at l^{th} stratum is given by:

$$f_l(m) = \frac{1}{\sqrt{2\pi}\sigma_l} e^{-\frac{m^2}{2\sigma_l^2}}, l = 1, 2, 3, ..., L \tag{3.61}$$

The average electrical signal power P_l of the bipolar OFDM signal at l^{th} stratum is also given by [65-66]:

$$P_l = E[x_l^2(t)] = \int_{-\infty}^{\infty} m^2 f_l(m) dm$$

$$= \sigma_l^2, \; l = 1, 2, 3, ..., L \tag{3.62}$$

But after clipping of negative samples, the average electrical signal power at each stratum is reduced by half. Let $x_l^{unp}(t)$ is the unipolar OFDM signal at l^{th} stratum after clipping the negative samples from $x_l(t)$, then the average electrical signal power $P_l^{"}$ of the unipolar OFDM signal $x_l^{unp}(t)$ at l^{th} stratum becomes:

$$P_l^{"} = E[(x_l^{unp}(t))^2] = \int_{0}^{\infty} m^2 f_l(m) dm$$

$$= \frac{\sigma_l^2}{2}, l = 1, 2, 3, ..., L \tag{3.63}$$

But, it is noted that the signal at each stratum are scaled and regenerated to equalize the length of signal at each stratum to the length of the signal at first stratum. Let $x_l^{"}(t)$ is the new scaled unipolar signal at l^{th} stratum, the average electrical signal power $P_l^{'}$ at l^{th} stratum becomes:

$$P_l^{'} = E[(x_l^{"}(t))^2] = \frac{P_l^{"}}{2^{l-1}}$$

$$= \frac{1}{2}\left(\frac{\sigma_l^2}{2^{l-1}}\right)$$

$$= \frac{\sigma_l^2}{2^l}, l = 1, 2, 3, ..., L \tag{3.64}$$

It is also possible to calculate the average electrical signal power of the complete transmitted STACO-OFDM signal after the combination of multiple OFDM frame from all available strata. Let $x_T(t)$ is the complete STACO-OFDM signal which contains both transmitted sub-frames on the two consecutive transmission sessions. The average electrical signal power P_{el}^{avg} of the complete STACO-OFDM symbol can be given by [56, 65,68]:

$$P_{el}^{avg} = E[x_T^2(t)] = E[(\sum_{l=1}^{L} x_l^{"}(t))^2]$$

$$= \sum_{l=1}^{L} E[(x_l^{"}(t))^2] + \sum_{l1=1}^{L} \sum_{\substack{l2=1 \\ l1 \neq l2}}^{L} E[x_{l1}^{"}(t)]E[x_{l2}^{"}(t)]$$

$$= \frac{1}{2}\sum_{l=1}^{L} \frac{\sigma_l^2}{2^{l-1}} + \sum_{l1=1}^{L} \sum_{\substack{l2=1 \\ l1 \neq l2}}^{L} (\frac{\phi(0)\sigma_{l1}}{\sqrt{2^{l1-1}}})(\frac{\phi(0)\sigma_{l2}}{\sqrt{2^{l2-1}}})$$

$$= \frac{1}{2}\sum_{l=1}^{L} \frac{\sigma_l^2}{2^{l-1}} + 2\phi^2(0) \sum_{l1=1}^{L} \sum_{\substack{l2=1 \\ l1 \neq l2}}^{L} \frac{\sigma_{l1}\sigma_{l2}}{\sqrt{2^{l1+l2}}}$$

$$= \frac{1}{2}\sum_{l=1}^{L} \frac{\sigma_l^2}{2^{l-1}} + \frac{1}{\pi} \sum_{l1=1}^{L} \sum_{\substack{l2=1 \\ l1 \neq l2}}^{L} \frac{\sigma_{l1}\sigma_{l2}}{\sqrt{2^{l1+l2}}} \quad (3.65)$$

On (3.65), $\phi(0)$ is the PDF of standard Gaussian distribution and the factors $2^{l-1}, 2^{l1-1}$ and 2^{l2-1} come from the amplitude scaling at each layer to conserve the symbol energy. It is well known that the PDF of standard normal distribution $\phi(\xi)$ at any point ξ can be given by :

$$\phi(\xi) = \frac{1}{\sqrt{2\pi}} e^{-\frac{1}{2}\xi^2} \quad (3.66)$$

Therefore, $\phi(0) = \frac{1}{\sqrt{2\pi}}$ is used on equation (3.65). From (3.64) and (3.65), it can be seen that the combination of OFDM signals from multiple strata increases the average electrical signal power of the entire system. By using (3.64) and (3.65), the electrical power increment α_l due to the

combination of signal from many strata in relative to the average electrical signal power of the signal at l^{th} stratum can be written in a form:

$$\alpha_l = \frac{P_{el}^{avg}}{P_l^{"}}, l = 1, 2, 3, ..., L \tag{3.67}$$

For AWGN channel, the signal to noise ratio (SNR) γ of STACO-OFDM signal based on energy per bit can be calculated as [56-57]:

$$\gamma = \frac{P_{el}^{avg}}{BN_o\eta_T} \tag{3.68}$$

On (3.68), B and N_o are the total employed bandwidth and the AWGN double sided spectral density respectively. Similarly, the SNR γ_l achieved at l^{th} stratum in terms of bit energy is given by the following formula as [56-57]:

$$\gamma_l = \frac{P_l^{"}}{BN_o\eta_l} \tag{3.69}$$

The SNR increment μ_l of the entire scheme compared to the SNR achieved at any l^{th} stratum can be calculated from equations (3.68) and (3.69) as:

$$\mu_l = \frac{\gamma}{\gamma_l} = \alpha_l(\frac{\eta_l}{\eta_T}) \tag{3.70}$$

3.4. Optical signal power

The average transmitted optical signal power of the OFDM signal at each stratum of STACO-OFDM is equal to the mean of the clipped and scaled signal. Therefore the average transmitted optical signal power P_l^o of the OFDM signal at l^{th} stratum can be given either based on the PDF of the distribution at that specific stratum or based on the PDF of standard Gaussian distribution as [56, 69]:

$$P_l^o = E[x_l^{"}] = \frac{1}{\sqrt{2^{l-1}}} \int_0^{\infty} m f_l(m)\, dm$$
$$= \frac{\phi(0)\sigma_l}{\sqrt{2^{l-1}}} \tag{3.71}$$
$$= \frac{\sigma_l}{\sqrt{\pi\ 2^l}}$$

The entire average optical signal power transmitted by the STACO-OFDM scheme is given by the mean of the distribution of the super positioned signal after combining all signals from all strata. The average optical signal power P_o^{avg} of STACO-OFDM scheme can be written in the following form.

$$P_o^{avg} = E[x_T(t)] = E[\sum_{l=1}^{L} x_l^{"}(t)]$$

$$= \phi(0)\sum_{l=1}^{L} \frac{\sigma_l}{\sqrt{2^{l-1}}} = \sum_{l=1}^{L} \frac{\sigma_l}{\sqrt{\pi\ 2^l}} \tag{3.72}$$

3.5. Theoretical BER of STACO-OFDM over AWGN channel

The theoretical BER bound achieved at each stratum of STACO-OFDM over AWGN channel can be derived from the BER formula of real bipolar M-QAM OFDM [52, 70] by accounting the SNR penalty introduced by the clipping and signal combination process. From equal power conserving property of unitary IFFT/FFT in time and frequency domain, the following relationship can be hold at l^{th} stratum of STACO-OFDM scheme [38, 71].

$$E[\sum_{k=0}^{N_l-1} |\, X_k^l\, |^2] = E[\sum_{n=0}^{N_l-1} |\, x_n^l\, |^2 = \sum_{n=0}^{N_l-1} E[|\, x_n^l\, |^2] \tag{3.73}$$

Where,

X_k^l : is the QAM symbol loaded on k^{th} subcarrier of l^{th} stratum of STACO-OFDM

x_n^l : is n^{th} sample of the bipolar time domain signal at l^{th} stratum of STACO-OFDM

Therefore, the average electrical signal power P_l of the bipolar OFDM signal at l^{th} stratum becomes:

$$P_l = \frac{1}{N_l}\sum_{n=0}^{N_l-1} E[|\, x_n^l\,|^2]$$

$$= \frac{2^{l-1}}{N}\sum_{n=0}^{\frac{N}{2^{l-1}}-1} E[|\, x_n^l\,|^2]$$

$$= \sigma_l^2, l = 1,2,3,...,L \qquad (3.74)$$

And from (3.73) and (3.74), we will have:

$$\frac{2^{l-1}}{N} E[\sum_{k=0}^{\frac{N}{2^{l-1}}-1} |\, X_k^l\,|^2] = \frac{2^{l-1}}{N}\sum_{n=0}^{\frac{N}{2^{l-1}}-1} E[|\, x_n^l\,|^2] = P_l \qquad (3.75)$$

If we assume symbols loaded on subcarriers at a particular stratum have average electrical signal power of $E[(X_k^l)^2] = P_l^{smb}$, the equation given on (3.75) can be written in the following form.

$$(\frac{2^{l-1}}{N})(\frac{N}{2^l})P_l^{sym} = P_l \qquad (3.76)$$

Hence, P_l^{sym} can be calculated as:

$$P_l^{smb} = E[|\, X_k^l\,|^2] = 2P_l \qquad (3.77)$$

To calculate the SNR of the QAM symbol transmitted at k^{th} sub carrier in terms of symbol power, the AWGN noise power at k^{th} sub carrier should be known. Let N_o is the single sided noise spectral density of AWGN, the noise variance σ_z^2 at each subcarriers is given by [71]:

$$\sigma_z^2 = E[|\, Z_k\,|^2] = \frac{1}{2}(N_o B_{sc})(\frac{N}{2^{l-1}}),\ l = 1,2,...,L \qquad (3.78)$$

On (3.78), B_{sc} is the bandwidth of sub carrier, $\frac{N}{2^{l-1}}$ term comes from the definition of unitary IFFT/FFT, and the factor $1/2$ appears because the information signal is assumed to be band limited to half of the total subcarriers. The signal to noise ratio SNR_k of the symbol transmitted at k^{th} sub carrier can be calculated from the symbol power and the associated AWGN variance as [8, 71]:

$$SNR_k = \frac{E[|X_k^l|^2]}{\sigma_z^2} = \frac{2^{l+1}P_l}{N_o B_{sc} N},\ l = 1,2,...,L \tag{3.79}$$

Therefore, the energy per bit to noise ratio $\gamma_l^{'}$ of the information transmitted at l^{th} stratum can be given by:

$$\gamma_l^{'} = \frac{SNR_k}{\log_2^{M_l}} = \frac{P_l(2^{l+1})}{N_o B_{sc} N(\log_2^{M_l})} = \frac{P_l(2^{l+1})}{N_o B(\log_2^{M_l})} \tag{3.80}$$

But, if N_{CP} is neglected in equation given on (3.58) for large number of available subcarriers, the formula for the spectral efficiency η_l of l^{th} stratum can be reduced to:

$$\eta_l = \frac{\log_2 M_l}{2^{l+1}},\ l = 1,2,...,L \tag{3.81}$$

Therefore from (3.80) and (3.81), $\gamma_l^{'}$ can be calculated as:

$$\gamma_l^{'} = \frac{P_l}{N_o B \eta_l} \tag{3.82}$$

It is noted that the above formula on (3.82) is based on the consideration of the bipolar OFDM signal at l^{th} stratum before the negative samples are clipped. After transmitting the clipped, the actual received signal on l^{th} stratum at the receiver has an average electrical power of $P_l^{'}$ which is equal to:

$$P_l^{'} = \frac{P_l}{2} = \frac{\sigma_l^2}{2}, l = 1,2,3,...,L \tag{3.83}$$

Where, the factor $1/2$ comes from clipping of negative samples at the transmitter end. Therefore, if Y_k^l is the QAM symbol received at k^{th} subcarrier of l^{th} stratum, then again by using Parseval's theorem:

$$\frac{2^{l-1}}{N}\sum_{k=0}^{\frac{N}{2^{l-1}}-1} E[|Y_k^l|^2] = \frac{P_l}{2} \tag{3.84}$$

Then, the average symbol power received at the subcarrier of l^{th} stratum becomes:

$$E[|Y_k^l|^2] = P_l = 2P_l^{"} \tag{3.85}$$

Then, the SNR on k^{th} subcarrier of l^{th} stratum at the receiver in terms symbol energy, SNR_k^R, can be calculated as:

$$SNR_k^R = \frac{E[|Y_k^l|^2]}{\sigma_z^2} = \frac{2^{l+1}P_l^{"}}{N_o B_{sc} N},\ l = 1,2,...,L \tag{3.86}$$

From (3.81), (3.83), (3.85), and (3.86), the SNR in terms of bit energy to noise ratio γ_l achieved on l^{th} stratum at the receiver is given by:

$$\gamma_l = \frac{SNR_k^R}{\log_2^{M_l}} = \frac{P_l}{2N_o B\eta_l} = \frac{P_l^{'}}{N_o B\eta_l} \tag{3.87}$$

But from equation given on (3.70), μ_l is defined as the ratio of the average electrical power of the unipolar STACO-OFDM signal to the average electrical power of the clipped and scaled unipolar OFDM signal at the l^{th} stratum. By considering P_{el}^{bp} is the average electrical power of the bipolar STACO-OFDM signal, the following relations can be made.

$$P_{el}^{bp} = 2P_{el}^{avg} \tag{3.88}$$

Let $\frac{E_b}{N_o}$ is the energy per bit to noise ratio of the bipolar STACO-OFDM; it can be calculated by using the following formula according to (3.68).

$$\frac{E_b}{N_o} = \frac{P_{el}^{bp}}{BN_0\eta_T} = \frac{2P_{el}^{avg}}{BN_0\eta_T} = 2\gamma \tag{3.89}$$

Then from equation (3.70), the bit energy to noise ratio at l^{th} stratum can be written as:

$$\gamma_l = \frac{\gamma}{\mu_l} = \frac{1}{2\mu_l}(\frac{E_b}{N_o}) \tag{3.90}$$

The theoretical BER bound of the information signal received at l^{th} stratum for AWGN channel can be calculated by using the BER formula of M-QAM modulation [70]. Therefore, BER_l which is the BER performance achieved at l^{th} stratum for AWGN channel can be written as:

$$BER_l \cong BER_{QAM}(M_l, \gamma_l) \cong BER_{QAM}(M_l, \frac{1}{2\mu_l}(\frac{E_b}{N_o}))$$

$$\cong \frac{4}{\log_2 M_l}(1-\frac{1}{\sqrt{M_l}})\sum_{i=1}^{\sqrt{M_l}/2}(Q((2i-1)\sqrt{\frac{3\log_2 M_l E_b}{2\mu_l(M_l-1)N_o}})) \tag{3.91}$$

The theoretical BER bound of the entire STACO-OFDM scheme can be obtained from the BER of each subsequent stratum. But since the number of transmitted bits at each stratum with in one frame duration is different, the percentage of contribution of BER from each stratum is different. Let N_{tot}^b, N_{er}^b and N_l^b are the total number of bits carried by all strata, the total number of erroneous bits received on all strata, and total number of bits transmitted on l^{th} stratum over one entire OFDM frame transmission time respectively. The BER bound BER_{STACO} of the proposed STACO-OFDM scheme over AWGN channel can be given by:

$$BER_{STACO} = \frac{N_{er}^b}{N_{tot}^b} = \frac{\sum_{l=1}^{L}(BER_l\ N_l^b)}{\sum_{l=1}^{L}N_l^b} \tag{3.92}$$

Where $N_l^b = N_l \log_2 M_l$ and N_l is the total number of information carrying sub carriers at l^{th} stratum. The BER formulas on (3.91) and (3.92) do not account for the error propagation from lower stratum to higher stratum during the successive demodulation process.

Similarly, the theoretical BER bound can be given in terms of the optical bit energy to noise ratio. The optical energy per bit to noise ratio (γ^{opt}) of STACO-OFDM can be calculated as follows [57].

$$\gamma^{opt} = \frac{P_o^{avg}}{BN_o\eta_T} \tag{3.93}$$

Then using equations (3.89) and (3.93); the ratio of electrical SNR to optical SNR in terms of bit energy, r, can be calculated as:

$$\left(\frac{E_b}{N_o}\right) \Big/ \gamma^{opt} = \frac{P_{el}^{bp}}{P_{avg}^{o}} = r \tag{3.94}$$

From equation (3.94), we can write the electrical SNR per bit in terms of optical SNR per bit as:

$$\frac{E_b}{N_o} = r\gamma^{opt} \tag{3.95}$$

Then by using equations (3.91) and (3.95), the theoretical BER at l^{th} stratum for AWGN channel can be calculated by the following formula [63, 70].

$$BER_l \cong \frac{4}{\log_2 M_l}\left(1-\frac{1}{\sqrt{M_l}}\right)\sum_{i=1}^{\sqrt{M_l}/2}\left(Q((2i-1)\sqrt{\frac{3\log_2 M_l (r\gamma^{opt})}{2\mu_l (M_l-1)}}\right)) \tag{3.96}$$

Then the overall theoretical BER of STACO-OFDM scheme over AWGN channel can be calculated by using the formula given as equation (3.92).

3.6. STACO-OFDM over multipath channel

In real world scenario, the transmitted information signal experiences multipath fading and dispersion while propagating through optical wireless channel. Multipath fading and dispersion are known for its challenge on the BER performance of wireless communication system during high speed communication [72-74]. Due to the frequency selectivity property of the optical wireless channel, the BER performance of the overall system is degraded due to the effect of sub

carriers experiencing low channel gain. As shown on Fig.3.5, the overall IM/DD and STACO-OFDM based OWC system can be represented by the baseband signal model.

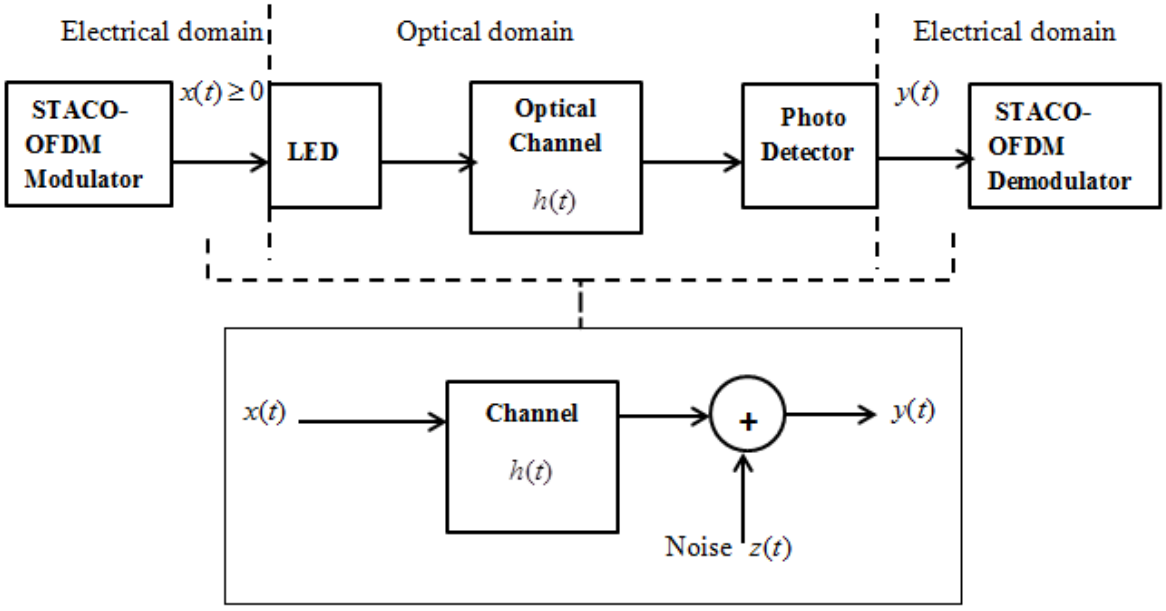

Figure 3. 5: Baseband model of IM/DD based OWC.

On Fig.3.5 $x(t)$, $h(t)$, $z(t)$ and $y(t)$ represent the transmitted electrical signal, the channel impulse response, the zero mean additive Gaussian noise (AWGN), and the received electrical signal respectively. The relationship between the transmitted and the received signal can be written as follows [38]:

$$y(t) = x(t) * h(t) + z(t) \tag{3.97}$$

On (3.97), $x(t)$ needs to be real and positive unipolar to fulfill the requirement of IM/DD system. In this thesis, the diffused optical link configuration is considered and celling bounce model [3, 18, 36, 75] is used to model diffused optical wireless channel configuration environment in indoor scenario. It uses a unit step function to model the CIR of diffused optical channel as follows:

$$h(t) = H(0)\frac{6a^6}{(t+a)^7}u(t) \tag{3.98}$$

Where, $a = 12\sqrt{\frac{11}{13}}D_{rms}$. D_{rms} and $H(0)$ are the channel delay spread introduced by the channel and the DC optical gain of the channel. As explained earlier on section (3.1), one complete STACO-OFDM frame is transmitted in the form of two sub frames in two transmission sessions. The two received time domain STACO-OFDM sub frames, $x_{r1}(t)$ and $x_{r2}(t)$, from the two consecutive transmission sessions can be written as:

$$x_{r1}(t) = x_{t1}(t) * h(t) + z_1(t) \tag{3.99}$$

$$x_{r2}(t) = x_{t2}(t) * h(t) + z_2(t) \tag{3.100}$$

Where, $h(t)$, $x_{t1}(t)$, $x_{t2}(t)$, $z_1(t)$, $z_2(t)$ are the channel impulse response, the analog versions of x_n^{t1}, the analog version of x_n^{t2}, AWGN noise added on the 1st sub frame, AWGN noise added on the 2nd sub frame respectively. As explained on section (3.1), the demodulation process is performed by adopting successive demodulation stratum by stratum. The 1st stratum information recovery is begun by subtracting $x_{r2}(t)$ from $x_{r1}(t)$ and padding $\frac{N}{2}$ zeros at the end of the output signal after subtraction operation. Since the received signal is changed in to its discrete form at the receiver, using discrete time representation as:

$$x_n^{r1} = x_n^{t1} * h_n + z_n^1 \tag{3.101}$$

$$x_n^{r2} = x_n^{t2} * h_n + z_n^2 \tag{3.102}$$

Where, z_n^{sf1} and z_n^{sf2} are the discrete noise signal added on the 1st and the 2nd sub frames respectively. To recover the 1st stratum information, x_n^{r2} is subtracted from x_n^{r1} and the obtained output signal y_n^1 becomes:

$$y_n^1 = x_n^{r1} - x_n^{r2}$$

$$= (x_n^{t1} - x_n^{t2}) * h_n + (z_n^{sf1} - z_n^{sf2})$$

$$= (x_n^{11} - x_n^{12}) * h_n + z_n$$

$$= x_n^{df} * h_n + z_n \tag{3.103}$$

On the above equation given on (3.103) z_n is the AWGN noise with single sided noise spectral density N_0 which is added in one complete OFDM frame and x_n^{df} is bipolar signal and exactly equal to the 1st half of the bipolar time domain signal at the first stratum (x_n^1) given on (3.6). In addition, the length of x_n^{df} is equal to $N/2 + N_{CP}$ and the length of h_n is equal to L where $N_{CP} \geq L$; hence, h_n is equal to zero for $n > L$. Therefore, the vector $[h_n]$ of channel impulse response can be written in vector form as:

$$[h_n] = [\underbrace{h_0 \; h_1 \; h_2 ... h_{L-1} \; 0 \; 0 \; 0 ... 0}_{\frac{N}{2} \text{ samples}}] \tag{3.104}$$

But we can write equation (3.103) by using summation as [76]:

$$y_n^1 = \sum_{l=0}^{L-1} h_l x_{n-l}^{df} + z_n, \; n = 0,1,2,...,N/2 + N_{CP} \tag{3.105}$$

The matrix representation for the above equation (3.105) becomes [76-77]:

$$[y^1] = [h][x^{df}] + [z] \tag{3.106}$$

Where $[y^1]$, $[x^{df}]$ and $[z]$ are $(N/2 + N_{CP})$ x 1 matrices while $[h]$ is $(N/2 + N_{CP})$ x $(N/2 + N_{CP})$ channel matrix. To recover the information carried by the 1st stratum, the first N_{CP} long samples should be removed from $[y^1]$ and $N/2$ zeros should be padded at the end of the signal. After the zero padding, $[y^1]$, $[x^{df}]$ and $[z]$ become N x 1 matrices with last $N/2$ samples are zero. Similarly $[h]$ becomes an N x N matrix. But $[x^{df}]$ is exactly similar to $[x^1] = [x_n^1]^T$ in which its last $N/2$ samples are clipped to zero. According to [11], the clipped signal can be given by:

$$[x^{df}] = R[x^1] + [d] \tag{3.107}$$

Where, R is a constant which is equal to 0.5 and $[d]$ is the clipping noise which is N x 1 matrix. But we can write $[x^1]$ in terms of IFFT matrix F^{-1} and frequency domain QAM symbol vector $[X^1]=[X_k^1]^T$. Therefore, the equation on (3.107) can be re-written as [77]:

$$[x^{df}]=R[F^{-1}][X^1]+[d] \tag{3.108}$$

Substituting equation (3.108) result on equation (3.106), the result becomes:

$$[y^1]=R[h][F^{-1}][X^1]+[d]+[z] \tag{3.109}$$

Taking FFT operation on the above signal given on (3.109) by using FFT matrix F [77]:

$$F[y^1]=R[F^{-1}][h][F][X^1]+F[d]+F[z]$$

$$=R[C][X^1]+F[d]+F[z] \tag{3.110}$$

Where, $[C]=[F^{-1}][h][F]$ is a diagonal matrix whose diagonal is equals to the Fourier transform of the channel impulse response $h[n]$ as:

$$H_k=F\{h_n\}, k, n=0,1,2,...,N-1 \tag{3.111}$$

The received frequency domain signal at each sub carriers on the 1st stratum becomes:

$$Y_k^1=RH_kX_k^1+D_k+Z_k, k=0,1,2,...,N-1 \tag{3.112}$$

Introducing zero forcing equalization for reducing the channel effect, then [36-37]:

$$\frac{Y_k^1}{RH_k}=X_k^1+\frac{D_k}{RH_k}+\frac{Z_k}{RH_k}, k=0,1,...,N-1 \tag{3.113}$$

On the above equation, it is also noted that the clipping noise only affect the odd subcarriers [11, 78]. Since the even subcarriers are not affected by the clipping noise, we can write the received symbols on the even sub carriers at the 1st stratum as:

$$\frac{Y_k^1}{RH_k}=X_k^1+\frac{Z_k}{RH_k}, k=2,4,6,...,N-2 \tag{3.114}$$

The information bits carried by the 1st stratum can be recovered by demodulating the above symbols received on even sub carriers. To recover the information carried by 2nd stratum, the recovered bits at the 1st stratum should be re-modulated again and processed in the same way as it was done at the transmitter. The re-modulated time domain sub frames are then affected by the CIR of the channel and subtracted from $x_{r1}(t)$ and $x_{r2}(t)$ to remove the contribution of the 1st stratum. By following similar mathematical analysis as it was done for the 1st stratum, the equalized QAM symbols received on odd subcarriers of the 2nd stratum will be in the following form:

$$\frac{Y_k^2}{RH_k} = X_k^2 + \frac{Z_k}{RH_k}, k = 1,3,5,...,\tfrac{N}{2}-1 \tag{3.115}$$

Then by demodulating the above resulted symbols after subtraction by conventional ACO-OFDM demodulator, it is possible to recover the information signal from odd subcarriers. Similarly, by re-modulating the bits recovered at 2nd stratum and subtracting it from the received signal, the equalized QAM symbols received on the 3rd stratum can be written as:

$$\frac{Y_k^3}{RH_k} = X_k^3 + \frac{Z_k}{RH_k}, k = 1,3,,...,\tfrac{N}{4}-1 \tag{3.116}$$

Then the bits stream carried by the 3rd stratum can be recovered by demodulating the above symbols using QAM demodulator. The bits carried by the other strata can also be recovered by using the same strategy stratum by stratum.

3.7. Theoretical BER of STACO-OFDM over multipath channel

3.7.1. BER in terms of electrical SNR

After passing through multipath optical channel, the average achieved SNR per bit at k^{th} sub carrier of the entire STACO-OFDM system is given by [19, 56-57]:

$$\gamma_k = \frac{|H_k|^2 P_{el}^{avg}}{BN_o\eta_T} \tag{3.117}$$

But the SNR per bit at k^{th} sub carrier has different values at different strata; the SNR per bit at k^{th} sub carrier of l^{th} stratum can be given by:

$$\gamma_{l,k} = \frac{|H_k|^2 P_l^{'}}{BN_o\eta_l} \tag{3.118}$$

The theoretical BER at the k^{th} sub carrier of l^{th} stratum can be given by the BER formula of M-QAM modulation as [70]:

$$BER_{l,k} = \frac{4}{\log_2 M_l}(1-\frac{1}{\sqrt{M_l}})\sum_{i=1}^{\sqrt{M_l}/2} Q((2i-1)\sqrt{\frac{3\log_2 M_l\ \gamma_{l,k}}{M_l-1}}\ ) \tag{3.119}$$

From the above equation, the overall BER at l^{th} stratum can be calculated as:

$$BER_l = \frac{1}{N_l^{\text{info}}}\sum_{k=1}^{\frac{N_l}{2}-1} BER_{l,k},\ l=1,2,3,...,L \tag{3.120}$$

Where, N_l^{info} is the number of information carrying subcarriers at l^{th} stratum. For the 1st stratum (i.e., $l=1$), k is even as $k=2,4,6,...,\frac{N}{2}-2$ since only even sub carriers are carrying information. For the rest of the strata k is odd as $k=1,3,5,...\frac{N_l}{2}-1$.

The theoretical BER bound of STACO-OFDM on multipath channel can be derived from the theoretical BER bound achieved at the available strata. Let S and N_l^{bits} stand for the total number of used strata and the total number of bits transmitted at l^{th} stratum in one complete OFDM frame transmission respectively, the BER of the overall STACO-OFDM system is then given by [11]:

$$BER_{tot} = \frac{\text{total No of erroneous bits per STACO-OFDM frame}}{\text{total No of transmitted bits per STACO-OFDM frame}}$$

$$= \frac{\sum_{l=1}^{L}(BER_l\ N_l^{bits})}{\sum_{s=1}^{L} N_l^{bits}} \tag{3.121}$$

3.7.2. BER in terms of optical power of transmitted signal

As pointed out before, Parseval's theorem can be applied at each stratum since unitary IFFT/FFT is used on each stratum [38, 50, 71, 79-80]. Therefore, at any l^{th} stratum the average electrical of the bipolar OFDM signal is equal to the signal variance σ_l^2 and can be given by the following formula.

$$\frac{2^{l-1}}{N}\sum_{n=0}^{\frac{N}{2^{l-1}}-1} E[|x_n^l|^2] = \frac{2^{l-1}}{N} E[\sum_{k=0}^{\frac{N}{2^{l-1}}-1} |X_k^l|^2] = \sigma_l^2, \quad l = 1,2,3,...,L \tag{3.122}$$

Then after clipping the negative samples of the signal the average electrical power $P_l^{'}$ of the unipolar signal at the l^{th} stratum will equal to the average symbol power of the received symbol Y_k^l as:

$$P_l^{'} = \frac{2^{l-1}}{N} E[\sum_{\substack{k=2,4|_{l=1} \\ k=1,3|_{l\neq 1}}}^{\substack{\frac{N}{2^{l-1}}-2|_{l=1} \\ \frac{N}{2^{l-1}}-1|_{l\neq 1}}} |Y_k^l|^2] = \frac{\sigma_l^2}{2}, l = 1,2,3,...,L \tag{3.123}$$

Then by using equations given on equations (3.71) and (3.123), $P_l^{'}$ can be written in terms of P_l^o which is the average optical power a l^{th} stratum as:

$$P_l^{'} = \pi (P_l^o)^2 (2^{l-1}),\ l = 1,2,3,....,L \tag{3.124}$$

Then from equation (3.123) and (3.124), equality relation can be given as:

$$\frac{2^{l-1}}{N} E[\sum_{\substack{k=2,4|_{l=1} \\ k=1,3|_{l\neq 1}}}^{\substack{\frac{N}{2^{l-1}}-2|_{l=1} \\ \frac{N}{2^{l-1}}-1|_{l\neq 1}}} |Y_k^l|^2] = \pi (P_l^o)^2 (2^{l-1}), l = 1,2,3,...,L \tag{3.125}$$

If we assume all the QAM symbols loaded on subcarriers at l^{th} stratum have equal average electrical signal power, we will have:

$$E[|\,\mathrm{Y}_k^l\,|^2] = 2^l \pi (P_l^o)^2 \tag{3.126}$$

But, since each symbol received at k^{th} subcarrier is attenuated by the channel gain $|H_k|$, the average electrical signal power of the attenuated symbol $\bar{Y}_k^l$ by the channel gain at k^{th} subcarrier of l^{th} stratum is given by:

$$E[|\,\bar{\mathrm{Y}}_k^l\,|^2] = 2^l \pi (P_l^o)^2 \,|H_k|^2 \tag{3.127}$$

To calculate the SNR of the QAM symbol received at k^{th} subcarrier, the AWGN noise power at k^{th} subcarrier should be known. Let N_o is the single sided noise spectral density; the noise variance σ_z^2 at each subcarriers is given by [71]:

$$\sigma_z^2 = E[|\,Z_k\,|^2] = (\frac{N_o B_{sc}}{2})(\frac{N}{2^{l-1}}), l = 1,2,3,...,L \tag{3.128}$$

Where, B_{sc} is the bandwidth of sub carrier and $\frac{N}{2^{l-1}}$ term comes from the definition of unitary IFFT/FFT. The SNR of the symbol received at k^{th} sub carrier is then given by [8, 71]:

$$SNR_k = \frac{E[|\,\mathrm{Y}_k^{sl}\,|^2]}{\sigma_z^2} = \frac{2^{2l}\pi (P_l^o)^2\,|H_k|^2}{N_o B_{sc} N}, l = 1,2,3,...,L \tag{3.129}$$

But for more accurate optical power efficiency performance assessment, writing SNR_k in terms of the total average optical power of the combined signal is vital. The average optical power P_o^{avg} of the combined signal $x_T(t)$ has been previously given on equation (3.72) [56, 68]. The optical power penalty α_l^o of the combined system with respect to the optical power at l^{th} stratum can be written based on equations (3.71) and (3.72) as:

$$\alpha_l^o = \frac{(P_o^{avg})^2}{(P_l^o)^2}, l = 1,2,3,...,L \tag{3.130}$$

Therefore, SNR_k can be written in terms of the overall transmitted optical power of STACO-OFDM system as:

$$SNR_k = \frac{2^{2l}\pi(P_o^{avg})^2 \mid H_k \mid^2}{N_o B_{sc} N \alpha_l^o}, l = 1,2,3,...,L \tag{3.131}$$

The SNR per bit $\gamma_{s,k}$ can also be calculated as:

$$\gamma_{l,k} = \frac{SNR_{l,k}}{\log_2 M_l} = \frac{2^{2l}\pi(P_o^{avg})^2 \mid H_k \mid^2}{N_o B_{sc} N \alpha_l^o (\log_2 M_l)}, l = 1,2,3,...,L \tag{3.132}$$

Then the BER at k^{th} sub carrier of l^{th} stratum become [70];

$$BER_{l,k} = \frac{4}{\log_2 M_l}(1 - \frac{1}{\sqrt{M_l}}) \sum_{i=1}^{\sqrt{M_l}/2} Q((2i-1)\sqrt{\frac{3(2^{2l})\pi(P_o^{avg})^2 \mid H_k \mid^2}{(M_l - 1)(B_{sc} N_o N \alpha_l^o)}}) \tag{3.133}$$

The total theoretical BER bound of the l^{th} stratum is then calculated by using the same formula as equation (3.120).

$$BER_l = \frac{1}{N_l^{\text{info}}} \sum_{k=1}^{\frac{N_l}{2}-1} BER_{l,k}, l = 1,2,3,...,L \tag{3.134}$$

The overall theoretical BER bound of STACO-ODM can be calculated by using similar formula defined as equation (3.121).

3.8. Adaptive optical OFDM for spectral efficiency enhancement

Optical wireless channel is characterized by frequency selective channel dynamics due to the availability of multipath fading and dispersion. The multipath channel effects on different subcarriers are different in magnitude during multicarrier communication. Subcarrier based rate adaptive optical OFDM modulation is a promising solution in enhancing the performance of indoor OWC in diffused optical wireless channel environment. Frequency selective property of the channel in frequency domain is the manifestation of time dispersive property of the channel in time domain which is known to introduce ISI in the system. Since STACO-OFDM modulation comprises ACO-OFDM modulator at each layer, investigating the performance of adaptive bit loading in ACO-OFDM is vital. Therefore, this section is dedicated to investigate the potential of

adaptive ACO-OFDM to enhance the spectral efficiency of indoor OWC in multipath channel environment. The system model of adaptive ACO-OFDM is presented on Fig.3.6. It is assumed that the channel information state is completely known by the transmitter and the receiver. The bit loading is done based on the current status of the channel gain of sub carriers. Since the channel state information is known by the transmitter and the receiver, it is possible to calculate the amount of the SNR to be achieved at each subcarrier for the current channel condition.

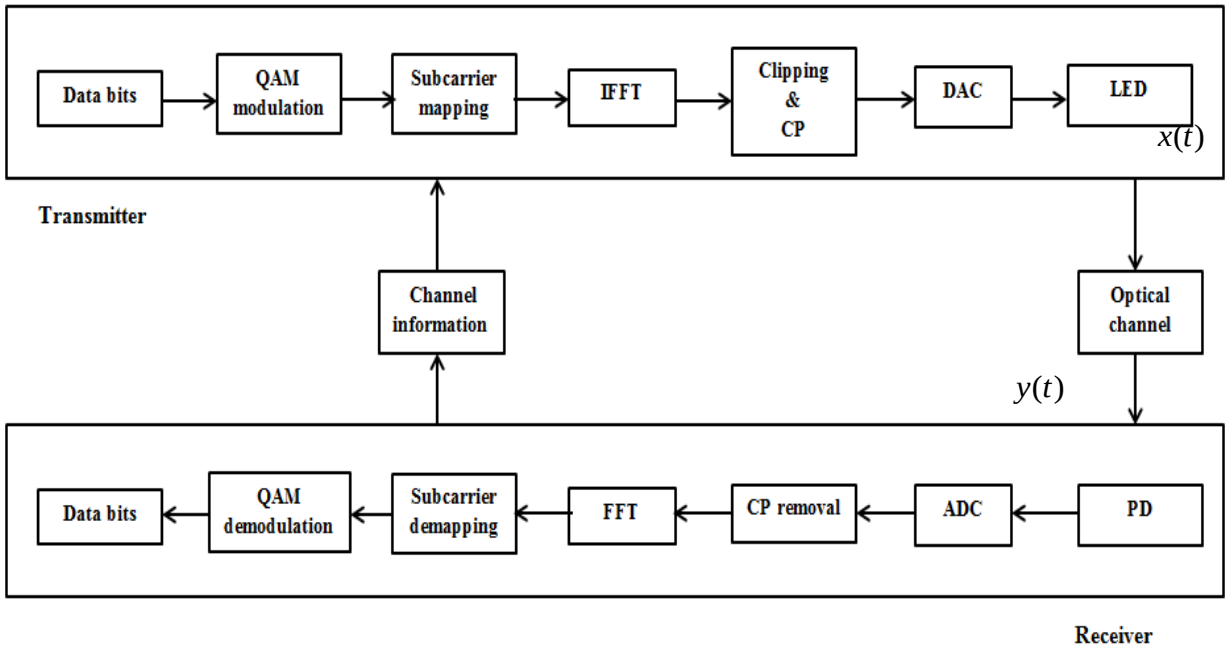

Figure 3. 6: Block diagram of rate adaptive ACO-OFDM.

γ_k^{ACO} of ACO-OFDM scheme at k^{th} subcarrier in terms of bit energy can be given by [17, 19]:

$$\gamma_k^{ACO} = \frac{1}{2}\left(\frac{|H_k|^2 E_b}{N_o}\right) \tag{3.135}$$

In equation (3.135), H_k is the channel gain of the k^{th} subcarrier whereas N_o is the AWGN spectral density. The factor $1/2$ on equation (3.135) comes from the clipping of negative samples at the transmitter. Target BER is set to avoid outage of the system. In this work, the target BER is set to be 10^{-3} which is equal to the minimum allowable BER value for voice communication. Using the BER formula of M-QAM modulation, the amount of required SNR γ to achieve the

target BER can be calculated for different level M-QAM modulations. The BER formula of M-QAM modulations is given as [70]:

$$BER = \frac{4}{\log_2 M}(1-\frac{1}{\sqrt{M}})\sum_{i=1}^{\sqrt{M_i}/2} Q((2i-1)\sqrt{\frac{3\log_2 M\ \gamma}{(M-1)}}\ )) \tag{3.136}$$

In this work, five different M-QAM modulations are considered for rate adaption. Those modulation formats are represented by $M_i - QAM$ as:

$$M_i = 2^{i+1},\ 1 \le i \le 4 \tag{3.137}$$

Therefore, the available modulation formats for rate adaption become 4-QAM, 8-QAM, 16-QAM, and 32-QAM, and the required SNR values γ_i to achieve a BER of 10^{-3} for those modulations can be represented as $\gamma_1, \gamma_2, \gamma_3, \gamma_4$ respectively. Since higher level modulations are not energy efficient, it is known that the following relation is true.

$$\gamma_1 < \gamma_2 < \gamma_3 < \gamma_4 \tag{3.138}$$

Then for each k^{th} sub carrier, the calculated SNR γ_k^{ACO} based on the current channel condition is compared with $\gamma_1, \gamma_2, \gamma_3, \gamma_4$. For certain $M_i\big|_{i\neq 0}$ to be chosen for adaption, the condition $\gamma_i \le \gamma_k^{ACO} < \gamma_{i+1}$ should be fulfilled. If γ_k^{ACO} is less than all required SNR ($\gamma_1, \gamma_2, \gamma_3, \gamma_4$), then no information is transmitted in that particular sub carrier. The rate adaption is done by the following algorithm using MATLAB code segment:

$M = [0\ 4\ 8\ 16\ 32]$ `% level of QAM MODULATION for rate adaption`

$\gamma_i = [\gamma_1\ \gamma_2\ \gamma_3\ \gamma_4]$ `% required SNR for target BER for those QAM mods`

$\gamma_k^{ACO} = [\gamma_1^{ACO}\ \gamma_3^{ACO}\ \gamma_5^{ACO} \ldots \gamma_{\frac{N}{2}-1}^{ACO}]$ `% achieved SNR on subcarriers using CIS`

for $i = 1 : length(\gamma_k^{ACO})$

snr_subc $= \gamma_k^{ACO}(i)$

$A = \gamma_i(\gamma_i \ge$ snr_subc$)$

$B = length(\gamma_i) - length(A)$

$D = M(B+1)$

$M_k(i) = D$ % chosen level of QAM on sub carrier for current CIS

end

Based on the chosen M_k on each information carrying odd sub carriers, different M_k-QAM symbols are loaded to those sub carriers.

3.8.1. Spectral efficiency of adaptive ACO-OFDM

Based on the obtained M_k for each sub carriers, it is possible to find the number of subcarriers N_{info} on which the information signal is transmitted, hence, N_{info} is the number of sub carriers having $M_k > 0$ after level of modulations are chosen for rate adaption at each odd sub carrier. The spectral efficiency Se_{ACO}^{ADP} provided by the adaptive ACO-OFDM can be calculated as [63]:

$$Se_{ACO}^{ADP} = \frac{1}{N + N_{CP}} \sum_{k=1,3,\ldots}^{N_{\text{info}}} \log_2 M_k \tag{3.139}$$

Where N_{CP} is the length of the cyclic prefix used.

Chapter 4

Results and Discussions

Simulations were performed to analyze and evaluate the spectral and energy efficiencies of the proposed STACO-OFDM in different channel environments, i.e. AWGN and multipath channels. The performances of STACO-OFDM are also compared with the major existing conventional state-of-the-art optical OFDM schemes (ACO-OFDM & DCO-OFDM) for IM/DD based OWC. The simulations are done for both AWGN and multipath channel environments to evaluate the performances in different optical channel scenarios. For the evaluation of energy efficiency, systems with equal spectral efficiencies (SE) of 1.5, 2, and 2.5 b/s/Hz are considered for all schemes (STACO/ACO/DCO-OFDM) for the sake of fair comparisons. The bit error rate (BER) is simulated for different amount of bit energy to noise ratio (E_b/N_o) to analyze the required amount of bit energy to achieve specific amount of BER while offering those given spectral efficiency values.

Moreover, the potential of adaptive OFDM to improve the spectral efficiency (SE) of OWC system is evaluated using simulations. In this work, frequency selective rate adaption capability is implemented on ACO-OFDM scheme since ACO-OFDM is the building component of STACO-OFDM at each stratum. The spectral efficiency of rate adaptive ACO-OFDM is also compared with the spectral efficiency offered by ACO-OFDM with fixed modulation schemes for a system having a target BER of 10^{-3} with no outage.

4.1. Spectral efficiency

Due to the limited modulation bandwidth of the LED in the transmitter, modulation schemes need to be spectrally efficient to realize high speed indoor OWC. Among previously proposed schemes, DCO-OFDM can offer good spectral efficiency but its energy inefficiency degrades its attractiveness for power constrained high speed OWC. On the other hand, ACO-OFDM scheme is attractive in terms of energy efficiency while its spectral efficiency (SE) is poor. Therefore, in

response to those challenges and issues on those major existing OFDM schemes, the proposed STACO-OFDM scheme in this thesis follows an optimized design strategy which is intended to deliver better spectral and energy efficiencies at the same time. Fig 4.1 shows the spectral efficiency of STACO/ACO/DCO-OFDM transmission schemes for 16-QAM modulation based on equations (2.21, 2.39, and 3.59). The effect of cyclic prefix is ignored since the number cyclic prefix is negligible in comparison to the number of total sub carriers.

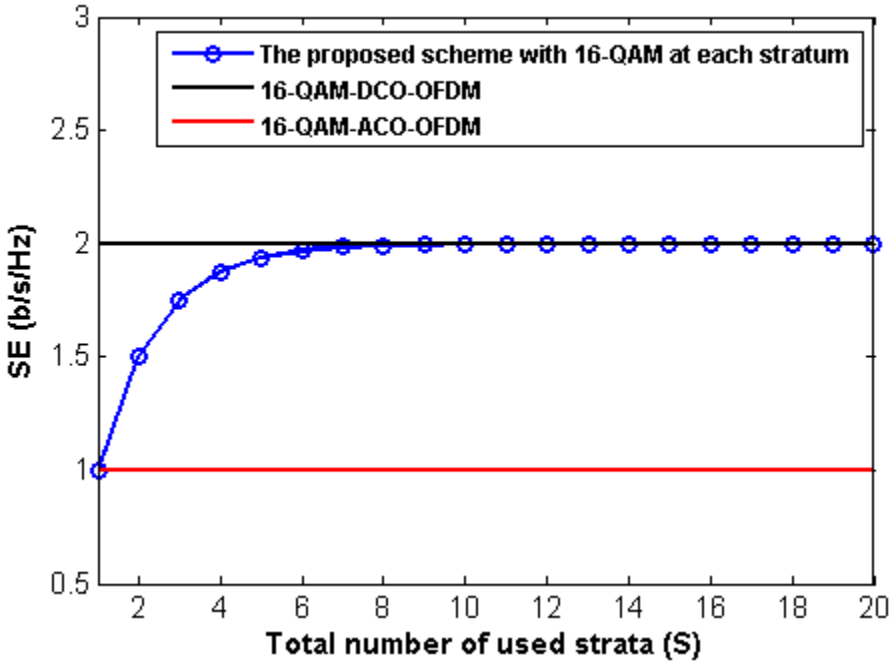

Figure 4. 1: Spectral efficiency of 16-QAM ACO-OFDM, 16-QAM DCO-OFDM, and 16-QAM STACO-OFDM.

In the case of STACO-OFDM, 16-QAM modulation is used at each stratum. As presented on Fig 4.1, ACO-OFDM offers a spectral efficiency (SE) of $1\ b/s/Hz$ with 16-QAM modulation while DCO-OFDM offers a spectral efficiency (SE) equals to $2\ b/s/Hz$ for same QAM modulation used. The spectral efficiency of STACO-OFDM increases with the number of used strata in the system. The increment of the spectral efficiency is becoming negligible and saturates at certain point when the number of strata becomes large enough in number. For about 7 used strata in the system, STACO-OFDM scheme has offered equal spectral efficiency ($\approx 2\ b/s/Hz$) as DCO-OFDM and better spectral efficiency compared to ACO-OFDM. To reduce the cost of the system, reducing the number of strata in STACO-OFDM is very important. Therefore, the number of strata

can be reduced by using different level M-QAM modulation at each stratum instead of fixed M-QAM modulation for all strata. Fig 4.2 shows the offered spectral efficiency when only three strata are used in STACO-OFDM with 32-QAM, 16-QAM, and 16-QAM modulations are used on the 1st , 2nd , and 3rd stratum respectively.

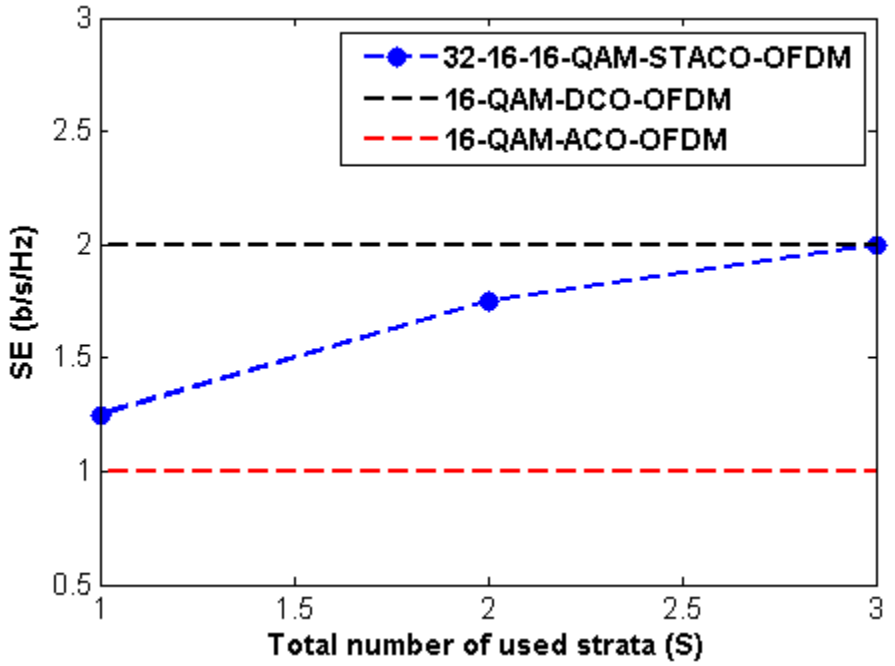

Figure 4. 2: Spectral efficiency of 16-QAM ACO-OFDM, 16-QAM DCO-OFDM, and 32-16-16-QAM STACO-OFDM.

The result on figure 4.2 reveals that 32-16-16-QAM –STACO-OFDM offers the same spectral efficiency as 16-QAM DCO-OFDM and better spectral efficiency compared to 16-QAM ACO-OFDM. But when choosing different QAM modulation at different strata, the trade off on the energy efficiency should be considered and should be minimized as much as possible. Hence, optimal size of M-QAM modulation should be chosen and used on each stratum to improve the energy efficiency of STACO-OFDM scheme.

4.2. Energy efficiency of STACO-OFDM over AWGN channel

In this section, the energy efficiency of STACO-OFDM over linear AWGN channel is evaluated using results from theoretical analysis and numerical simulations. The energy efficiency is analyzed by simulating the BER performance in terms of both RF signal and optical signal SNR per bit. The BER performance from the numerical simulation has shown a good agreement with the theoretical BER bound from theoretical analysis. The BER performance of the proposed STACO-OFDM is also compared with the BER performance of ACO-OFDM and DCO-OFDM offering similar spectral efficiencies. In this work, three spectral efficiency values (1.5, 2, 2.5 b/s/Hz) are considered for comparisons and for tracking the behaviour of STACO-OFDM and existing models while the transmission data rate is increased. The selected spectral efficiency values are also used for simulation of eu-OFDM in published literature [57]. Therefore, those values are selected for the sake of consistency for the performance comparisons of eU-OFDM and STACO-OFDM.

4.2.1. Electrical energy efficiency

The BER performance in terms of electrical SNR per bit (E_b/N_o) is used as a measurement for evaluating the electrical energy efficiency of STACO-OFDM in AWGN channel environment. The noise power, N_o is considered to be single sided AWGN spectral density in the simulation. The STACO-OFDM transmission scheme having three strata is considered with different optimal combination of M-QAM modulation at each stratum. Theoretical BER and the simulated BER of STACO-OFDM have shown good agreement with a very little variation since the propagated error from stratum to stratum during successive demodulation is not included in the theoretical BER bound. Energy efficiency performances are presented for a BER value of 10^{-5} since reliable communication can be achieved with most of forward error check (FEC) codes for BER values below 10^{-4} [57]. To observe the deviation introduced by the propagated errors, the BER performance of three strata STACO-OFDM with 16-QAM modulation at each stratum is simulated as shown in Fig. 4.3.

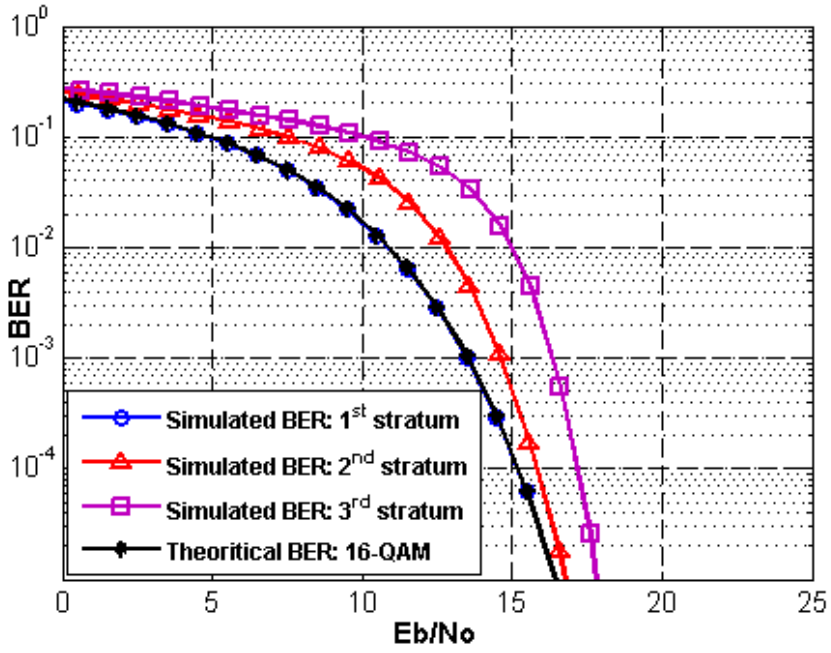

Figure 4. 3: BER of each stratum of 16-16-16-QAM STACO-OFDM in terms of effective SNR of each stratum.

As shown in Fig. 4.3, the simulated BER of the first stratum is equal to the theoretical BER bound since the only source of error is AWGN noise on this particular tier. On the other hand, the simulated BER on second and third strata have shown some deviations from the theoretical BER bounds since errors are propagated from first stratum to second stratum and from second stratum to third stratum during successive demodulation. Apart from the BER caused by AWGN, the simulated BER includes the bit errors which propagate from stratum to stratum and the theoretical BER bound accounts for only the BER introduced by AWGN. In STACO-OFDM, higher level strata are more affected by the propagated errors since errors are accumulated and transferred from all lower level strata. The result shown in Fig. 4.3 also confirms that the theoretical BER and the simulated BER of higher level strata are approaching to each other as the SNR of the transmitted signal is increased. As the SNR increased, the actual BER experienced at each stratum will be reduced and this will reduce the error propagating from one particular stratum to the next immediate stratum too.

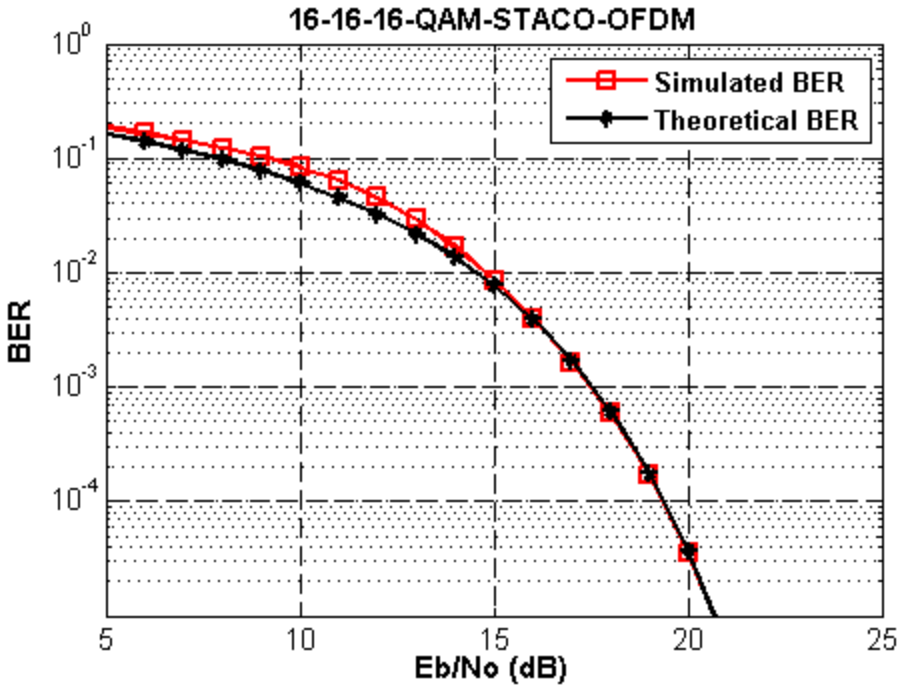

Figure 4. 4: Theoretical and simulated BER of 16-16-16-QAM STACO-OFDM.

The result presented on Fig. 4.4 shows the good agreement of the overall theoretical BER bound of STACO-OFDM given on equation (59) with the simulated BER from numerical simulations. The noise propagating from stratum to stratum becomes negligible as the SNR of the system is increased. The difference between the simulated and the theoretical BER is almost negligible for SNR values beyond 15 dB for 16-16-16-QAM STACO-OFDM scheme. Therefore, the slight deviation between the theoretical and simulated BER is also becoming negligible as the SNR is increasing.

The selection of M-QAM modulation format at each stratum of STACO-OFDM needs to be done carefully to achieve better energy efficiency. For example, 32-16-16-QAM-STACO-OFDM and 16-16-256-QAM-STACO-OFDM schemes offer equal spectral efficiency (SE) of 2b/s/Hz. The total BER of 32-16-16-QAM-STACO-OFDM and the BER at each stratum are given in Fig. 4.5 and Fig.4.6 respectively. As shown in Fig 4.5, the energy efficiency of 32-16-16-QAM-STACO-OFDM is better than the other counterpart. Avoiding of using non energy efficient higher level M-QAM modulation in STACO-OFDM scheme is very important to achieve better energy efficiency performance.

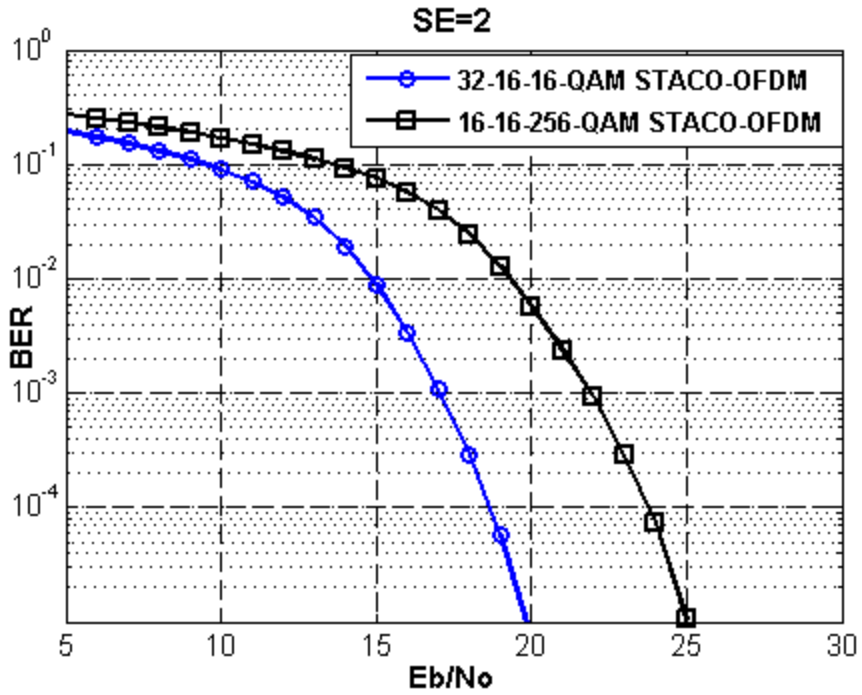

Figure 4.5: BER performance of 32-16-16-QAM STACO-OFDM and 16-16-256-QAM STACO-OFDM.

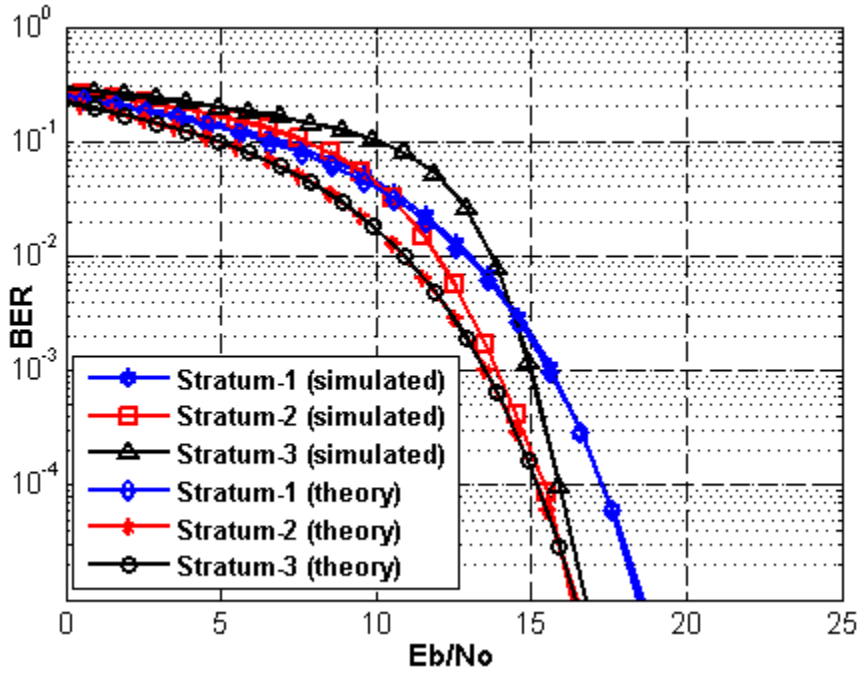

Figure 4. 6: BER of each stratum of 32-16-16-QAM STACO-OFDM in terms of effective SNR of each stratum.

As presented on Fig 4.5, 32-16-16-QAM-STACO-OFDM offers $5\ dB$ energy saving compared to 16-16-256-QAM-STACO-OFDM transmission schemes to achieve a BER of 10^{-5}. Therefore, 32-16-16-QAM is the optimal constellation size at the 1st, 2nd, and 3rd stratum to achieve better energy efficiency for spectral efficiency (SE) of 2 b/s/Hz. The scaling factors and the M-QAM combination used in the proposed STACO-OFDM are optimal and consistent with previous literature [57]. The BER performance of the 1st stratum is exactly equal to the theoretical BER bound as expected and the other strata experience some deviations as shown in Fig. 4.6.

After choosing the optimal constellation size at each stratum of STACO-OFDM, the electrical energy efficiency performance of STACO-OFDM is compared with the performance of ACO-OFDM and DCO-OFDM for three different spectral efficiencies. The optimal combinations of constellation size used for eU-OFDM on [57] are also adopted for STACO-OFDM in this work. The performance of ACO-OFDM and DCO-OFDM used for comparisons in this work are consistent with the simulation results reported on published literatures [17, 19, 56-57, 81].

Fig. 4.7, 4.8, and 4.9 show the comparisons of BER performance as a function of electrical SNR per bit in dB for the proposed STACO-OFDM scheme, DCO-OFDM, and ACO-OFDM for similar spectral efficiencies (SE) of 1.5, 2, and 2.5 bits/s/Hz respectively. Similar spectral efficiencies are chosen for all schemes for the purpose of keeping the same data rate while comparing their energy efficiency performances. For the considered spectral efficiency values, the level of QAM modulation for DCO-OFDM and ACO-OFDM are obtained from equations (2.21) and (2.39) respectively by ignoring the length of cyclic prefix.

For spectral efficiency of 1.5 bits/s/Hz, 16-8-4-QAM modulations are used for the proposed STACO-OFDM scheme, meaning that, 16-QAM at 1st stratum, 8-QAM at 2nd stratum, and 4-QAM at 3rd stratum are used. 64-QAM ACO-OFDM and 8-QAM DCO-OFDM with 7 dB DC bias are used for comparisons for systems delivering spectral efficiency of 1.5 bits/s/Hz. As shown on Fig. 4.7, the BER performance of STACO-OFDM scheme shows better performance with around 3 dB electrical energy saving compared to ACO-OFDM and 3.9 dB electrical energy savings compared to DCO-OFDM to achieve a BER of 10^{-5} for SE of 1.5 bits/s/Hz.

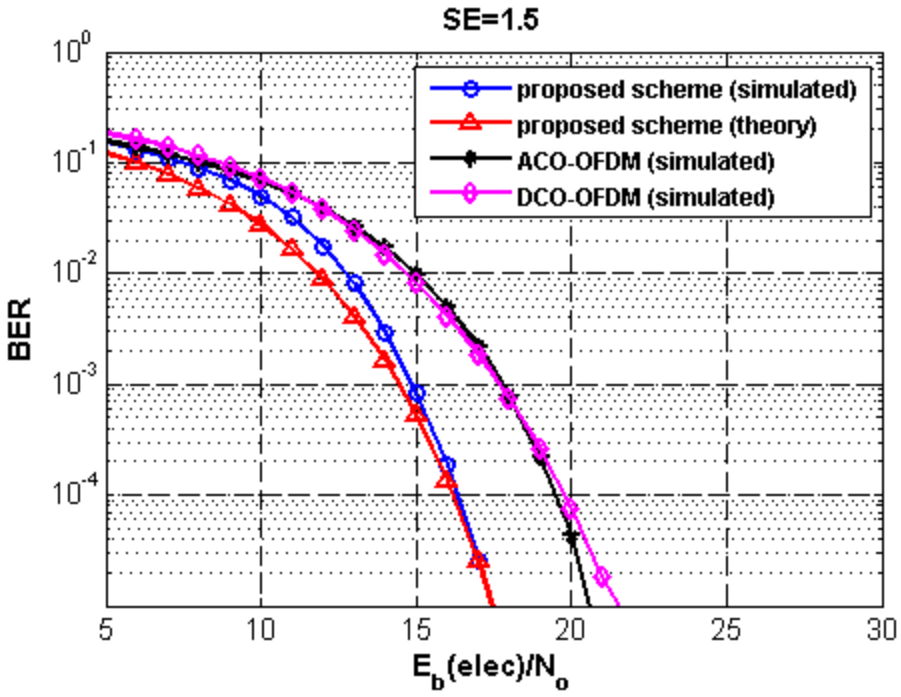

Figure 4. 7: BER performance of 16-8-4-QAM STACO-OFDM, 64-QAM ACO-OFDM, and 8-QAM DCO-OFDM in terms of electrical SNR.

In comparison to ACO-OFDM scheme, the performance degradation of DCO-OFDM starts for SNR values above 19 dB. This is because of the increment of the clipping distortion in DCO-OFDM with the increment of the signal power since fixed amount of DC bias is used in DCO-OFDM scheme. The BER performance improvement of 16-8-4-QAM STACO-OFDM in comparison to 64-QAM ACO-OFDM and 8-QAM DCO-OFDM roughly starts at the SNR value of 8 dB.

For offered spectral efficiency of 2 bits/s/Hz, 32-16-16 QAM STACO-OFDM proposed scheme is compared with 256-QAM ACO-OFDM and 16-QAM DCO-OFDM with 7.5 dB DC-bias. Again the proposed scheme shows better electrical energy saving which is about 2.5 dB compared to DCO-OFDM and 5.5 dB compared to ACO-OFDM to achieve a BER of 10^{-5} as presented on Fig. 4.8. In comparison to 256-QAM ACO-OFDM and 16-QAM DCO-OFDM, the BER performance improvements of 32-16-16 QAM STACO-OFDM begin at SNR values of 7 dB and 12 dB respectively.

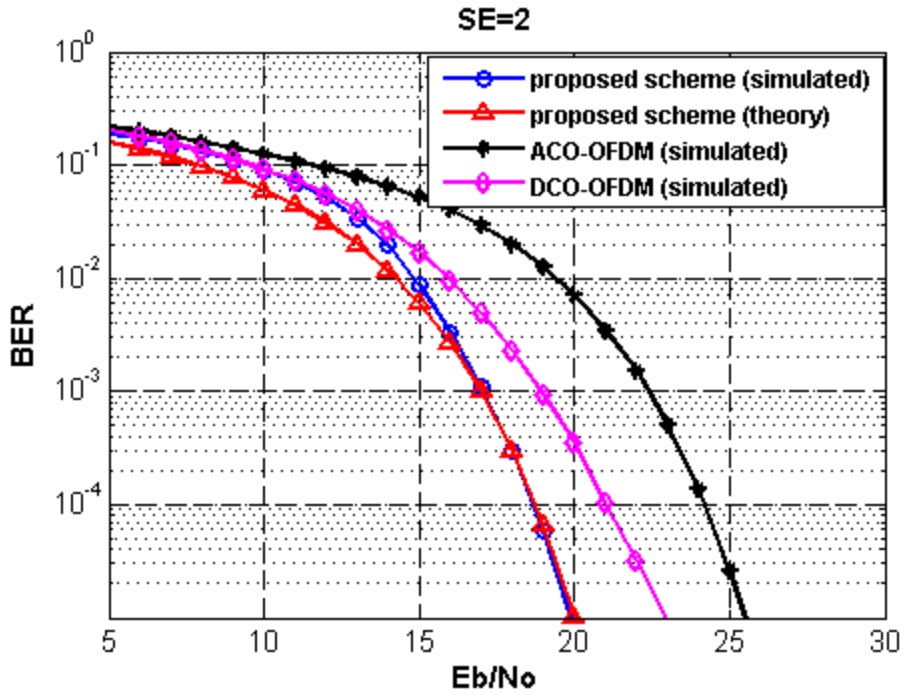

Figure 4. 8: BER performance of 32-16-16-QAM STACO-OFDM, 256-QAM ACO-OFDM, and 16-QAM DCO-OFDM in terms of electrical SNR.

For spectral efficiency of 2.5 bits/s/Hz, 64-64-16-QAM STACO-OFDM scheme is compared with 1024-QAM ACO-OFDM and 32-QAM DCO-OFDM with 8 dB DC-bias as shown on Fig. 4.9. To achieve a BER of 10^{-5}, the proposed STACO-OFDM scheme shows around 3 dB electrical energy saving compared to DCO-OFDM and 7.5dB electrical energy saving compared to ACO-OFDM scheme.

For higher spectral efficiency such as 2.5 bits/s/Hz, the BER performance or energy efficiency gap between the proposed STACO-OFDM scheme and ACO-OFDM has become wider. While increasing spectral efficiency, the SNR penalty of ACO-OFDM in relative to STACO-OFDM and DCO-OFDM schemes will increase since higher level M-QAM modulation is used in ACO-OFDM to fill the spectral efficiency gap. Using large constellation QAM symbols affects the energy efficiency of ACO-OFDM since higher level QAM modulations are known for their energy inefficient performances. Therefore, DCO-OFDM outperforms ACO-OFDM in Fig. 4.8 because of the usage of 256-QAM in ACO-OFDM to fill the spectral efficiency gap.

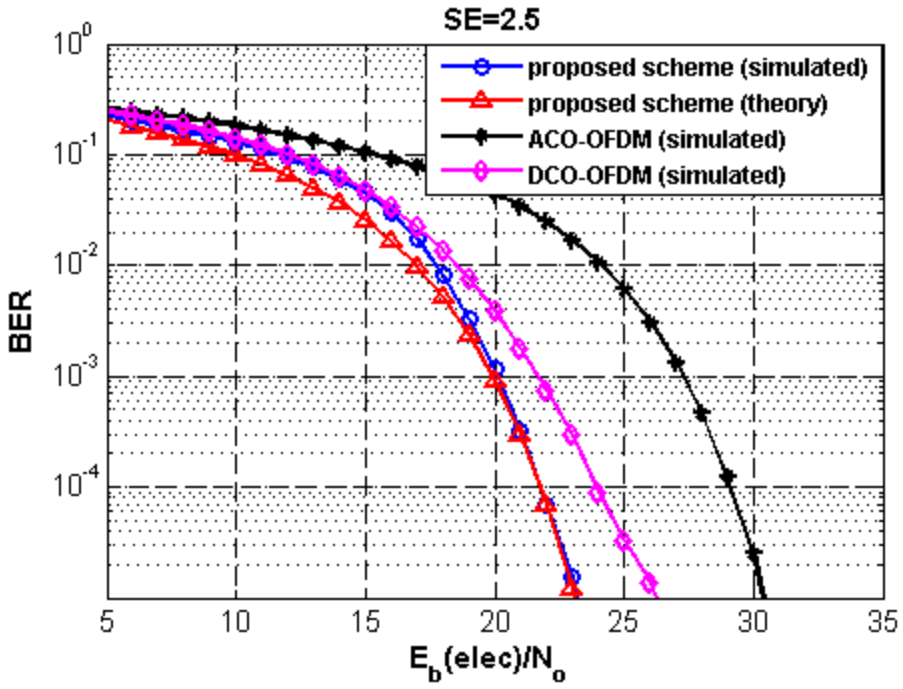

Figure 4. 9: BER performance of 64-64-16-QAM STACO-OFDM, 1024-QAM ACO-OFDM, and 32-QAM DCO-OFDM in terms of electrical SNR.

4.2.2. Optical energy efficiency

The permissible level of optical signal power for optical wireless communication is limited due to the regulation of skin and eye safety. Even if good SNR level is needed to realize good quality of communication services, the electrical power of transmitted signal is constrained to certain level to keep the emitted optical signal from the LED in acceptable range. Therefore, the transmission scheme in OWC should be efficient in terms of optical signal power usage to achieve better BER performance. In this section, the optical power efficiency of STACO-OFDM, ACO-OFDM, and DCO-OFDM are compared to each other using numerical simulations of BER performance in terms of optical SNR per bit for AWGN channel environment. In Fig.4.10, 4.11, and 4.12, the BER performance of the three schemes as a function of optical energy per bit to noise power ratio ($E_{b(opt)}/N_o$) are presented.

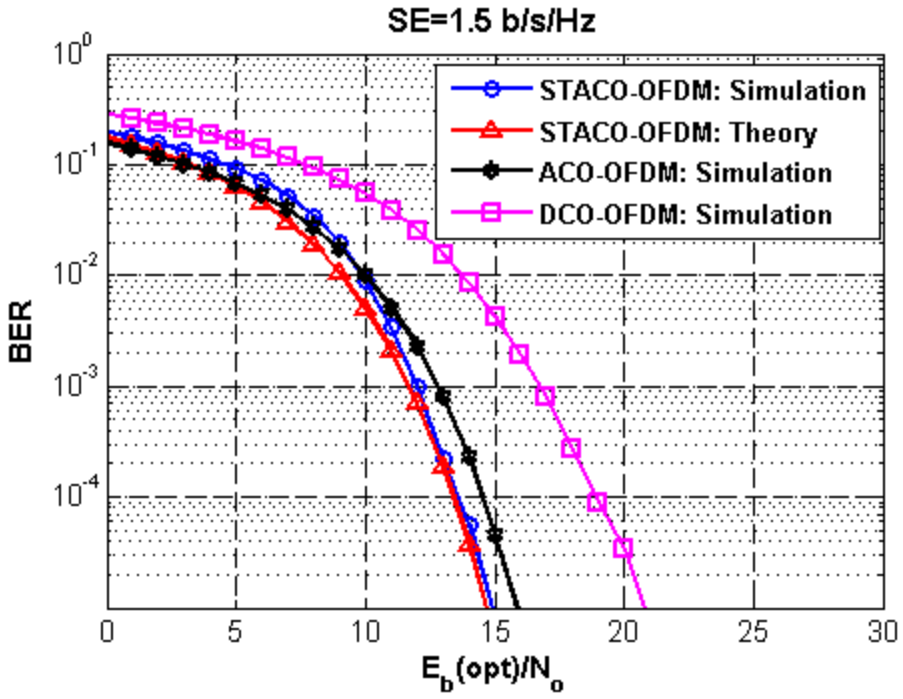

Figure 4. 10: BER performance of 16-8-4-QAM STACO-OFDM, 64-QAM ACO-OFDM, and 8-QAM DCO-OFDM in terms of optical SNR.

As shown on Fig.4.10, for spectral efficiency (SE) of 1.5 bits/s/Hz, the proposed STACO-OFDM scheme provides better optical energy efficiency compared to both ACO-OFDM and DCO-OFDM schemes. To achieve a BER of 10^{-5}, STACO-OFDM saves optical energy of around 5.7 dB and 0.9 dB compared to DCO-OFDM and ACO-OFDM respectively. For spectral efficiency (SE) of 2 bits/s/Hz, STACO-OFDM scheme provides optical energy saving of 3.2 dB compared with ACO-OFDM. But compared to DCO-OFDM, it has shown superior optical energy efficiency with around 5.1 dB optical energy saving to achieve a BER of 10^{-5} as shown on Fig.4.11.

For spectral efficiency (SE) of 2.5 bits/s/Hz, STACO-OFDM scheme shows better performance in terms of optical energy saving compared to both ACO-OFDM and DCO-OFDM as presented on Fig.4.12. Both ACO-OFDM and DCO-OFDM schemes have experienced about 5 dB optical energy penalties compared to STACO-OFDM scheme to achieve BER of 10^{-5} with 2.5 b/s/Hz systems.

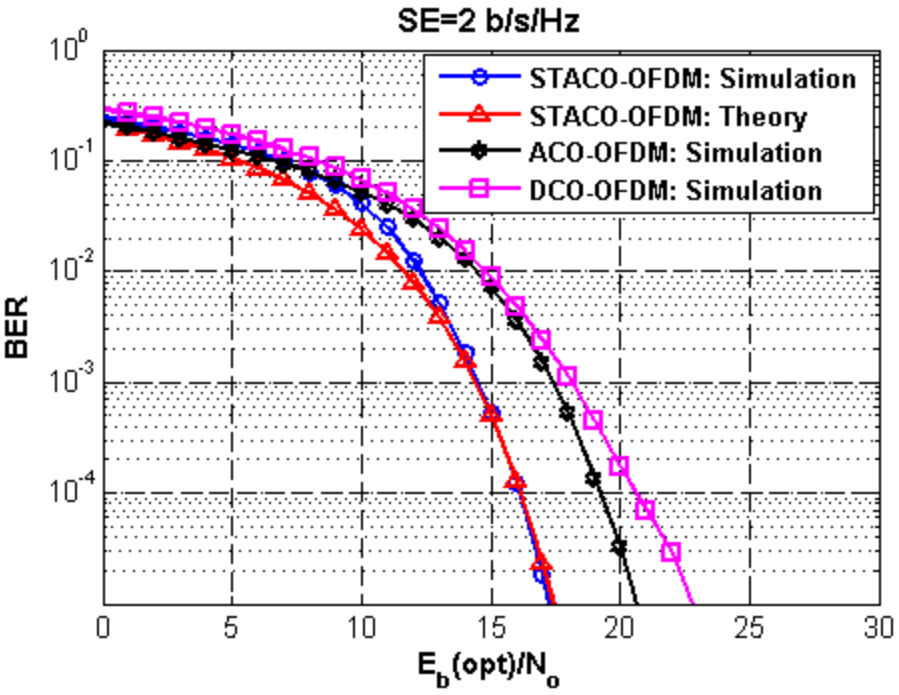

Figure 4. 11: BER performance of 32-16-16-QAM STACO-OFDM, 256-QAM ACO-OFDM, and 16-QAM DCO-OFDM in terms of optical SNR.

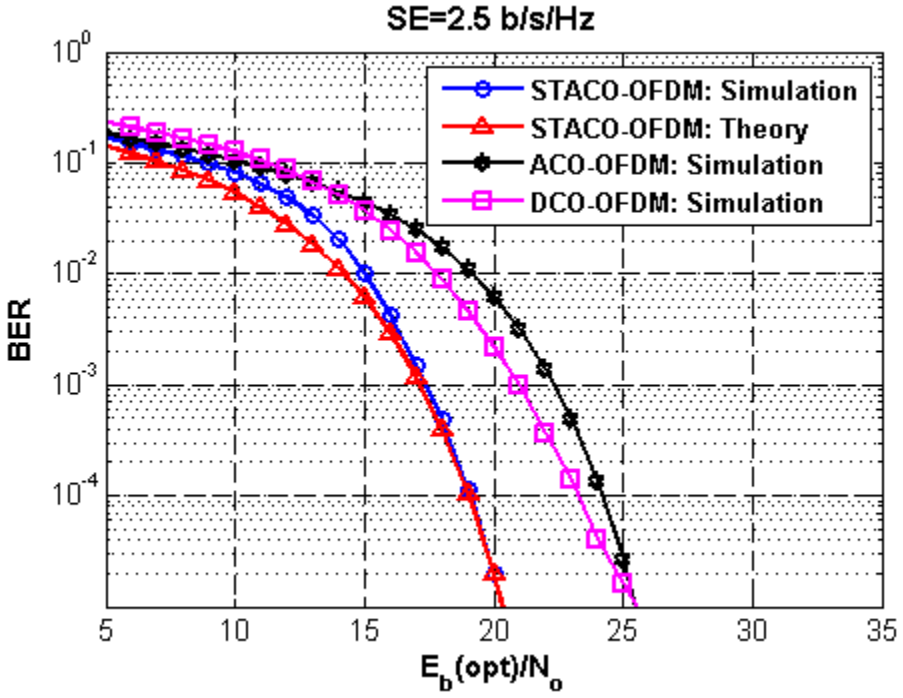

Figure 4. 12: BER performance of 64-64-16-QAM STACO-OFDM, 1024-QAM ACO-OFDM, and 32-QAM DCO-OFDM in terms of optical SNR.

The previously presented results for BER vs. optical SNR conclude that the optical power efficiency of ACO-OFDM is more affected for higher spectral efficiencies due to usage of energy inefficient large constellation sized QAM modulations. In addition, the BER performance of DCO-OFDM is relatively affected for large optical SNR values due to the increment of clipping distortion. The amplitude and power of the transmitted signal become large for large SNR values; hence, many samples are left in negative regions even after adding the DC-bias for DCO-OFDM scheme. Therefore, many samples will be clipped to zero and the clipping distortion becomes high and affects the BER performance of DCO-OFDM.

4.3. Energy efficiency of STACO-OFDM over multipath channel

The performance of the proposed STACO-OFDM over multipath optical wireless channel is investigated and analyzed in this section. Performance comparisons have also been done with ACO-OFDM and DCO-ODM transmission schemes over a multipath channel. Purely diffused optical wireless channel physical link configuration is considered on this part of the research. The Ceiling bounce model is used to characterize and model the optical wireless channel impulse response. Simple zero forcing equalization is used in all scheme to reduce the effect of the multipath channel on the performance of the systems. The BER vs. electrical SNR and BER vs. optical power are simulated to analyze the electrical energy efficiency and optical power efficiency of the system respectively. The characteristic of defused optical channel is also investigated using time domain and frequency domain simulation of the optical channel impulse response. The following major simulation parameters listed on table 4.1 are used during BER performance simulations of STACO-OFDM, DCO-OFDM, and ACO-OFDM. The total employed bandwidth ($f_s = 100MHz$) is chosen for simulation since the modulation bandwidth of LED is less than 200 MHz [26]. The measured channel delay spread for typical room is in the range of 2-20 ns as indicated in [3, 38]. Therefore, the delay spread (10 and 20 ns) are chosen to be in the rage of delay spread reported in [3, 38].

Table 4.1: Major simulation parameters of BER simulation over multipath channel

OFDM parameters			
IFFT/FFT size	2048		
Cyclic prefix length	64		
Sampling frequency (f_s)	100 MHz		
Channel delay spread (D_{rms})	10ns, 20ns		
Modulation Techniques			
STACO-OFDM/eU-OFDM	Stratum-1	Stratum-2	Stratum-3
	16-QAM	8-QAM	4-QAM
	32-QAM	16-QAM	16-QAM
	64-QAM	64-QAM	16-QAM
ACO-OFDM	64, 256, 1024-QAM		
DCO-OFDM	8, 16, 32-QAM		
Spectral efficiency	≈1.5, 2, and 2.5 bits/s/Hz		
Bit rate	145 Mbs, 194 Mbs, 242 Mbs		

4.3.1. Diffused optical wireless channel impulse response

The samples of the channel impulse response are generated based on ceiling bounce model by using equation (2.7). The simulation parameters used to generate the CIR are given on table 4.1 of section (4.3). The channel is generated for two scenarios of channel delay spread, i.e. $D_{rms} = 10 \; and \; 20 \; ns$. Fig.4.13 shows the discrete time simulation result of normalized time domain CIR of the diffused optical channel h_n for channel delay spread of 10 ns and 20 ns.

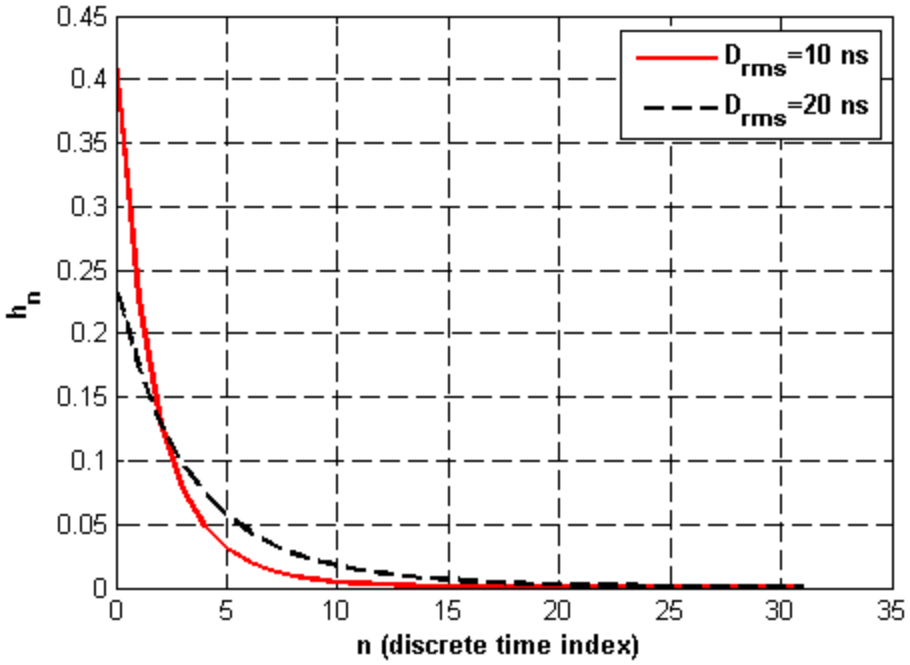

Figure 4. 13: The normalized time domain CIR from celling bounce model for $D_{rms} = 10, 20\ ns$.

The time duration between two discrete points is equal to the sampling time ($T_s = 1/f_s$) as listed previously on table 4.1. The channel samples are generated with consideration of no blocking object which blocks the reflected light from reaching to the receiver. A total of 64 samples length cyclic prefix is used in all three schemes to mitigate inter-symbol interference (ISI). In the proposed STACO-OFDM scheme, the length of the cyclic prefix is set to be 32 for each sub frames which are transmitted in to two consecutive sessions. To achieve similar spectral efficiency for the three schemes for fair comparisons, 64 samples long cyclic prefix is used for ACO-OFDM and DCO-OFDM schemes. The result in Fig.4.13 confirms that 32 samples long cyclic prefix is enough to avoid ISI since the magnitude of h_n is almost zero for samples beyond the 12th sample.

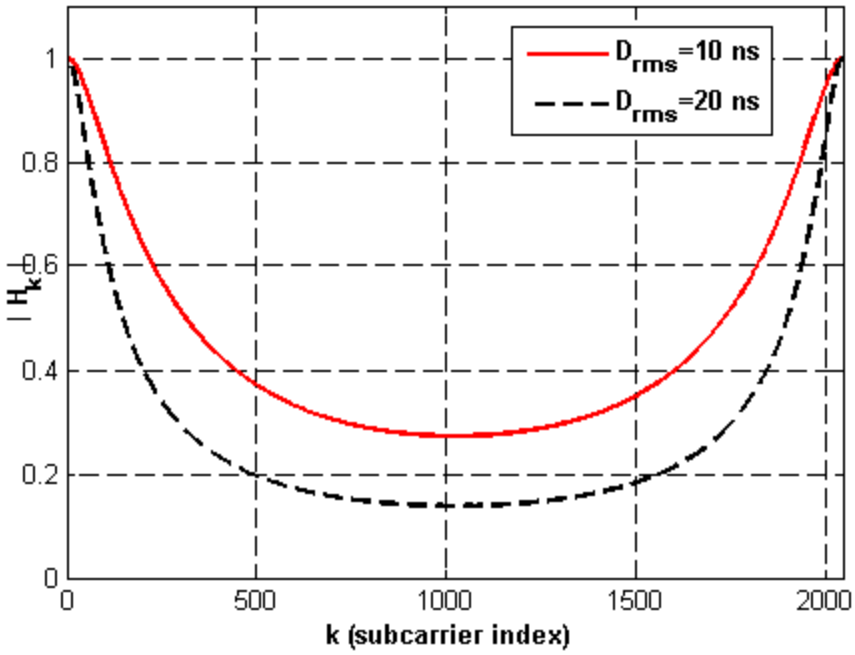

Figure 4. 14: Frequency domain subcarrier gain for CIR with $D_{rms} = 10,\ 20\ ns$.

The plot on Fig.4.14 is the frequency domain subcarrier gain of the optical wireless channel for the normalized CIR with D_{rms} of (10 ns, 20 ns). The simulation results in Fig.4.14 shows that the optical wireless channel has low pass nature [3, 82] and becoming more frequency selective when the quantity of D_{rms} is increased. The subcarriers near to the zero frequency are relatively in better condition to achieve relatively better SNR since they have relatively higher channel gain. Moreover, while D_{rms} is increasing, the channel gain of the subcarriers are decreasing, hence, it is difficult to achieve enough SNR for better BER performance while the quantity of the channel delay becomes large. The second half of subcarriers (with index k>1023) are not used for information carriage due to the imposed Hermitian symmetry.

4.3.2. Electrical energy efficiency

To compare the electrical energy efficiencies of the three schemes, the BER performances versus electrical E_b/N_o are analyzed for the three modulation schemes having similar spectral efficiencies and bitrates. As shown in Fig. 4.15, the simulation result and the theoretical BER bound of STACO-ODM has shown good agreement apart from the inclusion of residual error

introduced by the successive demodulation on the simulated BER. Starting from electrical SNR of 27 dB, the theoretical and simulated BER have overlapped for STACO-OFDM based system over a channel with D_{rms} of 10 ns.

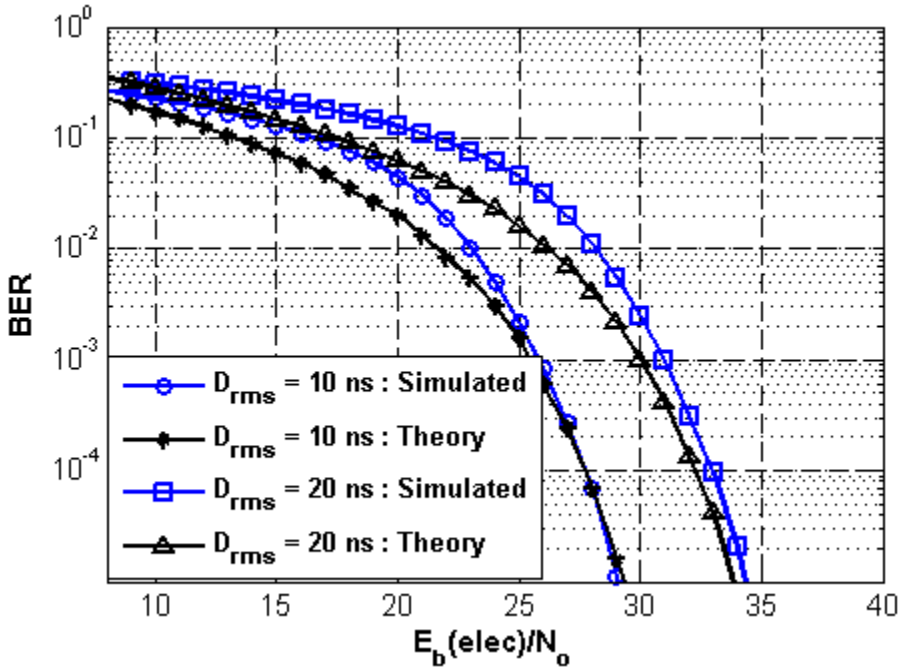

Figure 4. 15: Theoretical and simulated BER of STACO-OFDM for spectral efficiency of 2 b/s/Hz.

For STACO-OFDM transmission scheme over channel having D_{rms} of 20 ns, the theoretical and simulated BER are going to overlap slowly since the achieved BER at each stratum is higher due to the significant amount multipath effect of the channel. Therefore, the gap between the theoretical and simulated BER is relatively visible because of the significant amount of bit errors propagated from stratum to stratum for the channel with large D_{rms}. Hence, the propagated residual BER from lower to higher stratum due to the successive demodulation technique is relatively higher for channel having D_{rms} of 20 ns compared to the channel with D_{rms} of 10 ns. The result on Fig. 4.16 presented the comparison of the three schemes in terms of electrical energy efficiency for the system providing spectral efficiency (SE) and bitrate of 1.5 bits/s/Hz and 145 Mb/s respectively over diffused optical channel.

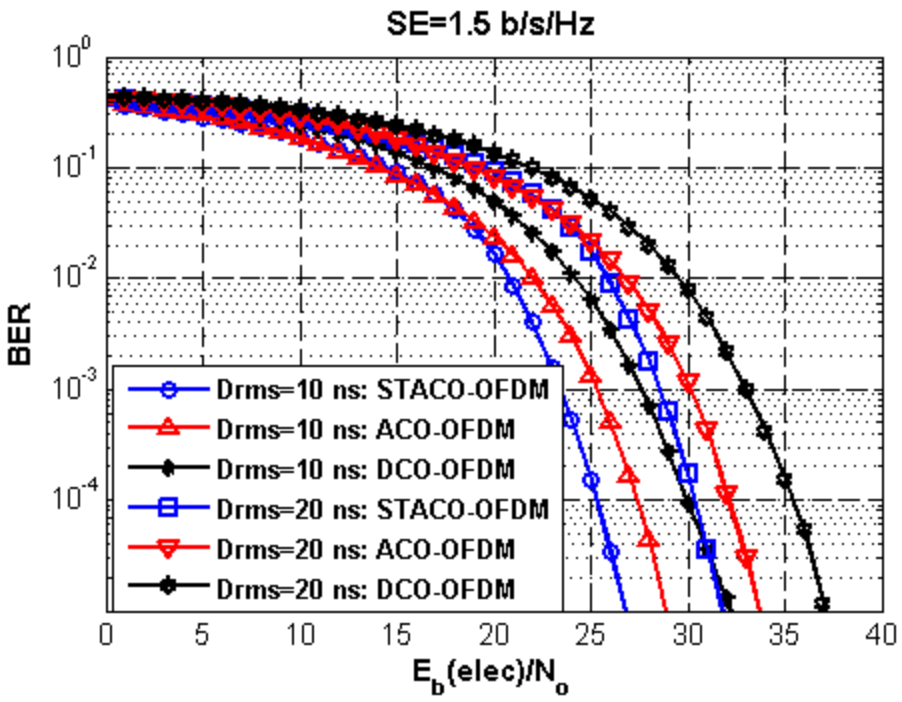

Figure 4. 16: BER Vs. electrical SNR performance of STACO-OFDM, ACO-OFDM and DCO-OFDM with spectral efficiency of 1.5 bits/s/Hz over multipath channel with $D_{rms} = 10,\ 20\ ns$.

As the simulation result shows, to achieve a BER of 10^{-5} over multipath channel having delay spread of 10 and 20 ns, the proposed STACO-OFDM requires E_b/N_o of about 26.8 dB and 31.8 dB respectively. Among the two considered channel scenarios, the QAM symbols at each information carrying subcarrier are more attenuated when the channel D_{rms} is equals to 20 ns. On the other hand, to achieve a BER of 10^{-5} over multipath channel having delay spread of 10 and 20 ns, the proposed STACO-OFDM delivers electrical energy savings of about 2.1 dB and 1.9 dB respectively compared to ACO-OFDM and about 5.3 dB and 5.2 dB electrical energy savings respectively compared to DCO-OFDM. In Fig. 4.17, the BER performances with respect to electrical SNR are given for the three schemes providing spectral efficiency (SE) of 2 bits/s/Hz and a bit rate of 194 Mb/s. As the simulated results confirm, the proposed STACO-OFDM scheme outperforms both ACO-OFDM and DCO-OFDM for frequency selective multipath channel with the given channel delay spreads.

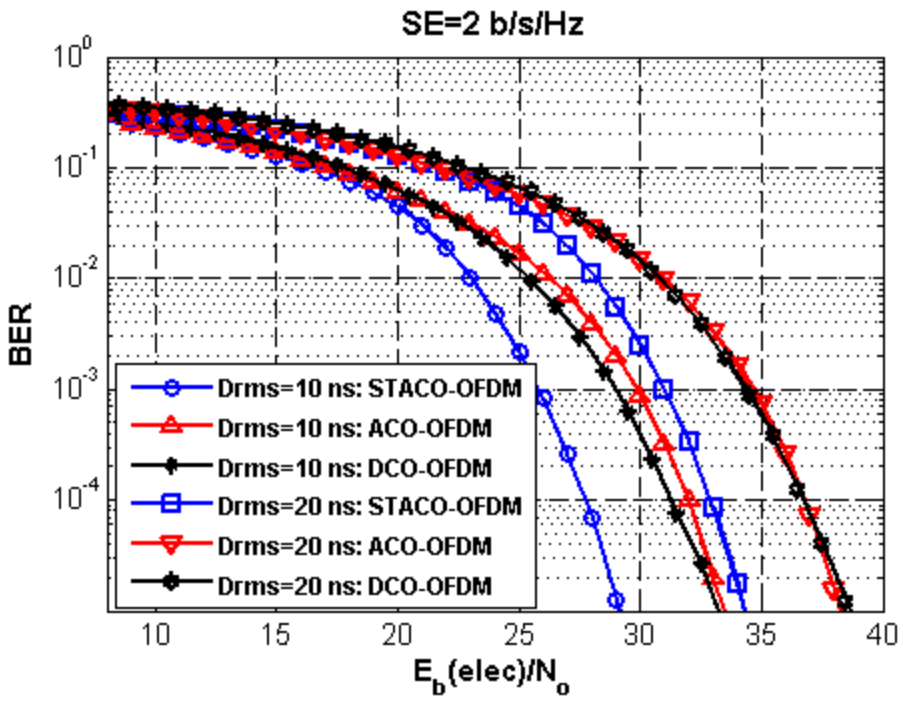

Figure 4. 17: BER Vs. electrical SNR performance of STACO-OFDM, ACO-OFDM and DCO-OFDM with spectral efficiency of 2 bits/s/Hz over multipath channel with $D_{rms} = 10,\ 20\ ns$.

STACO-OFDM provides electrical energy savings of about 4.3 dB and 4.5 dB compared to DCO-OFDM and ACO-OFDM respectively to achieve a BER of 10^{-5} over multipath fading channel having 10 ns delay spread. To achieve the same BER (10^{-5}) over multipath channel having D_{rms} of 20 ns, STACO-OFDM shows 4.3 dB electrical energy savings compared to both ACO-OFDM and DCO-OFDM. For lager SNR values, the performance of DCO-OFDM starts degrading (due to the maximization of clipping distortion with increment of transmitted signal power) in comparison to ACO-OFDM. The BER performances of the three schemes over multipath channel for system having spectral efficiency (SE) of 2.5 bits/s/Hz and bitrate of 242 Mb/s are given in Fig. 4.18. Over the channel having D_{rms} of 10 ns, STACO-OFDM requires SNR of 32.2 dB to achieve BER of 10^{-5} while DCO-OFDM and ACO-OFDM schemes require SNR of 36.4 dB and 38.5 dB respectively. For the second scenario ($D_{rms} = 20ns$), SNR values of about 37.3 dB, 41.8 dB, and 43.2 dB are required by STACO-OFDM, DCO-OFDM, and ACO-OFDM respectively to achieve a BER of 10^{-5}. Therefore, In comparison to DCO-OFDM, the proposed STACO-OFDM

has offered an electrical energy savings of about 4.2 dB and 4.5 dB to achieve a BER of 10^{-5} over multipath channel having D_{rms} of 10 ns and 20 ns respectively.

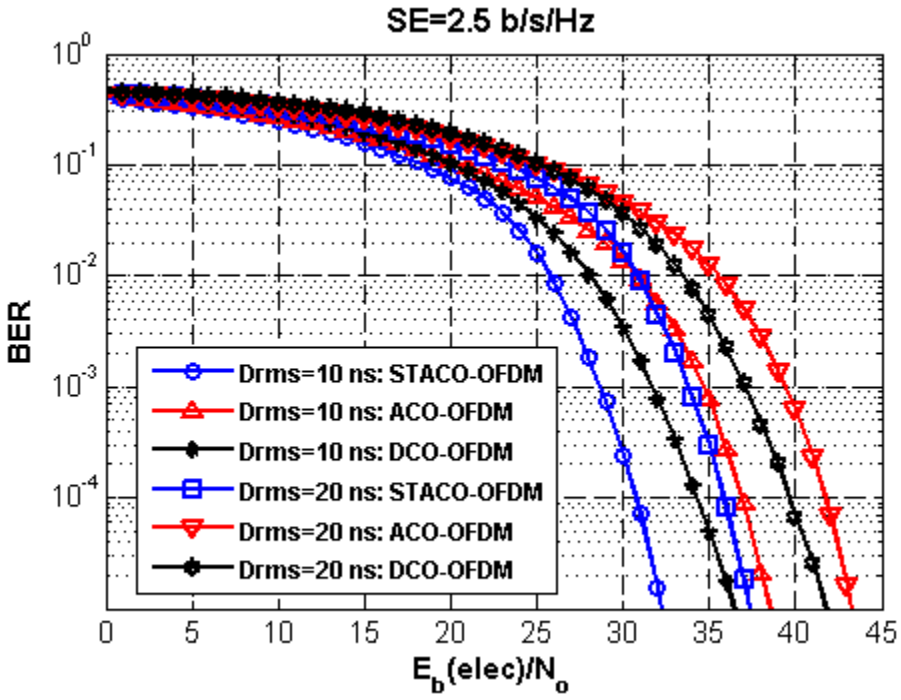

Figure 4. 18: BER Vs. electrical SNR performance of STACO-OFDM, ACO-OFDM and DCO-OFDM with spectral efficiency of 2.5 bits/s/Hz over multipath channel with $D_{rms} = 10,\ 20\ ns$.

Moreover, STACO-OFDM offer electrical energy saving of about 6.3 dB and 5.9 dB compared to ACO-OFDM scheme at channel delay spread of 10 ns and 20 ns respectively.

The overall presented simulation results on section (4.3) also show that, when the spectral efficiency increases the SNR penalty of ACO-OFDM in comparison to STACO-OFDM is increased since higher order QAM modulations are used in ACO-OFDM to fill the spectral efficiency gap. Constellation points are close to each other in higher order QAM modulations; hence, they are vulnerable to the effects of multipath channel. Higher order QAM modulations are not also energy efficient in general. To achieve a better BER over multipath channel having relatively larger channel delay spread, the electrical power of the transmitted signal should be high to achieve enough effective SNR. But while increasing the electrical power of the transmitted signal, the peak of the negative samples also increase in negative region and this will introduce large clipping noise for the case of DCO-OFDM since many samples are still left in negative region even after adding a fixed DC bias. Therefore, as the presented results show, DCO-OFDM is more affected by multipath fading due to the presence of unavoidable clipping noise. The presented

results also revealed that the residual noise propagating from stratum to stratum during successive demodulation of STACO-OFDM signal affects the energy efficiency of STACO-OFDM for large channel delay spreads. For relatively large delay spreads, the propagated bit error is relatively large since the achieved BER at each stratum becomes relatively high for large channel delay spread values.

4.3.3. Optical power efficiency

To evaluate the BER performance of the three modulation schemes in terms of transmitted optical power (P_o), the parameters listed in table 4.2 are used in addition to the main parameters listed on table 4.1.

Table 4.2: Simulation parameters for simulation of BER in terms of optical power.

Simulation parameters	
DC channel gain (H_0)	10^{-6}
Noise spectral density (N_o)	3.05×10^{-23}
Transmitted optical power (P_o)	$25-40$ *dBm*

The channel parameters (D_{rms}, H_0, N_o) in Table 4.2 for simulation are consistent with experimentally measured channel parameters presented in literature [3]. The result from numerical simulation and the theoretical BER bound given at equations (53) and (70) have shown good agreement as shown on Fig.4.19. The BER vs. P_o (transmitted optical power) performances of the three optical OFDM schemes over multipath channel having a delay spread of $10\,ns$ are presented in Fig. 4.20, 4.21, and 4.22 for spectral efficiencies (SE) of 1.5, 2 & 2.5 b/s/Hz respectively. For a system delivering spectral efficiency (SE) of 1.5b/s/Hz, STACO-OFDM shows better performance with approximately 0.6 dB and 2.8 dB optical energy savings to achieve a BER of 10^{-5} compared to ACO-OFDM and DCO-OFDM respectively as shown on Fig. 4.20. For sections of the graph below SNR values of 29 dB, ACO-OFDM has outperformed STACO-OFDM due to the significant amount residual errors propagating from stratum to stratum during successive demodulation. But it will not be a draw back for STACO-OFDM since ACO-OFDM is better only in high BER region above BER values of 10^{-2}.

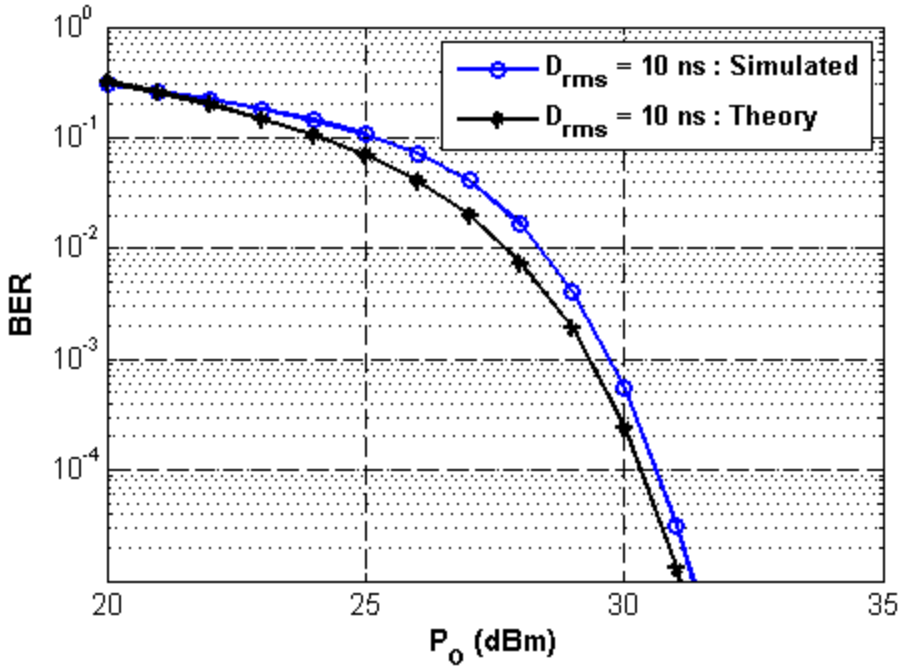

Figure 4. 19: Theoretical and simulated BER of STACO-OFDM in terms of transmitted optical power for a system with spectral efficiency of 1.5 b/s/Hz over channel with D_{rms} of 10 ns.

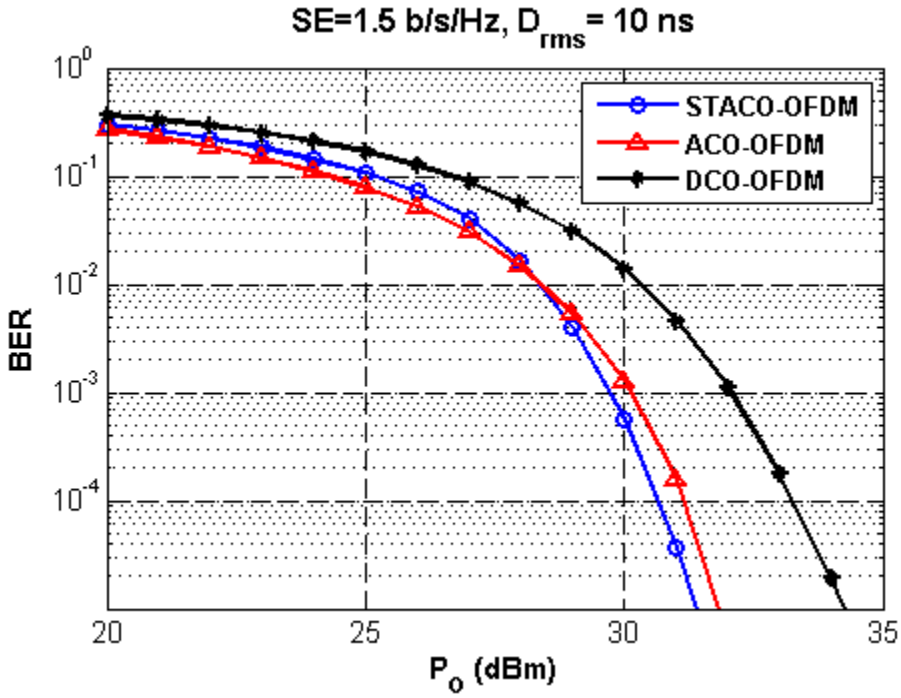

Figure 4. 20: BER Vs. optical power performance of STACO-OFDM, ACO-OFDM and DCO-OFDM with spectral efficiency of 1.5 bits/s/Hz over multipath channel with $D_{rms} = 10\ ns$.

As the simulation results revealed in Fig. 4.21, STACO-OFDM saves about 1.5 dB optical energy compared to ACO-OFDM and 2.5 dB optical energy compared to DCO-OFDM for the system offering spectral efficiency (SE) of 2b/s/Hz with achieved BER of 10^{-5}.

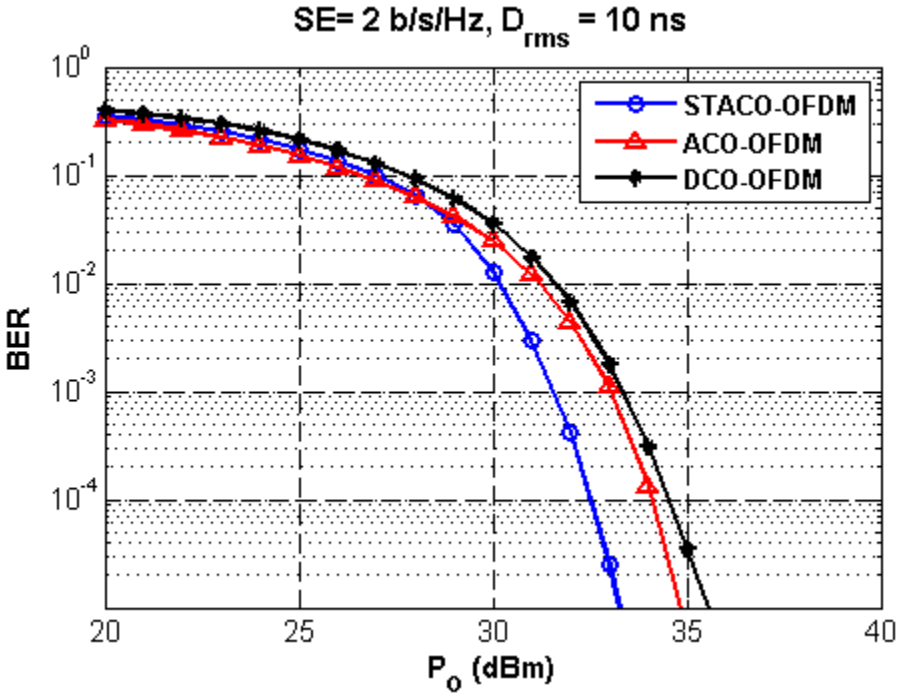

Figure 4. 21: BER Vs. optical power performance of STACO-OFDM, ACO-OFDM and DCO-OFDM with spectral efficiency of 2 bits/s/Hz over multipath channel with $D_{rms} = 10\ ns$.

The optical power penalty of ACO-OFDM with respect to STACO-OFDM is increased because of higher level QAM (256-QAM) usage to equalize the spectral efficiency of ACO-OFDM to 2b/s/Hz. Due to the energy inefficient properties of higher level QAM modulations; the power penalty of ACO-OFDM becomes large. Similarly, as the results on Fig. 4.22 confirmed, the STACO-OFDM scheme outperforms both ACO-OFDM and DCO-OFDM for the system providing a spectral efficiency (SE) of 2.5b/s/Hz. STACO-OFDM needs 35.3 dBm optical powers to achieve a BER of 10^{-5} while DCO-OFDM and ACO-OFDM need optical power of 37.5 dBm and 37.7 dBm respectively to achieve the same BER.

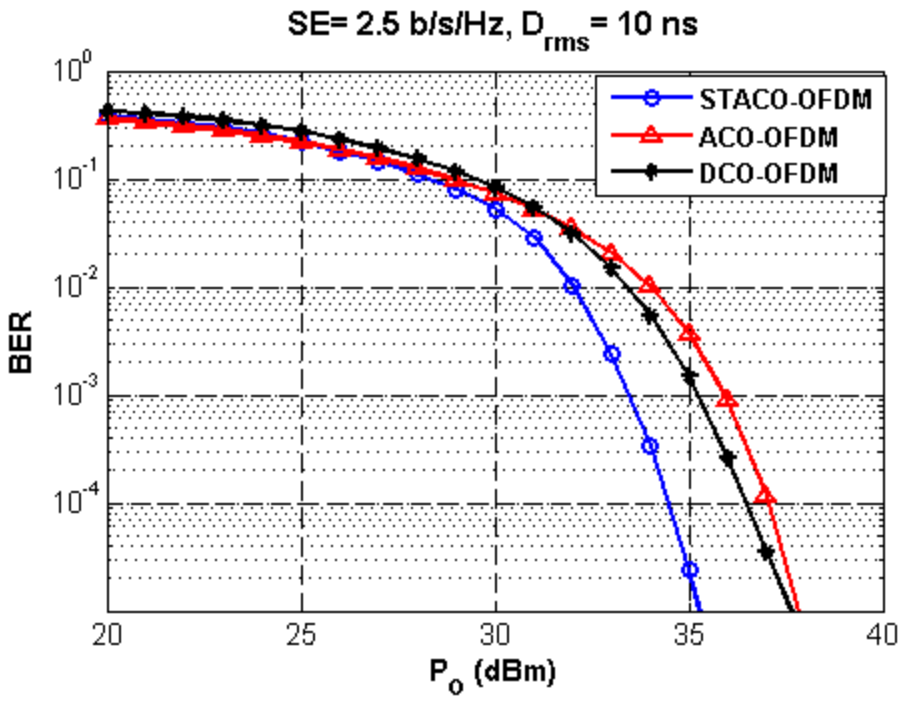

Figure 4. 22: BER Vs. optical power performance of STACO-OFDM, ACO-OFDM and DCO-OFDM with spectral efficiency of 2.5 bits/s/Hz over multipath channel with $D_{rms} = 10\ ns$.

Therefore compared to ACO-OFDM and DCO-OFDM schemes, the overall presented results have shown that STACO-OFDM provides better optical power efficiency which has huge significance for solving drawbacks of optical power constraints to meet eye and skin safety regulations in indoor optical wireless communications.

4.4. Performance comparisons of STACO-OFDM and eU-OFDM on multipath channel

The BER/energy efficiency performance of STACO-OFDM and eU-OFDM is compared to each other for multipath channel having D_{rms} values of 10 ns and 20 ns. The comparisons are done by evaluating the required electrical SNR (E_b/N_o) values to achieve a BER value of 10^{-5}. The BER performance of both schemes offering spectral efficiency (SE) of 1.5 b/s/Hz is given in Fig. 4.23.

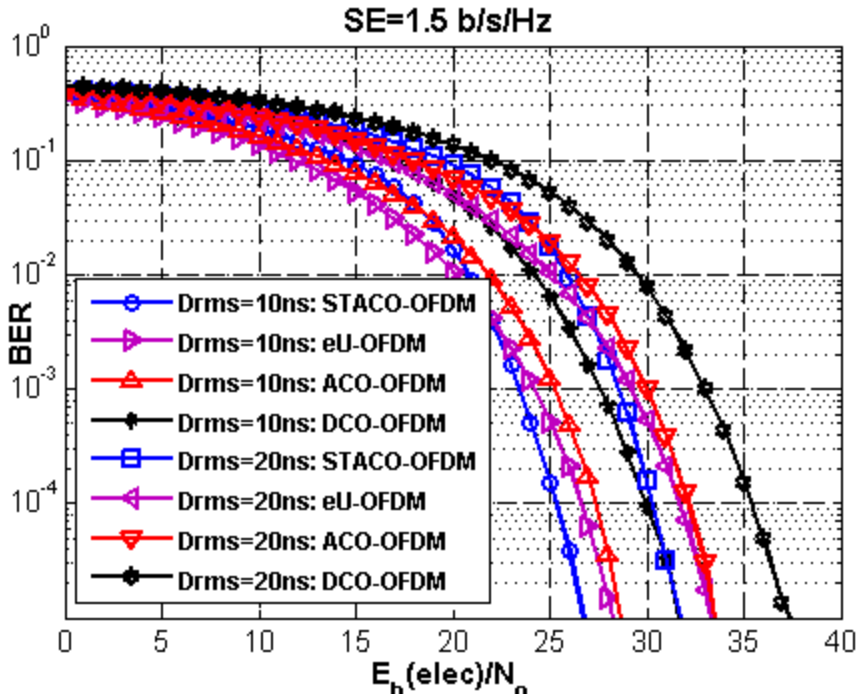

Figure 4.23. BER performance of STACO-OFDM, eU-OFDM, ACO-OFDM, and DCO-OFDM for offered SE of 1.5 b/s/Hz.

The simulation result given in Fig. 4.23 has revealed that STACO-OFDM has offered electrical energy savings of about 1.2 dB and 1.6 dB compared to eU-OFDM over multipath channel with D_{rms} values of 10 ns and 20 ns respectively. Nonetheless, eU-OFDM has shown slightly better performance compared to both ACO-OFDM and DCO-OFDM schemes.

As shown in Fig. 4.24, the STACO-OFDM has outperformed the eU-OFDM scheme for the system offering a spectral efficiency (SE) of 2 b/s/Hz. As the simulation results confirmed, eU-OFDM scheme has introduced electrical energy penalties of about 1.2 dB and 1.6 dB compared to STACO-OFDM scheme over channels with D_{rms} of 10 ns and 20 ns respectively.

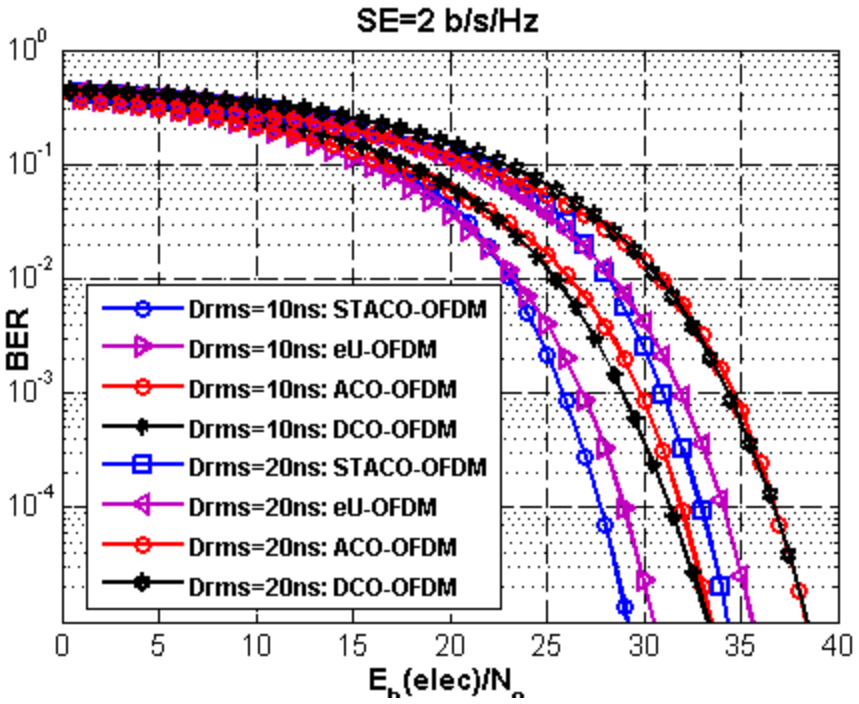

Figure 4.24. BER performance of STACO-OFDM, eU-OFDM, ACO-OFDM, and DCO-OFDM for offered SE of 2 b/s/Hz.

Similarly, the simulation results has confirmed that STACO-OFDM can offer better energy efficiency compared to eU-OFDM for the system delivering spectral efficiency (SE) of 2.5 b/s/Hz. As given in Fig. 4.25, the results from simulation have concluded that STACO-OFDM provides electrical energy savings of about 3.1 dB and 3.7 dB compared to eU-OFDM scheme over channels having delay spread of 10 ns and 20 ns respectively.

According to results given in section (4.2.1) and [57], both STACO-OFDM and eU-OFDM schemes have shown approximately close BER performances as a function of electrical SNR for linear AWGN channel. Nevertheless, the results presented on this section have shown that STACO-OFDM can offer better BER performance compared to eU-OFDM on frequency selective multipath channel. As given in Fig.4.14, the optical wireless channel has low pass nature and the subcarriers on high frequency region are more attenuated by the effect of the channel. The eU-OFDM utilizes those subcarriers in low and high frequency region at each layer for transmission of information bits [56, 57]. On the other hand, STACO-OFDM avoids utilizing those high frequency subcarriers on higher depth strata. Therefore, the usages of high frequency region subcarriers on all layers reduce the BER performance of eU-OFDM.

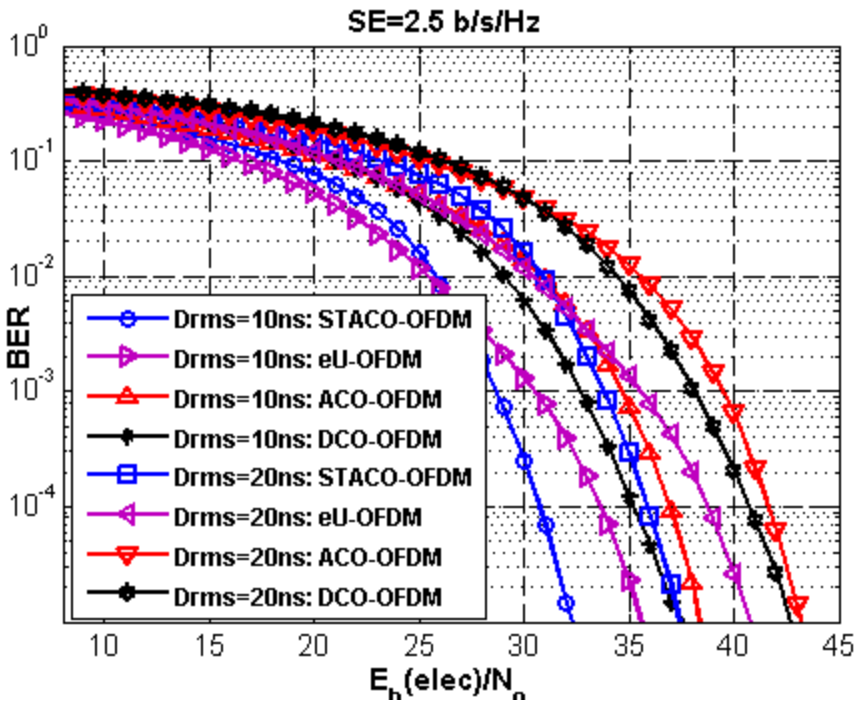

Figure 4.25. BER performance of STACO-OFDM, eU-OFDM, ACO-OFDM, and DCO-OFDM for offered SE of 2.5 b/s/Hz.

Moreover, due to its efficient signal generation and demodulation strategies, STACO-OFDM has lower system latency compared to eU-OFDM. For same M-QAM modulation used on all of the available L strata of both eU-OFDM and STACO-OFDM schemes, the latency introduced at the transmitter of STACO-OFDM scheme is approximately less than the latency experienced at the transmitter of eU-OFDM by a factor of $2^L - 1$. For example, if we consider $L = 3$ for both schemes, $7(\log_2 M)(N/2-1)$ bits should be received at the transmitter of eU-OFDM before transmission while $(\log_2 M)(7N/16-1)$ bits are enough for the case of STACO-OFDM. Furthermore, the latency introduced at the receiver of STACO-OFDM is also lower compared to eU-OFDM since the frame length of STACO-OFDM scheme is less than the frame length of eU-OFDM by a factor of 2^L [56, 57]. Therefore, STACO-OFDM scheme has better advantage over eU-OFDM for latency sensitive real-time communications. Furthermore, implementing one tap frequency domain channel equalization is easier in STACO-OFDM than in eU-OFDM. To perform frequency domain channel equalization on l^{th} layer of eU-OFDM, the CIR of the channel should be constant throughout 8 frames duration. On contrary, the channel effect can be equalized

successfully in STACO-OFDM as long as the channel is invariant over one frame duration. Therefore, STACO-OFDM can be used on applications involving fast channel dynamics scenario.

4.5. Performance of rate adaptive ACO-OFDM

4.5.1. Spectral efficiency

In this section, the potential of adaptive optical OFDM transmission scheme in enhancing the spectral efficiency of OWC system on multipath channel is investigated. In this work, rate adaptive capability is employed on ACO-OFDM transmission scheme to evaluate the effect of employing adaptive capability to improve spectral efficiency. Since STACO-OFDM comprises of ACO-OFDM schemes at each stratum, ACO-OFDM is chosen for investigating the potential of rate adaptive OFDM for optical wireless communication over multipath channel. Therefore, the spectral efficiency of adaptive ACO-OFDM is simulated and the results are compared to the performance of ACO-OFDM with fixed modulation schemes. For fixed modulation schemes, subcarriers that are suitable in achieving the target BER with that particular fixed modulation scheme are loaded with zero QAM with no information transmission over them. The following parameters listed in table 4.3 are used during the simulations.

Table 4.3: Simulation parameters for rate adaptive ACO-OFDM.

Simulation parameters	
Number of subcarriers (N)	2048
Cyclic prefix (CP)	32
Sampling frequency (f_s)	100 MHz
Channel delay spread (D_{rms})	10 ns
Modulations	4,8,16,32-QAM
Target BER	10^{-3}

The samples of channel impulse response are generated by using ceiling bounce model with consideration of no blocking object between transmitter and receiver. The result of discrete time

simulation of the channel impulse response is presented in Fig. 4.26. The simulation result in Fig.4.23 confirms that 32 samples length CP is enough since the magnitude of the channel is almost negligible beyond the 8th sample. Fig.4.27 shows the frequency domain simulation of the channel for D_{rms} of 10 ns. The optical wireless channel has low pass nature and the sub carriers near to dc are in good conditions for transmission of information bits. In Fig. 4.28, the BER performance of adaptive ACO-OFDM with a target BER of 10^{-3} is presented for different magnitudes of electrical SNR in terms of bit energy. The simulation results show that the target BER (10^{-3}) is achieved and no outage of system is going to happen. The transitions from 8 to 16-QAM and from16 to 32-QAM are can be seen at 12 and 16 dB respectively. The channel state information (CSI) is assumed to be known by both transmitter and receiver.

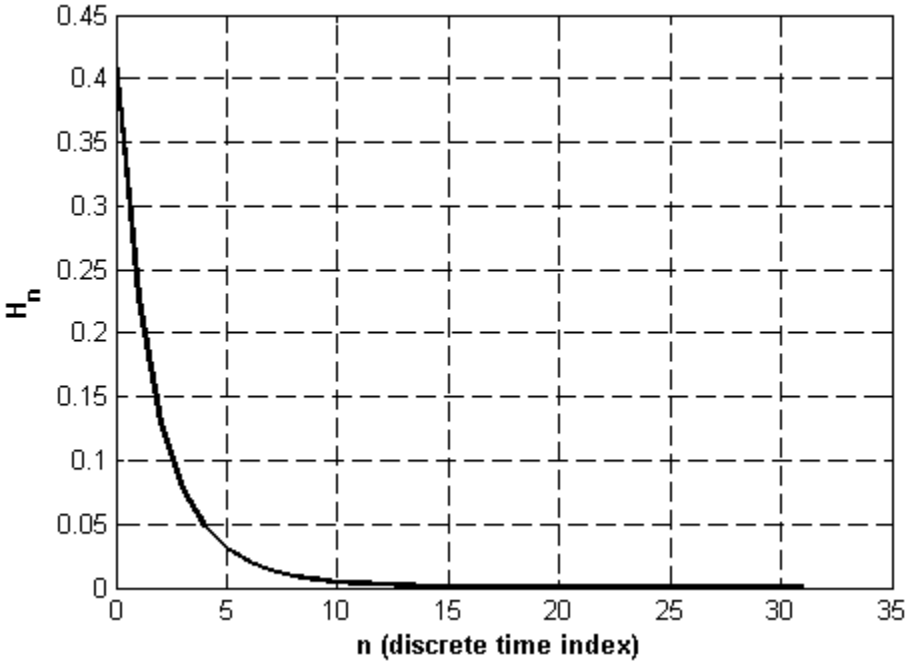

Figure 4. 26: Channel impulse response in time domain.

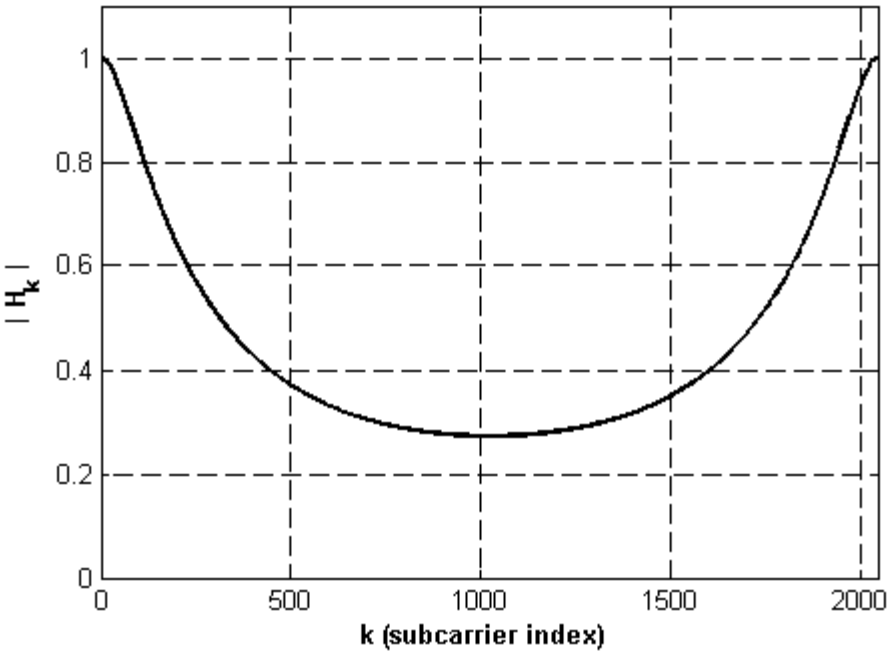

Figure 4. 27: Channel impulse response in frequency domain.

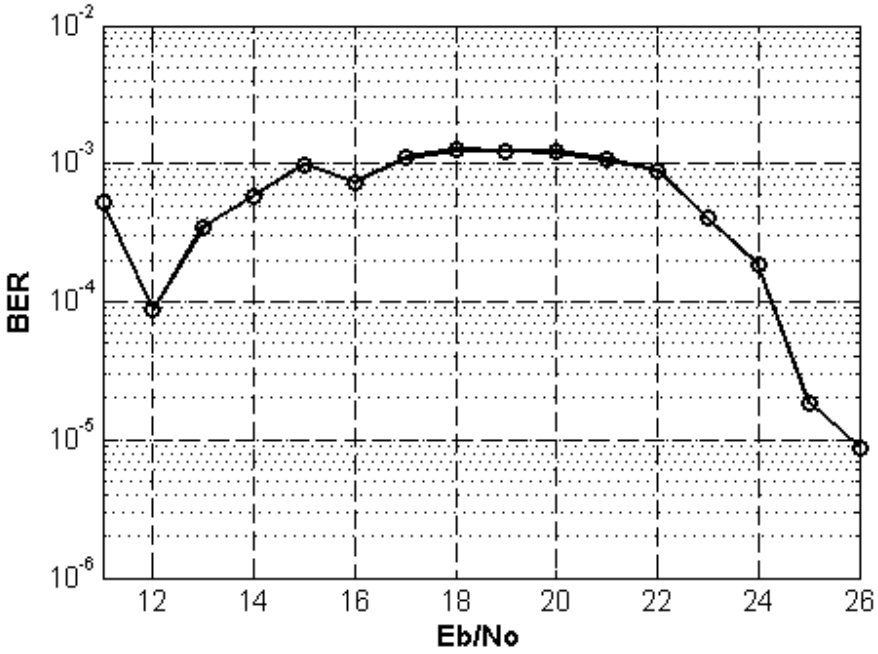

Figure 4. 28: BER performance of rate adaptive ACO-OFDM for target BER of 10^{-3}.

The comparisons of adaptive M-QAM ACO-OFDM scheme to fixed M-QAM ACO-OFDM scheme in terms of spectral efficiency are presented on Fig. 4.29.

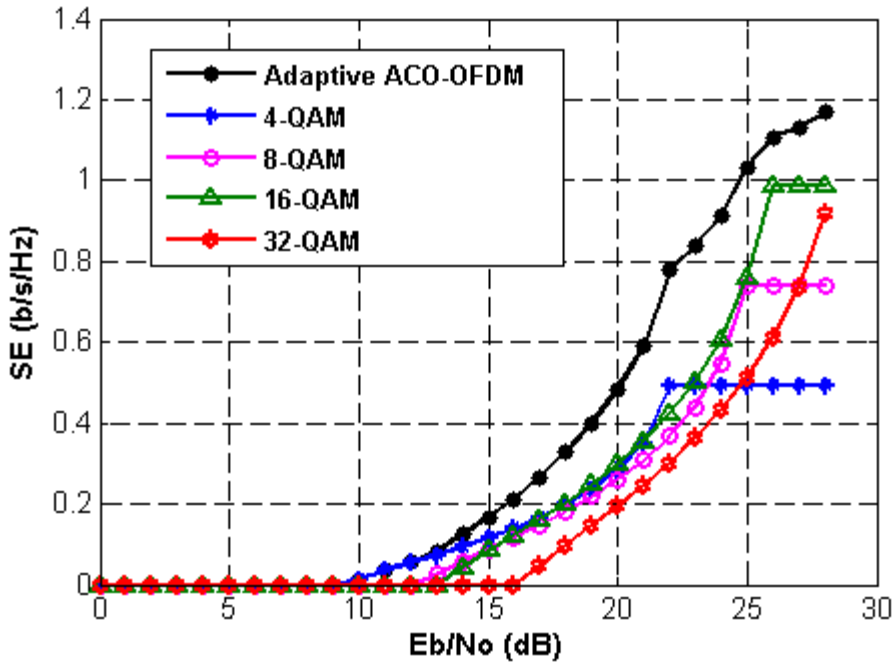

Figure 4. 29: Spectral efficiencies of rate adaptive ACO-OFDM and fixed modulation schemes for target BER of 10^{-3}.

The simulation results presented in Fig. 4.29 confirmed that the rate adaptive ACO-OFDM can offer better spectral efficiencies compared to those obtained from fixed M-QAM (4,8,16,32-QAMs) ACO-OFDM modulation schemes. For electrical SNR (E_b/N_o) of 25 dB, the rate adaptive ACO-OFDM offers a spectral efficiency of around 1 b/s/Hz while fixed 8-QAM ACO-OFDM and 16-QAM ACO-OFDM schemes offer a spectral efficiency of around 0.75 b/s/Hz. Moreover, fixed 4-QAM ACO-OFDM and 32-QAM ACO-OFDM modulations offer a spectral efficiency of 0.5 b/s/Hz for the same amount of electrical SNR (25 dB). The 32–QAM ACO-OFDM scheme offers less spectral efficiency because the achieved SNR, γ_k^{ACO}, at many subcarriers are not enough to achieve the target BER. Therefore, many subcarriers are left empty without data transmission.

4.5.2. Bits allocation on subcarriers of adaptive ACO-OFDM

The bit allocation for subcarriers in the frequency selective rate adaptive ACO-OFDM scheme is dependent on the magnitude of the channel gain of information carrying subcarriers.

As shown on Fig. 4.30 the bits allocation for adaptive ACO-OFDM is as follows; the odd indexed subcarriers ranging from 1st to 427th subcarrier are loaded with 5 bits, 429th to 791th are loaded

with 4 bits, and 793th to 1023th are loaded with 3 bits. Since the channel has a low pass characteristic as presented in Fig. 4.27, higher indexed subcarriers are loaded with fewer bits since they are more affected by frequency selectivity nature of the channel.

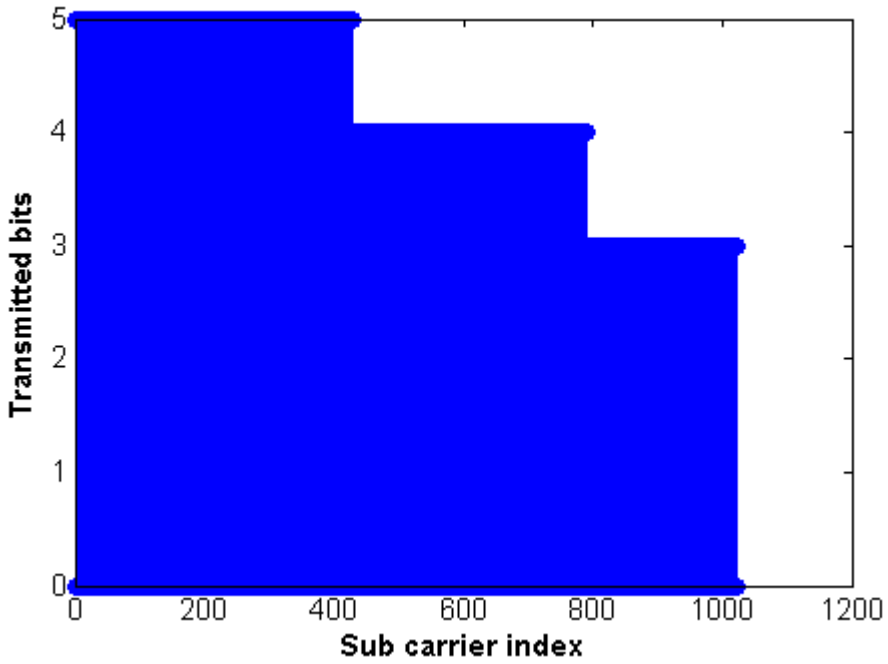

Figure 4. 30: Adaptive ACO-OFDM sub carriers' bits allocation for E_b/N_o of 25 dB.

For 16-QAM based fixed modulation ACO-OFDM scheme, odd subcarriers ranging from 1-791 are loaded with 4 bits while odd subcarriers from index 793-1023 are loaded with zero bits as shown in Fig. 4.31. The subcarriers from index 793-1023 are significantly affected by the channel frequency selectivity and it is not possible to achieve the target BER if they are loaded with 4 bits. Similarly, only odd subcarriers ranging from index 1-427 are loaded with 5 bits for fixed modulation based ACO-OFDM with 32-QAM scheme as presented in Fig. 4.32. No transmission is done on subcarriers beyond 427th subcarrier since their condition is too worse to achieve the target BER for the given E_b/N_o (25 dB). For fixed 32-QAM ACO-OFDM scheme, most of the odd subcarriers are left empty; hence, the achieved spectral efficiency is lower for the given E_b/N_o of 25 dB.

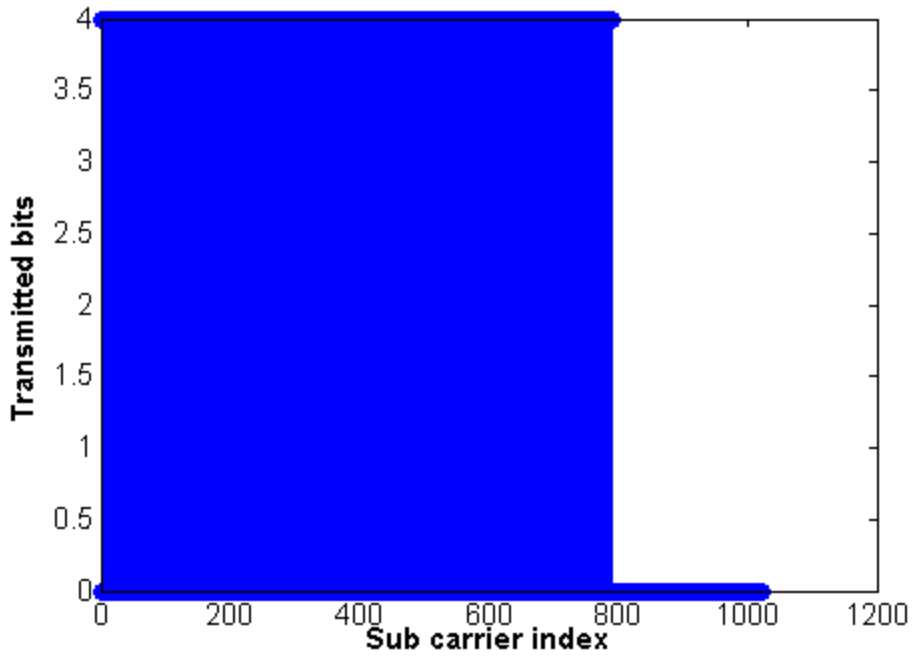

Figure 4. 31: Fixed 16-QAM ACO-OFDM sub carriers' bits allocation for E_b/N_o of 25 dB.

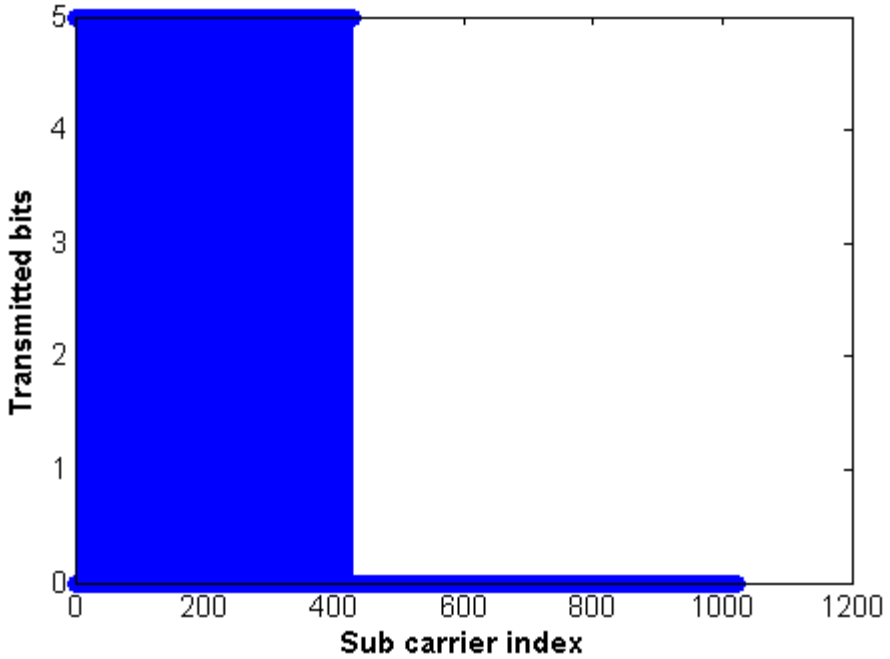

Figure 4. 32: Fixed 32-QAM ACO-OFDM sub carriers' bits allocation for E_b/N_o of 25 dB.

Chapter 5

Conclusions and Recommendations

In this research work, the performance of different unipolar OFDM schemes for IM/DD based optical wireless communication have been investigated for both AWGN and multipath optical wireless channel environments. The conventional well known state-of-the-art unipolar OFDM schemes such as ACO-OFDM and DCO-OFDM has been investigated with detailed analysis. The existing strength, weakness, and challenges of these unipolar OFDM schemes in relation to communication performances have been identified. The ACO-OFDM scheme has good energy efficiency but it has no good spectral efficiency. On the contrary, DCO-OFDM is energy inefficient scheme and it has good spectral efficiency. Moreover, a novel unipolar OFDM scheme called stratified asymmetrically clipped optical OFDM (STACO-OFDM) with a stratified architecture has been proposed in response to the weakness and challenges of ACO-OFDM and DCO-OFDM schemes. Furthermore, a well detailed and suitable theoretical and simulation analysis is given for the proposed scheme. Closed form theoretical formulas are also derived for both BER performance and spectral efficiency of the proposed unipolar STACO-OFDM scheme and compared to simulation results. The performances of the proposed STACO-OFDM scheme have also been compared to the performances of ACO-OFDM and DCO-OFDM in terms of spectral and energy/power efficiencies.

In addition, the potential of adaptive optical OFDM to enhance the spectral efficiency of OWC over frequency selective (dispersive) channel has been investigated by implementing frequency selective rate adaptive capability on ACO-OFDM. The spectral efficiency of rate adaptive M-QAM ACO-OFDM has been also compared to the spectral efficiency of fixed M-QAM ACO-OFDM scheme for purely diffused optical wireless physical link configuration.

5.1. Conclusions

The proposed STACO-OFDM has a stratified architecture in which even subcarriers are utilized on the first stratum and odd subcarriers are utilized on the rest of strata to carry information bits. In this thesis, a proper and detailed theoretical and simulation frame works has been given for the proposed STACO-OFDM scheme based on both AWGN and multipath channels. The formula for calculating spectral efficiency of STACO-OFDM is also accurately derived. The theoretical BER bound of STACO-OFDM is also derived in well detailed manner and compared to the simulated BER for both linear AWGN and multipath channel scenarios. As a result, very good agreements have been achieved between the theoretical BER bound and the simulated BER. The simulated BER is obtained by counting erroneously received bits in simulation environment whereas the theoretical BER is calculated from the derived BER formulas. Based different performance metrics such as spectral efficiency, energy efficiency and BER performance, performance comparisons have been made between STACO-OFDM scheme and well adopted ACO-OFDM and DCO-OFDM schemes both for linear AWGN and multipath channel environments. The results obtained from simulation have confirmed that STACO-OFDM has better performance compared to both ACO and DCO-OFDM schemes. On the other hand, the design complexity and cost of STACO-OFDM is high compared to both ACO and DCO-OFDM schemes.

5.1.1. Spectral efficienc

The spectral efficiency of STACO-OFDM is compared with the spectral efficiency of ACO-OFDM and DCO-OFDM for the same M-QAM modulation used on all the three schemes. For enough number of used strata, STACO-OFDM has offered equivalent spectral efficiency with DCO-OFDM and better spectral efficiency compared to ACO-OFDM. For five available strata, STACO-OFDM is able to offer 97 % of the spectral efficiency offered by DCO-OFDM and almost double the spectral efficiency offered by ACO-OFDM. The STACO-OFDM scheme has offered a spectral efficiency of 2 b/s/Hz by using 16-QAM on six strata which is equals to the spectral efficiency of the 16-QAM-DCO-OFDM. The 16-QAM-ACO-OFDM has offered a spectral efficiency of 1 b/s/Hz which is inferior performance compared to 16-QAM-DCO-OFDM and STACO-OFDM.

5.1.2. Energy efficiency

The energy efficiency of STACO-OFDM has been evaluated using both theoretical and simulation analysis in terms of BER vs. electrical SNR/optical SNR/optical power both for AWGN and multipath channel scenarios. Performance comparisons based on energy efficiency are also made between the three schemes (STACO-OFDM, ACO-OFDM, and DCO-OFDM) offering equal spectral efficiencies. Overall, the simulation and theoretical results have shown that STACO-OFDM is able to offer better electrical and optical energy efficiency compared to both ACO-OFDM and DCO-OFDM schemes. For both linear AWGN and multipath channels, the electrical energy savings of STACO-OFDM in comparison with ACO-OFDM and DCO-OFDM scheme has roughly started at achieved BER value of 10^{-1}.

Compared to ACO-OFDM in AWGN channel environment, the STACO-OFDM scheme offered 3, 5.5, and 7.5 dB electrical energy savings and 0.9, 3.2, and 5 dB optical energy savings at spectral efficiencies of 1.5, 2, 2.5 b/s/Hz respectively. The STACO-OFDM scheme also offered 3.9, 2.5, and 3 dB electrical energy savings and 5.7, 5.1, and 5 dB optical energy savings at spectral efficiencies of 1.5, 2, 2.5 b/s/Hz respectively compared to DCO-OFDM for AWGN channel situations.

In 10 ns rms delay spread multipath channel situations, the STACO-OFDM scheme offered 2.1, 4.5, and 6.3 dB electrical energy savings and 0.6, 1.5, and 2.4 dB optical energy savings at spectral efficiencies of 1.5, 2, 2.5 b/s/Hz respectively compared to ACO-OFDM. In comparison to DCO-OFDM at 10 ns channel delay spread, the STACO-OFDM scheme has shown 5.3, 4.3, and 4.2 dB electrical energy savings and 2.8, 2.5, and 2.2 dB optical energy savings at spectral efficiencies of 1.5, 2, 2.5 b/s/Hz respectively. In channel delay spread of 20 ns, the electrical energy savings of the STACO-OFDM scheme are 1.9, 4.3, and 6.3 dB at spectral efficiencies of 1.5, 2, 2.5 b/s/Hz respectively compared to ACO-OFDM. The DCO-OFDM scheme incurred electrical energy penalty of 1.9, 4.3, and 6.3 dB at spectral efficiencies of 1.5, 2, 2.5 b/s/Hz respectively compared to STACO-OFDM at 20 ns channel delay spread.

5.1.3. Performance of adaptive optical OFDM

The performance of frequency selective rate adaptive ACO-OFDM has been investigated in terms of offered spectral efficiency and comparisons have been made to the fixed M-QAM based ACO-OFDM on diffused optical wireless link configuration. The M-QAM modulation with $M = 4,8,16,32$ have been considered for rate adaption on AO-OFDM for system having a target BER of 10^{-3}. The simulation results have shown that adaptive M-QAM ACO-OFDM can offer better spectral efficiency compared to fixed M-QAM ACO-OFDM schemes. For SNR values, $E_b/N_o = 25\ dB$, adaptive ACO-OFDM has offered a spectral efficiency of $\approx 1\ b/s/Hz$ while those fixed M-QAM based ACO OFDM schemes offered a spectral efficiency less than $0.75\ b/s/Hz$.

5.2. Recommendations

Zero level single sided signal clipping has been considered at the optical front end of STACO-OFDM in the overall theoretical analysis and simulations given in chapter (3) and chapter (4). However, the time domain OFDM signal in OWC might experience double sided signal clipping in some scenarios due to the limited dynamic range of the LED at the transmitter. Therefore, future work in this area may include the development of analytical frame work and simulation analysis for the effect of non-linear distortion due to double sided signal clipping on the performance of STACO-OFDM. Furthermore, the potential of bit and power loading algorithms can be investigated for performance improvement of STACO-OFDM in a realistic optical channel in the future work.

References

[1] S.K. Yong and C. Chong, "An overview of multigigabit wireless through millimeter wave technology: potentials and technical challenges," EURASIP Journal of Wireless Communication Networks, vol. 2007, no. 1, pp. 50-50, Jan. 2007.

[2] P. Cheolhee and T. Rappaport, "Short-range wireless communications for nextgeneration networks: UWB, 60 GHz millimeter-wave WPAN, and zigbee," IEEE Wireless Communications, vol. 14, no. 4, pp. 70-78, 2007.

[3] J. Kahn and J. Barry, "Wireless infrared communications," in Proceedings of the IEEE, 1997.

[4] P. Barker and A. Boucouvalas, "Performance modeling of the IrDA protocol for infrared wireless communications," IEEE Communications Magazine, vol. 36, no. 12, p. 113–117, 1998.

[5] D. K. Borah, A. C. Boukouvalas, C. C. Davis, and S. H. H. Yiannopoulos, "A review of communication-oriented opticalwireless systems," EURASIP Journal on Wireless Communications and Networking, vol. 2012, no. 1, p. 91, Mar. 2012.

[6] Z. Ghassemlooy, S. Arnon, M. Uysal, Z. Xu, and J. Cheng, "Emerging Optical Wireless Communications-Advances and Challenges," IEEE Journal on Selected Areas in Communications, vol. 33, no. 9, pp. 1738 - 1749, Sept. 2015.

[7] N. Fernando, "Non-coherent OFDM Techniques," PhD thesis, Monash University, 2014.

[8] J. Armstrong, "OFDM for Optical Communications," Journal of Lightwave Technology, vol. 27, no. 3, pp. 189 - 204, Feb. 2009.

[9] L. Litwin, "An introduction to multicarrier modulation," IEEE Potentials , vol. 19, no. 2, pp. 36 - 38, May 2000.

[10] S. K. Hashemi, Z. Ghassemlooy, L. Chao, and D. Benhaddou, "Orthogonal frequency division multiplexing for indoor optical wireless communications using visible light LEDs," in IEEE International Symposium on Communication Systems, Networks and Digital Signal Processing (CNSDSP), Graz, Austria, 2008.

[11] J. Armstrong and A. Lowery, "Power Efficient Optical OFDM," Electronics Letters, vol. 42, no. 6, p. 370–372, March 16, 2006.

[12] C. V. N. Index, "Global mobile data traffic forecast update, 2016-2021," Mar. 2017.

[13] J. R. Barry, Wireless Infrared Communications, Springer, 1994.

[14] Z. Ghassemlooy, W. Popoola, and S. Rajbhandari, Optical wireless communications: system and channel modeling with MATLAB, 1st ed., CRC press, 2012.

[15] J. B. Carruthers and J. M. Kahn, "Multiple-subcarrier Modulation for Nondirected Wireless Infrared Communication," IEEE Journal on Selected Areas in Communications, vol. 14, no. 3, p. 538–546, April 1996.

[16] T. Ohtsuki, "Multiple–Subcarrier Modulation in Optical Wireless Communications," IEEE Communications Magazine, vol. 41, no. 3, p. 74–79, Mar. 2003.

[17] J. Armstrong and B. J. C. Schmidt, "Comparison of Asymmetrically Clipped Optical OFDM and DC-Biased Optical OFDM in AWGN," IEEE Communications Letters, vol. 12, vol. 12, no. 5, p. 343–345, May 2008.

[18] N. Fernando, Y. Hong, and E. Viterbo, "Flip-OFDM for optical wireless communications," in IEEE Information Theory Workshop, Paraty, Brazil, 2011.

[19] D. Tsonev, S. Sinanovic, and H. Haas, "Novel Unipolar Orthogonal Frequency Division Multiplexing (U-OFDM) for Optical Wireless," in IEEE Vehicular Technology Conference (VTC Spring), Yokohama, Japan, 2012.

[20] A. G. Bell, "Selenium and the Photophone," Nature, vol. 22, no. 569, p. 500–503, 1880.

[21] R. N. Hall, G. E. Fenner, J. D. Kingsley, T. J. Soltys, and R. O. Carlson, "Coherent Light Emission from GaAs Junctions," Physical Review Letter, vol. 9, no. 9, p. 366–369, Nov. 1962.

[22] M. I. Nathan, W. P. Dumke, G. Burns, and F. H. Dill, "Stimulated Emission of Radiation from GaAs p-n Junctions," ppl. Physical Letter, vol. 1, no. 3, p. 62, 1962.

[23] K.K. Wong, T. O'Farrell, and M. Kiatweerasakul, "Infrared wireless communication using spread sprectrum techniques," in IEE Proceedings of Optoelectronics, 2000.

[24] K. K. Wong and T. O'Farrell, "Spread spectrum techniques for indoor wireless IR communications," IEEE Wireless Communications, vol. 10, no. 2, pp. 54-63, Apr. vol. 10, pp. , 2003.

[25] H. Elgala, R. Mesleh, and H. Haas, "Indoor Optical Wireless Communication: Potential and State-of-the-Art," IEEE Communication Magazine., vol. 49, no. 9, pp. 56-62, 2011.

[26] V. Jungnickel, A. Forck, T. Haustein, U. Krueger, V. Pohl, and C. von Helmolt, "Electronic tracking for wireless infrared communication," IEEE Transactions on Wireless Communications, vol. 2, no. 5, pp. 989 - 999, Sept 2003.

[27] J. Liu, W. Noonpakdee, H. Takano, and S. Shimamoto, "Foundational Analysis of Spatial Optical Wireless Communication Utilizing Image Sensor," in IEEE International Conference on Imaging Systems and Techniques (IST), Penang, Malaysia, 2011.

[28] I. Takai, S. Ito, K. Yasutomi, K. Kagawa, M. Andoh, and S. Kawahito, "LED and CMOS Image Sensor Based Optical Wireless Communication System for Automotive Applications," IEEE Photonnic Journal, vol. 5, no. 5, Oct. 2013.

[29] Z. Wang, D. Tsonev, S. Videv, and H. Haas, "Towards self-powered solar panel receiver for optical wireless communication," in IEEE International Conference in Communications (ICC), Sydney, Australia, 2014.

[30] S. Schmid, G. Corbellini, S. Mangold, and T. Gross, "An LED-to-LED Visible Light Communication System with Software-based Synchronization," in IEEE Globecom Workshops (GC Wkshps), Anaheim, CA, USA, 2012.

[31] D. Giustiniano, N. Tippenhauer, and S. Mangold, "Low-complexity Visible Light Networking with LED-to-LED communication," in IFIP Wireless Days (WD), Dublin, Ireland, 2012.

[32] R. Mesleh, R. Mehmood, H. Elgala, and H. Haas, "An Overview of Indoor OFDM/DMT Optical Wireless Communication Systems," in IEEE International Symposium on Communication Systems, Networks and Digital Signal Processing (CSNDSP), Newcastle, U.K, 2010.

[33] H. Elgala, R. Mesleh, and H. Haas, "Indoor Broadcasting via White LEDs and OFDM," IEEE Transactions on Consumer Electronics, vol. 55, no. 3, p. 1127–1134, Aug. 2009.

[34] J. V. G. Grubor, "Adaptive modulation technique for broadband communication in indoor optical wireless systems,"PhD thesis, University of Berlin, 2009.

[35] J.B. Carruthers and J.M Kahn, "Modelling of Nondirected Wireless Infrared Channel," IEEE Transactions on Communication, vol. 45, no. 10, pp. 1260-1268, Oct. 1997.

[36] S. K. Wilson and J. Armstrong, "Transmitter and receiver methods for improving asymmetrically-clipped optical OFDM," IEEE Transactions on Wireless Communications, vol. 8, no. 9, p. 4561–4567, Sep. 2009.

[37] P. Saengudomlert, "On the Benefits of Pre-Equalization for ACO-OFDM and Flip OFDM Indoor Wireless Optical Transmissions over Dispersive Channels," journal of Lightwave technology, vol. 32, no. 1, pp. 70 - 80, Jan. 2014.

[38] J. Panta, P. Saengudomlert, and K. Sripimanwat, "Performance Improvement of ACO-OFDM Indoor Optical Wireless Transmissions Using Partial Pre-Equalization," ECTI Transactions on Electrical Engineering., Electronics, and Communications., vol. 14, no. 1, pp. 1-11, Feb. 2015.

[39] F. R. Gfeller and U. Bapst, "Wireless in-house data communication via diffuse infrared radiation," Proceedings of the IEEE, vol. 67, no. 11, pp. 1474-1486, Nov. 1979.

[40] G. P. Agrawal, Fiber-Optic Communication Systems, John Wiley and Sons, 1997.

[41] K. Schneider and H. Zimmermann, Highly Sensitive Optical Receivers, Springer, 2006.

[42] F. Tavernier and M. Steyaert, High-Speed Optical Receivers with Integrated Photodiode in Nanoscale CMOS, Springer, 2011.

[43] T. Hunziker, "Multicarrier Modulation Techniques for Bandwidth Efficient Fixed Wireless Access Systems," 2002.

[44] J. Vucic, C. Kottke, S. Nerreter, K. D. Langer, and J. W. Walewski, "513 Mbit/s Visible Light Communications Link Based on DMT-Modulation of a White LED," Journal of Lightwave Technology, vol. 28, no. 24, p. 3512–3518, Dec. 2010.

[45] H. Elgala, R. Mesleh, H. Haas, and B. Pricope, "OFDM Visible Light Wireless Communication Based on White LEDs," in Proceedings of the 64th IEEE Vehicular Technology (VTC) , Dublin, Ireland, 2007.

[46] S. Dimitrov, S. Sinanovic, and H. Haas, "Signal Shaping and Modulation for Optical Wireless Communication," IEEE/OSA Journal on Lightwave Technology (IEEE/OSA JLT), vol. 30, no. 9, p. 1319–1328, May 2012.

[47] H. Elgala, R. Mesleh, and H. Haas, "Practical Considerations for Indoor Wireless Optical System Implementation using OFDM," in Proceedings of the IEEE 10th International Conference on Telecommunications (ConTel), Zagreb, Croatia, 2009.

[48] R. Mesleh, H. Elgala, and H. Haas, "Performance Analysis of Indoor OFDM Optical Wireless Communication Systems," in IEEE Wireless communication and networking conference, Shanghai, China, 2012.

[49] J. Panta, P. Saengudomlert, and K. Sripimanwat, "Optimization of operating BW for indoor optical wireless OFDM transmission with IM/DD," in International Conference on Electrical Engineering/Electronics, Computer, Telecommunication and Information Technologies (ECTI-CON), Nakhon Ratchasima, Thailand, 2014.

[50] S. Dimitrov, S. Sinanovic, and H. Haas, "A comparison of OFDM-based modulation schemes for OWC with clipping distortion," in IEEE GLOBECOM Workshops , Houston, TX, USA, 2011 .

[51] P. Saengudomlert, J. Panta, and K. Sripimanwat, "Optimal sizing of QAM constellation for indoor optical wireless OFDM transmissions without bandwidth limitation," in IEEE International Electrical Engineering Congress (iEECON), Chonburi, Thailand, 2014.

[52] S. Dimitrov, S. Sinanovic, and H. Haas, "Clipping Noise in OFDM-based Optical Wireless Communication Systems," IEEE Transactions on Communications (IEEE TCOM), vol. 60, no. 4, p. 1072–1081, Apr. 2012.

[53] S. Dimitrov, H. Haas, Principles of LED Light Communications: Towards Networked Li-Fi, Cambridge University Press, 2015.

[54] J. I. Yong, "Modulation and demodulation apparatuses and methods for wired/wireless communication system," United States Patent and Trademark Office (USTPO), 2011.

[55] S. D. Dissanayake, and J. Armstrong, "Comparison of ACO-OFDM, DCO-OFDM and ADO-OFDM in IM/DD systems," Journal of Lightwave Technology, vol. 31, no. 7, pp. 1063-1072, Apr. 2013.

[56] D. Tsonev, S. Videv, and H. Haas, "Unlocking spectral efficiency in intensity modulation and direct detection," IEEE Journal of Selected Areas in Communications, vol. 33, no. 9, pp. 1758-1770, Sept. 2015.

[57] M. S. Islim, D. Tsonev, and H. Haas, "A Generalized Solution to the Spectral Efficiency Loss in Unipolar Optical OFDM-based Systems," in IEEE International Conference on Communications (ICC), London, UK, 2015.

[58] P. S. Chow, J. M. Cioffi, and J. A. C. Bingham, "A practical discrete multi-tone transceiver loading algorithm for data transmission over spectrally shaped channels," IEEE Transactions on Communications., vol. 43, no. 234, p. 773–775, 1995 .

[59] C. Y. Wong, R.S. Cheng, K.B. Lataief, and R.D. Murch, "Multiuser OFDM with adaptive subcarrier, bit, and power allocation," IEEE Journal of Selected Areas in Communications, vol. 17, no. 10, pp. 1747 - 1758, Oct. 1999.

[60] N. Zervos and I. Kalet, "Optimized decision feedback equalization versus optimized orthogonal frequency division multiplexing for high-speed data transmission over the local cable network," in IEEE Conference on Communications, Boston, USA, 1989.

[61] A. Czylwik, "Adaptive OFDM for wideband radio channels," in Global Telecommunication Conference (GLOBECOM), London, UK, 1996.

[62] O. Gonzalez, R. Perez-Jimenez, S. Rodriguez, J. Rabadan, and A. Ayala, "Adaptive OFDM system for communications over the indoor wireless optical channel," IEE Proceedings - Optoelectronics, vol. 153, no. 4, p. 139–144, Aug. 2006 .

[63] N. Kalikulov and R. C. Kizilirmak, "Adaptive OFDM for VLC systems with multiple transmitters," in IEEE Wireless Symposium (IWS), Shanghai, China, 2016.

[64] J. Grubor, V. Jungnickel, and K. D. Langer, "Adaptive Optical Wireless OFDM System with Controlled Asymmetric Clipping," in IEEE Conference Signals, Systems and Computers, Pacific Grove, USA, 2007.

[65] X. Li, R. Mardling, and J. Armstrong, "Channel Capacity of IM/DD Optical Communication Systems and of ACO-OFDM," in Proeedings of IEEE International Conference on Communications, Glasgow, UK, 2007.

[66] B. P. Lathi and Z. Ding, Modern Digital and Analog Communication Systems, 4th ed., Oxford University Press, 2009.

[67] S. Haykin and M. Moher, An Introduction to Analog and Digital Communications, 2nd ed., Wiley, 2006.

[68] J. Burkardt, "The Truncated Normal Distribution," Graduate students seminar, Florida State University,Departmentof Scientific Computing, 2014

URL: http://people.sc.fsu.edu/~jburkardt/presentations/ truncated normal 2014 fsu.pdf

[69] M. Mossaad, "Theoretical Analysis and Simulation of IM/DD Optical OFDM Systems," McMaster Universit, URL: http://www.academia.edu/19322099.

[70] F. Xiong, Digital Modulation Techniques, 2nd ed., Artech House Press, 2006.

[71] X. Li and J. Vucic, "On the Capacity of Intensity-Modulated Direct-Detection Systems and the Information Rate of ACO-OFDM for Indoor Optical Wireless Applications," IEEE transactions on communications, vol. 60, no. 3, pp. 799 - 809, Mar. 2012.

[72] K.R. Panta and J. Armstrong, "Effects of clipping on the error performance of OFDM in frequency selective fading channels," IEEE Transactions on Wireless Communications, vol. 3, no. 2, pp. 668 - 671, Mar. 2004.

[73] H. Steendam and M. Moeneclaey, "Analysis and optimization of the performance of OFDM on frequency-selective time-selective fading channels," IEEE Transactions on Communications, vol. 47, no. 12, pp. 1811 - 1819, Dec. 1999.

[74] J. Foerster, "The effects of multipath interference on the performance of UWB systems in an indoor wireless channel," in IEEE Vehicular Technology Conference, Rhodes, Greece, 2001.

[75] S. Rajbhandari, Z. Ghassemlooy, and M. Angelova, "Bit error performance of diffuse indoor optical wireless channel pulse position modulation system employing artificial neural networks for channel equalization," IET Optoelectronics, vol. 3, no. 4, pp. 169 - 179, Aug. 2009.

[76] L. Rugini, P. Banelli, and G. Leus, "OFDM Communications over Time-Varying Channels," in Wireless Communications Over Rapidly Time-Varying Channels, Academic Press, 2011, pp. 285-297.

[77] B. Muquet, Z. Wang, G. B. Giannakis, M. de Courville, and P. Duhamel, "Cyclic Prefixing or Zero Padding for Wireless Multicarrier Transmissions," IEEE transactions on communications, vol. 50, no. 12, pp. 2136 - 2148, Dec. 2002.

[78] D. Tsonev, S. Sinanovic, H. Haas, "Complete Modeling of Nonlinear Distortion in OFDM-Based Optical Wireless Communication," Journal of Lightwave Technology , vol. 31, no. 18, pp. 3064 - 3076, Sept. 2013 .

[79] S. Dimitrov, S. Sinanovic , and H. Haas, "Double-Sided Signal Clipping in ACO-OFDM Wireless Communication Systems," in IEEE International Conference on Commun. (ICC), , Kyoto, Japan, 2011.

[80] K.R. Rao, D. N. Kim, and J. J. Hwang, "Two-Dimensional Discrete Fourier Transform," in Fast Fourier Transform - Algorithms and Applications, Springer, 2010, pp. 127-170.

[81] D. Dissanayake, K. Panta, and J. Armstrong, "A novel technique to simultaneously transmit ACO-OFDM and DCO-OFDM in IM/DD systems," in IEEE GLOBECOM Workshops (GC Wkshps), Houston, USA, 2011.

[82] S. K. Wilson and J. Armstrong, "Digital Modulation Techniques for Optical Asymmetrically-Clipped OFDM," in *IEEE Wireless Commun. and Net. Conference (WCNC)* , Las Vegas, USA, 2008.

Appendices

A. Phase of diffused optical CIR in frequency domain

The magnitude of phase of the diffused optical wireless CIR generated by ceiling bounce model for channel delay spread of 10 ns and 20 ns is given in Fig. A.1 as follows.

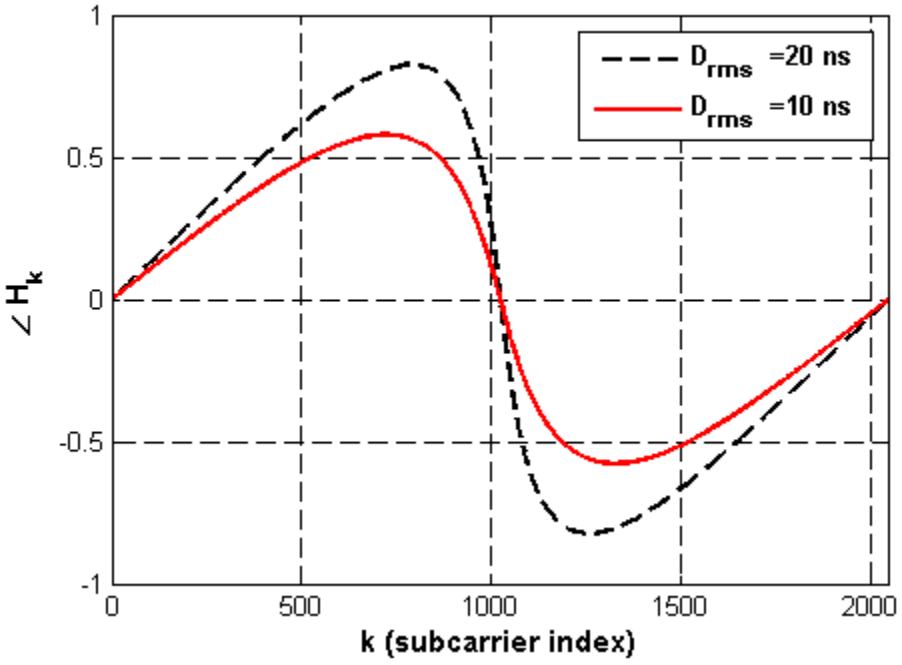

Figure. A.1: the angle of the frequency domain channel impulse response in radian.

B. Matlab code for BER simulation of STACO-OFDM

B.1 STACO-OFDM over linear AWGN channel

```
N_aco1=2048; % IFFT points at 1st stratum
N_aco2=1024; % IFFT points at 2nd stratum
N_aco3=512;  % IFFT points at 3rd stratum
N_4=2048;    % IFFT points for ACO-OFDM and DCO-OFDM stratum
M_aco1=16;   % Level of QAM modulation at 1st stratum of STACO-OFDM
M_aco2=8;    % Level of QAM modulation at 2nd stratum of STACO-OFDM
M_aco3=4;    % Level of QAM modulation at 3rd stratum of STACO-OFDM
M_aco4=64;   % Level of QAM modulation for ACO-OFDM
M_dco=8;     % Level of QAM modulation for DCO-OFDM
N_data_dco=3069;  % bits transmitted in one DCO-OFDM frame
N_data1=2044;     % bits transmitted at the 1st stratum in one STCO-OFDM frame
N_data2=768;      % bits transmitted at the 2nd stratum in one STCO-OFDM frame
N_data3=256;      % bits transmitted at the 3rd stratum in one STCO-OFDM frame
N_data4=3072;     % bits transmitted at in one ACO-OFDM frame
N_Iteration=500;  % size of iteration for numerical simulation
EbNo_aco=[-13:1:30]; % SNR in terms of energy per bit to noise ratio in dB
se1=(4*511)/2048;    % spectral efficiency at 1st stratum of STACO-OFDM
se2=0.375;           % spectral efficiency at 2nd stratum of STACO-OFDM
se3=0.125;           % spectral efficiency at 3rd stratum of STACO-OFDM
se_total=se1+se2+se3; % spectral efficiency the overall STACO-OFDM scheme
beta1=10^(-1.8/20);   % scaling factor at 1st stratum of STACO-OFDM
beta2=10^(1.4/20);    % scaling factor at 2nd stratum of STACO-OFDM
beta3=10^(5/20);      % scaling factor at 3rd stratum of STACO-OFDM
EbNo_act_dco=EbNo_aco+7;
%creating modulation and demodulation objects
H_dco=modem.qammod(M_dco); %16QAM object
H_dco.InputType='Bit';
H_dco.SymbolOrder='gray'; %to get gray code
```

```
H_aco1=modem.qammod(M_aco1); %32QAM object
H_aco1.InputType='Bit';
H_aco1.SymbolOrder='gray';
H_aco2=modem.qammod(M_aco2); %16QAM object
H_aco2.InputType='Bit';
H_aco2.SymbolOrder='gray'; %to get gray
H_aco3=modem.qammod(M_aco3); %16QAM object
H_aco3.InputType='Bit';
H_aco3.SymbolOrder='gray';
H_aco4=modem.qammod(M_aco4); %64QAM object
H_aco4.InputType='Bit';
H_aco4.SymbolOrder='gray';
m=sqrt((10^0.7)-1); % dc bias for DCO-OFDM
for aa_aco=1:length(EbNo_aco)
ebNo_aco=EbNo_aco(aa_aco);
SNR_dco=EbNo_aco(aa_aco)+7+10*log10(3);% Effective SNR of DCO-OFDM
%TRANSMITTER
for (k=1:N_Iteration)
generate_data_aco1=randi([0 1],N_data1,1); %Bits generation for 1st stratum of STACO-OFDM
generate_data_aco2=randi([0 1],N_data2,1); %Bits generation for 2nd stratum of STACO-
OFDM
generate_data_aco3=randi([0 1],N_data3,1); %Bits generation for 3rd stratum of STACO-
OFDM
%%%%%%%%%%%%%%%%%%%%%%%%%%%%%%%%%%%%%%%%%%%%%%%%%
generate_data_aco4=randi([0 1],N_data4,1); %Bits generation for ACO-OFDM
generate_data_dco=randi([0 1],N_data_dco,1); %Bits generation for DCO-OFDM
%%%%%%%%%%%%%%%%%%%%%%%%%%%%%%%%%%%%%%%%%%%%%%%%%
X_aco1=modulate(H_aco1, generate_data_aco1);%QAM modulation at 1st stratum of STACO-
OFDM
X_aco2=modulate(H_aco2, generate_data_aco2);%QAM modulation at 2nd stratum of STACO-
OFDM
```

```
X_aco3=modulate(H_aco3, generate_data_aco3);%QAM modulation at 3rd stratum of STACO-
OFDM
%%%%%%%%%%%%%%%%%%%%%%%%%%%%%%%%%%%%%%%%%%%%%%%
X_aco4=modulate(H_aco4, generate_data_aco4);%QAM modulation for ACO-OFDM
X_dco=modulate(H_dco, generate_data_dco);%QAM modulation for DCO-OFDM
%%%%%%%%%%%%%%%%%%%%%%%%%%%%%%%%%%%%%%%%%%%%%%%
hermitian_symetric_aco1=[0;X_aco1;0;conj(flipud(X_aco1))]; %hrmitian symm at 1st stratum
parellel_serial_aco1=reshape( hermitian_symetric_aco1,1,length( hermitian_symetric_aco1));%
serial to parallel
zero_table_aco1=zeros(1,N_aco1); %zeros generation
zero_table_aco1(1:2:end)=parellel_serial_aco1; %odd carriers are loaded with zero
ifft_data_aco1=ifft(zero_table_aco1.');% IFFT
ifft_data_aco111=-1.*ifft_data_aco1;  % flipping of samples polarity
ifft_data_aco1(1025:end)=ifft_data_aco111(1025:end);% flipped samples on 2nd subframe
clipped1_aco1=max(ifft_data_aco1,0); %asymmetrically clipping of negative samples
clipped_aco1=(1/beta1)*(clipped1_aco1.');%scaling
clipped_aco1_new1= clipped_aco1(1:1024);% 1st sub frame of 1st stratum
clipped_aco1_new2= clipped_aco1(1025:end);% 2nd sub frame of 1st stratum
p1=(norm(clipped_aco1_new1)^2)/length(clipped_aco1_new1);% electrical power
p12=(norm(clipped_aco1_new2)^2)/length(clipped_aco1_new2);% electrical power
%%%%%%%%%%%%%%%%%%%%%%%%%%%%%%%%%%%%%%%%%%%%%%%
hermitian_symetric_aco2=[X_aco2;conj(flipud(X_aco2))]; %hrmitian symm 2nd stratum
parellel_serial_aco2=reshape( hermitian_symetric_aco2,1,length(
hermitian_symetric_aco2));% seri to parall.
zero_table_aco2=zeros(1,N_aco2); %zeros generation.
zero_table_aco2(2:2:end)=parellel_serial_aco2; % even carriers are loaded with zeros
%%%%%%%%%%%%%%%%%%%%%%%%%%%%%%%%%%%%%%%%%%%%%%%
ifft_data_aco2=ifft(zero_table_aco2.');% IFFT operation
clipped1_aco2=max(ifft_data_aco2,0); %assymetrically clipping
clipped_aco2=(1/beta2)*(1/sqrt(2))*(clipped1_aco2.'); % scaling at 2nd stratum
p2=(norm(clipped_aco2)^2)/length(clipped_aco2);% Electrical power
```

```
%%%%%%%%%%%%%%%%%%%%%%%%%%%%%%%%%%%%%%%%%%%%%%%
hermitian_symetric_aco3=[X_aco3;conj(flipud(X_aco3))]; %hrmitian symm at 3rd stratum
parellel_serial_aco3=reshape( hermitian_symetric_aco3,1,length(
hermitian_symetric_aco3));%seri to paral.
zero_table_aco3=zeros(1,N_aco3); %zeros generation
zero_table_aco3(2:2:end)=parellel_serial_aco3; % even carriers are loaded with zeros
%%%%%%%%%%%%%%%%%%%%%%%%%%%%%%%%%%%%%%%%%%%%%%%%%
 ifft_data_aco3=ifft(zero_table_aco3.'); %IFFT opren.
 clipped1_aco3=max(ifft_data_aco3,0); %asymmetrically clipping of negative samples
 clipped_aco3=(1/beta3)*(1/2)*(clipped1_aco3.');% scaling
 clipped_aco3_new=[clipped_aco3 clipped_aco3]; % merging to construct subframes
 p3=(norm(clipped_aco3_new)^2)/length(clipped_aco3_new);% electrical power
%%%%%%%%%%%%%%%%%%%%%%%%%%%%%%%%%%%%%%%%%%%%%%%%%%%
 hermitian_symetric_aco4=[X_aco4;conj(flipud(X_aco4))]; %hrmitian symm for ACO-OFDM
 parellel_serial_aco4=reshape( hermitian_symetric_aco4,1,length( hermitian_symetric_aco4));
 zero_table_aco4=zeros(1,N_4); %zeros gen.
 zero_table_aco4(2:2:end)=parellel_serial_aco4; % even carriers are loaded with zeros
 ifft_data_aco4=ifft(zero_table_aco4.');%IFFT oprn.
 clipped1_aco4=max(ifft_data_aco4,0); %asymmetrically clipping of negative samples
 clipped_aco4=clipped1_aco4.';
%%%%%%%%%%%%%%%%%%%%%%%%%%%%%%%%%%%%%%%%%%%%%%%%%%%
 hermitian_symetric_dco=[0;X_dco;0;conj(flipud(X_dco))]; %hrmitian symm for DCO-OFDM
  parellel_serial_dco=reshape( hermitian_symetric_dco,1,length( hermitian_symetric_dco));
  ifft_data_dco=ifft(parellel_serial_dco.'); %IFFT
  p=(norm(ifft_data_dco)^2)/length(ifft_data_dco);% electrical power
  pp=m*sqrt(p);% dc bias on samples
  dc_ifft_data_dco=ifft_data_dco+pp;% dc bias added on samples
  clipped1_dco=max(dc_ifft_data_dco,0); %asymmetrically clipping of negative samples
  clipped_dco=clipped1_dco.';
%%%%%%%%%%%%%%%%%%%%%%%%%%%%%%%%%%%%%%%%%%%%%%%%%%%
```

```
DATA_tot_1=clipped_aco1_new1+ clipped_aco2+clipped_aco3_new;% 1st subframe of
STACO-OFDM for 1st trans. session
DATA_tot_2=clipped_aco1_new2+ clipped_aco2+clipped_aco3_new;% 2nd subframe of
STACO-OFDM for 2nd trans. session
p4_new1=(norm(DATA_tot_1)^2)/length(DATA_tot_1);% electrical power
p4_new2=(norm(DATA_tot_2)^2)/length(DATA_tot_2);% electrical power
p4= p4_new1+ p4_new2;
%%%%%%%%%%%%%%%%%%%%%%%%%%%%%%%%%%%%%%%%%%%%%%%%%%%%%%%%%%%%%%%%%%%%%%%%
alpha1=(p4/(2*p1))*(se1/se_total);% SNR per bit increment of STACO-OFDM wrt 1st stratum
alpha2=(p4/(2*p2))*(se2/se_total);% SNR per bit increment of STACO-OFDM wrt 2nd stratum
alpha3=(p4/(2*p3))*(se3/se_total);% SNR per bit increment of STACO-OFDM wrt 3rd stratum
SNR1=ebNo_aco+10*log10(4)+10*log10(se_total/se1)-10*log10(2);% effective SNR of
STACO-OFDM
SNR2=ebNo_aco+10*log10(6)-10*log10(2);%effective SNR of ACO-OFDM
%%%%%%%%%%%%%%%%%%%%%%%%%%%%%%%%%%%%%%%%%%%%%%%%%%%%%%%%%%%%%%%%%%%%%%%%
rx_aco_new1=awgn(DATA_tot_1,SNR1,'measured');% Adding AWGN samples
rx_aco_new2=awgn(DATA_tot_2,SNR1,'measured');% Adding AWGN samples
rx_aco_singl=awgn(  clipped_aco4,SNR2,'measured');% Adding AWGN samples
rx_dco=awgn(clipped_dco,SNR_dco,'measured');% Adding AWGN samples
%sucessive demodulation for STACO-OFDM information recovery
rx4_aco55=rx_aco_new1(1:end)-rx_aco_new2(1:end);% subtracting 2nd subframe from 1st
subframe
rx4_aco55555=(beta1)*(rx4_aco55); % removing the scaling factor form 1st stratum info
zero_table_aco11_new=zeros(1,N_aco1); % zero generation
zero_table_aco11_new(1:1:1024)=rx4_aco55555; % padding of zeros
J_J4_aco=fft(zero_table_aco11_new');   % FFT opration
f_aco= J_J4_aco(1:2:N_aco1);%removing odd carriers
p_aco=2*f_aco((2:512),:); %1st half of the data
p_k_aco=p_aco;
%%%%%%%%%%%%demodulation object
  H2_aco=modem.qamdemod(H_aco1);
```

```
   H2_aco.OutputType='Bit';
   H2_aco.SymbolOrder='gray';
   demodulate_data_aco=demodulate(H2_aco, p_k_aco);%demodulation of symbols
   demodulate_data2_aco=reshape(demodulate_data_aco,1,N_data1);
%%%%%%%%%%%%%%%%%%%%%%%%%%%%%%%%%%%%%%%%%%%%%%%%%%
 % remodulating the iformation recovered at 1st stratum
    X_aco11=modulate(H_aco1, demodulate_data_aco);
    hermitian_symetric_aco11=[0;X_aco11;0;conj(flipud(X_aco11))]; %hrmitian symm
    parellel_serial_aco11=reshape( hermitian_symetric_aco11,1,length
    (hermitian_symetric_aco11));
     zero_table_aco11=zeros(1,N_aco1); %zeros gen
     zero_table_aco11(1:2:end)=parellel_serial_aco11; % odd carriers are loaded with zeros
     ifft_data_aco11=ifft(zero_table_aco11.');
     ifft_data_aco11111=-1.*ifft_data_aco11;
     ifft_data_aco11(1025:end)=ifft_data_aco11111(1025:end);
     clipped1_aco11=max(ifft_data_aco11,0); %asymmetrically clipping
     clipped_aco11=(1/beta1)*(clipped1_aco11.');
     clipped_aco1_new11= clipped_aco11(1:1024);
     clipped_aco1_new22= clipped_aco11(1025:end);
%%%%%%%%%%%%%%%%%%%%%%%%%%%%%%%%%%%%%%
 % 2nd stratum information recoverey
     rx_aco11= rx_aco_new1(1:end)-clipped_aco1_new11(1:end);% removing contribution
     of 1st  stratum
     rx_aco111=rx_aco_new2(1:end)-clipped_aco1_new22(1:end);%removing
     contribution   of 1st stratum
     rx4_aco1=rx_aco11(1:end)+rx_aco111(1:end);% adding subframes for 2nd stratum
     rx4_aco12=(sqrt(2)/2)*rx4_aco1;% removing the scaling
     rx4_aco13=(beta2)*(rx4_aco12.');%removing the scaling
     J_J4_aco1=fft(rx4_aco13);% FFT oprn.
    f_aco1= J_J4_aco1(2:2:N_aco2);%removing even carriers
  p_aco1=f_aco1((1:256),:); %1st half of the data
```

```
  p_k_aco1=2*p_aco1;
%%%%%%%%%%%%%%%%%%%%%%%%%%%%%%%%%%%%%%%%%%%%%%
 % demodulation of symbols at 2nd stratum
  H2_aco1=modem.qamdemod(H_aco2);
  H2_aco1.OutputType='Bit';
  H2_aco1.SymbolOrder='gray';
  demodulate_data_aco1=demodulate(H2_aco1, p_k_aco1);%demodulation of symbols
  demodulate_data2_aco1=reshape(demodulate_data_aco1,1,N_data2);
%%%%%%%%%%%%%%%%%%%%%%%%%%%%%%%%%%%%%%%%%%%%%%
 % remodulation of information recovered at 2nd stratum
   X_aco22=modulate(H_aco2, demodulate_data_aco1);
   hermitian_symetric_aco22=[X_aco22;conj(flipud(X_aco22))]; %hrmitian symm
   parellel_serial_aco22=reshape( hermitian_symetric_aco22,1,length
   (hermitian_symetric_aco22));
   zero_table_aco22=zeros(1,N_aco2); %zeros generation
   zero_table_aco22(2:2:end)=parellel_serial_aco22; % even carriers are loaded with zeros
   ifft_data_aco22=ifft(zero_table_aco22.');% IFFT
  clipped1_aco222=max(ifft_data_aco22,0); %asymmetrically clipping
  clipped_aco222=(1/beta2)*(1/sqrt(2))*(clipped1_aco222.');
%%%%%%%%%%%%%%%%%%%%%%%%%%%%%%%%%%%%%%%%%%%%%%
  % 3Rd stratum information recovery
  rx_aco221_new1=rx_aco11(1:end)-clipped_aco222(1:end);%removing contribution
  of 3rd stratum information
  rx_aco221_new2=rx_aco111-clipped_aco222;%removing contribution of
  3rd stratum information
   rx4_aco2=rx_aco221_new1(1:512)+rx_aco221_new1
  (513:1024)+ rx_aco221_new2(1:512) +rx_aco221_new2(513:1024);
   rx4_aco22=(1/2)*rx4_aco2;% removing scaling factor
   rx4_aco222=(beta3)*(rx4_aco22.');% removing scaling factor
   J_J4_aco2=fft(rx4_aco222);% FFT oprn.
 f_aco2= J_J4_aco2(2:2:N_aco3);%removing even carriers
```

```
 p_aco2=f_aco2((1:128),:); %1st half of the data
 p_k_aco2=2*p_aco2;
%%%%%%%%%%%%%%%%%%%%%%%%%%%%%%%%%%%%%%%%%%%%%%%%%%%%%%%%%%%
% demodulation of symbols at 3rd stratum
 H2_aco2=modem.qamdemod(H_aco3);
 H2_aco2.OutputType='Bit';
 H2_aco2.SymbolOrder='gray';
 demodulate_data_aco2=demodulate(H2_aco2, p_k_aco2);%demodulation of symbols
 demodulate_data2_aco2=reshape(demodulate_data_aco2,1,N_data3);
%%%%%%%%%%%%%%%%%%%%%%%%%%%%%%%%%%%%%%%%%%%%%%%%%%%%%%%%%%%
% information recovery for ACO-OFDM
 rx4_aco_singl=rx_aco_singl.';
 J_J4_aco_singl=fft(rx4_aco_singl);%FFT
 f_aco_singl= J_J4_aco_singl(2:2:N_4);%removing even carriers
 p_aco_singl=f_aco_singl((1:512),:); %1st half of the data
 p_k_aco_singl=2*p_aco_singl;
%%%%%%%%%%%%%%%%%%%%%%%%%%%%%%%%%%%%%%%%%%%%%%%%%%%%%%%%%%%
% demodulation of symbols for ACO-OFDM
H4_aco=modem.qamdemod(H_aco4);
H4_aco.OutputType='Bit';
H4_aco.SymbolOrder='gray';
demodulate_data_aco_singl=demodulate(H4_aco,p_k_aco_singl);%demodulation of symbols
demodulate_data2_aco_singl=reshape(demodulate_data_aco_singl,1,N_data4);
%%%%%%%%%%%%%%%%%%%%%%%%%%%%%%%%%%%%%%%%%%%%%%%%%%%%%%%%%%%
% information recovery for DCO-OFDM
 rx4_dco=rx_dco.';
 rx4_dco1=rx4_dco-pp;% removing DC bias
 J_J4_dco=fft(rx4_dco1);
 p_dco=J_J4_dco((2:1024),:); %1st half of the data
%%%%%%%%%%%%%%%%%%%%%%%%%%%%%%%%%%%%%%%%%%%%%%%%%%%%%%%%%%%
 % demodulation of symbols for ACO-OFDM
```

```
H2_dco1=modem.qamdemod(H_dco);
H2_dco1.OutputType='Bit';
H2_dco1.SymbolOrder='gray';
demodulate_data_dco=demodulate(H2_dco1, p_dco);%demodulation of symbols
demodulate_data2_dco1=reshape(demodulate_data_dco,1,N_data_dco);
%%%%%%%%%%%%%%%%%%%%%%%%%%%%%%%%%%%%%%%%%%%%%%%%%%%%%%%%%%%%%%%%%%%%%%%%%%%%
[nErr1 bErr1(aa_aco,k)]=symerr( generate_data_aco1,demodulate_data_aco);% BER and
eranious bits at 1st stratum
[nErr2 bErr2(aa_aco,k)]=symerr( generate_data_aco2,demodulate_data_aco1);% BER and
eranious bits at 2nd stratum
[nErr3 bErr3(aa_aco,k)]=symerr( generate_data_aco3,demodulate_data_aco2);% BER and
eranious bits at 3rd stratum
%%%%%%%%%%%%%%%%%%%%%%%%%%%%%%%%%%%%%%%%%%%%%%%%%%%%%%%%%%%%%%%%%%%%%%%%%%%%
[nErr4 bErr4(aa_aco,k)]=symerr( generate_data_aco4,demodulate_data_aco_singl);%BER and
eranious bitsfor ACO-OFDM
[nErr5 bErr5(aa_aco,k)]=symerr( generate_data_dco,demodulate_data_dco);%BER and
erroneous bits for DCO-OFDM
%%%%%%%%%%%%%%%%%%%%%%%%%%%%%%%%%%%%%%%%%%%%%%%%%%%%%%%%%%%%%%%%%%%%%%%%%%%%
[Y(aa_aco,k)]=nErr1+nErr2+nErr3;% Total erranious for one complete STACO-OFDM frame
X=length(generate_data_aco1)+length(generate_data_aco2)+length(generate_data_aco3);% total
transmitted bits in one STACO-OFDM frame
end
end
Z=mean(Y')/X;% average BER of STACO-OFDM
EB1=EbNo_aco-10*log10(alpha1)-10*log10(2);% Effective SNR per bit at 1st stratum
EB2=EbNo_aco-10*log10(alpha2)-10*log10(2);% Effective SNR per bit at 2nd stratum
EB3=EbNo_aco-10*log10(alpha3)-10*log10(2);% Effective SNR per bit at 2nd stratum
EB6=EbNo_aco;
width = 5;     % Width in inches
height = 3.5;    % Height in inches
alw = 0.75;    % AxesLineWidth
```

```
fsz = 11;      % Fontsize
lw = 2;      % LineWidth
msz = 8;       % MarkerSize
figure(1)
pos = get(gcf, 'Position');
set(gcf, 'Position', [pos(1) pos(2) width*100, height*100]); %<- Set size
set(gca, 'FontSize', fsz, 'LineWidth', alw); %<- Set properties
semilogy(EB6,Z,'bo-',EB6,mean(bErr4'),'ko-',EbNo_act_dco,mean(bErr5'),'
mo- ','linewidth',lw);grid on;
set(gca,'GridLineStyle','--')
xlim([5 30])
ylim([0.00001 1])
xlabel('E_b(elec)/N_o')
ylabel('BER')
legend('proposed scheme (simulated)','ACO-OFDM (simulated)','DCO-OFDM (simulated)')
title('SE=1.5')
```

B.2 STACO-OFDM over frequency selective multipath channel

```
N_aco1=2048;% IFFT points at 1st stratum
N_aco2=1024;% IFFT points at 2nd stratum
N_aco3=512;% IFFT points at 3rd stratum
Ncp=64;% CICLIC PREFIX
M_aco1=16;   % Level of QAM modulation at 1st stratum of STACO-OFDM
M_aco2=8;    % Level of QAM modulation at 2nd stratum of STACO-OFDM
M_aco3=4;    % Level of QAM modulation at 3rd stratum of STACO-OFDM
N_data1=2044;% bits transmitted at the 1st stratum in one STCO-OFDM frame
N_data2=768;% bits transmitted at the 2nd stratum in one STCO-OFDM frame
N_data3=256;% bits transmitted at the 3rd stratum in one STCO-OFDM frame
N_Iteration=2000;% size of iteration for numerical simulation
EbNo_aco=[-9:1:40];  % SNR in terms of energy per bit to noise ratio in dB
```

```
DRMS=[10:10:20]; % delay spread of channel in ns
se1=(4*511)/2112; % spectral efficiency at 1st stratum of STACO-OFDM
se2=768/2112;% spectral efficiency at 2nd stratum of STACO-OFDM
se3=256/2112;% spectral efficiency at 3rd stratum of STACO-OFDM
se_total=se1+se2+se3;% spectral efficiency the overall STACO-OFDM scheme
beta1=10^(-1.8/20);   % scaling factor at 1st stratum of STACO-OFDM
beta2=10^(1.4/20);    % scaling factor at 2nd stratum of STACO-OFDM
beta3=10^(5/20);      % scaling factor at 3rd stratum of STACO-OFDM
%creating modulation and demodulation objects
H_aco1=modem.qammod(M_aco1); %32QAM object
H_aco1.InputType='Bit';
H_aco1.SymbolOrder='gray';
H_aco2=modem.qammod(M_aco2); %16QAM object
H_aco2.InputType='Bit';
H_aco2.SymbolOrder='gray'; %to get gray code
H_aco3=modem.qammod(M_aco3); %16QAM object
H_aco3.InputType='Bit';
H_aco3.SymbolOrder='gray';
for i=1:length(DRMS)
Drms=DRMS(i);
Drms=Drms*(10^-9);% setting the Drms to  nano second
for aa_1=1:length(EbNo_aco)
ebNo_aco=EbNo_aco(aa_1);
%TRANSMITTER
for (k=1:N_Iteration)
generate_data_aco1=randi([0 1],N_data1,1); %Bits generation for 1st stratum of STACO-
OFDMgenerate_data_aco2=randi([0 1],N_data2,1); %Bits generation for 2nd stratum of
STACO-OFDMgenerate_data_aco3=randi([0 1],N_data3,1); %Bits generation for 3rd stratum of
STACO-OFDM
%%%%%%%%%%%%%%%%%%%%%%%%%%%%%%%%%%%%%%%%%%%%%%%%%%%%%%%%%%%%%%%%%%%%%%%%%%%%%%
```

```
X_aco1=modulate(H_aco1, generate_data_aco1);%QAM modulation at 1st stratum of STACO-
OFDM
X_aco2=modulate(H_aco2, generate_data_aco2);%QAM modulation at 2nd stratum of STACO-
OFDM
X_aco3=modulate(H_aco3, generate_data_aco3);%QAM modulation at 3rd stratum of STACO-
OFDM
%%%%%%%%%%%%%%%%%%%%%%%%%%%%%%%%%%%%%%%%%%%%%%%
hermitian_symetric_aco1=[0;X_aco1;0;conj(flipud(X_aco1))]; %hrmitian symm at 1st stratum
parellel_serial_aco1=reshape( hermitian_symetric_aco1,1,length( hermitian_symetric_aco1));%
serial to parallel
zero_table_aco1=zeros(1,N_aco1);  %zeros generation
zero_table_aco1(1:2:end)=parellel_serial_aco1;% odd carriers are loaded with zeros
ifft_data_aco1=ifft(zero_table_aco1.');% IFFT oprn.
ifft_data_aco111=-1.*ifft_data_aco1;% flipping of samples polarity
ifft_data_aco1(1025:end)=ifft_data_aco111(1025:end);% flipped samples on 2nd subframe
clipped1_aco1=max(ifft_data_aco1,0); %asymmetrically clipping of negative samples
clipped_aco1_new1_1= clipped_aco1(1:1024);% 1st sub frame of 1st stratum
clipped_aco1_new1=[clipped_aco1_new1_1(993:1024) clipped_aco1_new1_1(1:1024)];%
addition of CP
clipped_aco1_new2_1= clipped_aco1(1025:end);% 2nd sub frame of 1st stratum
clipped_aco1_new2=[clipped_aco1_new2_1(993:1024) clipped_aco1_new2_1(1:1024)];%
addition of CP
%%%%%%%%%%%%%%%%%%%%%%%%%%%%%%%%%%%%%%%%%%%%%%%
hermitian_symetric_aco2=[X_aco2;conj(flipud(X_aco2))]; %hrmitian symm 2nd stratum
parellel_serial_aco2=reshape( hermitian_symetric_aco2,1,length( hermitian_symetric_aco2));%
serial to parallel
zero_table_aco2=zeros(1,N_aco2); %zeros generation
zero_table_aco2(2:2:end)=parellel_serial_aco2; % even carriers are loaded with zeros
%%%%%%%%%%%%%%%%%%%%%%%%%%%%%%%%%%%%%%%%%%%%%%%
 ifft_data_aco2=ifft(zero_table_aco2.');% IFFT operation
clipped1_aco2=max(ifft_data_aco2,0).';% asymmetrically clipping
```

```
clipped_aco2_new=[clipped1_aco2(993:1024) clipped1_aco2(1:end)] ; % addition of CP
clipped_aco2=(1/beta2)*(1/sqrt(2))*(  clipped_aco2_new);  % scaling at 2nd stratum
%%%%%%%%%%%%%%%%%%%%%%%%%%%%%
hermitian_symetric_aco3=[X_aco3;conj(flipud(X_aco3))]; %hrmitian symm at 3rd stratum
parellel_serial_aco3=reshape( hermitian_symetric_aco3,1,length( hermitian_symetric_aco3));%
serial to parallel.
zero_table_aco3=zeros(1,N_aco3); %zeros generation
zero_table_aco3(2:2:end)=parellel_serial_aco3; % even carriers are loaded with zeros
%%%%%%%%%%%%%%%%%%%%%%%%%%%%%%%%%%%%%%%%%%%%%%%%%%%%%%%%%%%%%%%%%%%%%%%%%%%%%%%%
 ifft_data_aco3=ifft(zero_table_aco3.');%IFFT opren.
 clipped1_aco3=max(ifft_data_aco3,0); % asymmetrically clipping
 clipped_aco3=(1/beta3)*(1/2)*(clipped1_aco3.');% scaling
 clipped_aco3_new1=[clipped_aco3 clipped_aco3];% merging to construct subframes
 clipped_aco3_new=[clipped_aco3_new1(993:1024) clipped_aco3_new1(1:end)];% addition
 of CP
%%%%%%%%%%%%%%%%%%%%%%%%%%%%%%%%%%%%%%%%%%%%%%%%%%%%%%%%%%%%%%%%%%%%%%%%%%%%%%%%
DATA_tot_1=clipped_aco1_new1+ clipped_aco2+clipped_aco3_new;% 1st subframe of
STACO-OFDM
DATA_tot_2=clipped_aco1_new2+ clipped_aco2+clipped_aco3_new;% 2nd subframe of
STACO-OFDM
%%%%%%%%%%%%%%%%%%%%%%%%%%%%%%%%%%%%%%%%%%%%%%%%%%%%%%%%%%%%%%%%%%%%%%%%%%%%%%%%
 %CHANNEL IMPULSE RESPONSE
 Tsamp=10*(10^(-9)); % sampling time
  a = 12*sqrt(11/13)*Drms;% parameter for ceiling bounce model
  K = 32;% channel tap or length
  k1 = 1:K;
  h =((6*a^6)./(((k1*Tsamp) + a).^7));% channel impulse response samples
  h=h./sum(h);% normalizing for signal energy conservation
  %%%%%%%%%%%%%%%%%%%%%%%%%%%%%%%%%%%%%%%%%%%%%%%%%%%%%%%%%%%%%%%%%%%%%%%%%%%%%%%%
   X1=zeros(1,2048);
   X1(1:32)=h;
```

```
Y1=fft(X1);% channel 2048-point FFT
Y1_1=Y1(3:2:1023);% channel magnitude at even subcarriers
X11=zeros(1,1024);
X11(1:32)=h;
Y11=fft(X11);% channel 1024-point FFT
Y11_1=Y11(2:2:512);% channel magnitude at odd subcarriers
X111=zeros(1,512);
X111(1:32)=h;
Y111=fft(X111);% channel 512-point FFT
Y111_1=Y111(2:2:256);% channel magnitude at odd subcarriers
%%%%%%%%%%%%%%%%%%%%%%%%%%%%%%%%%%%%%%%%%%%%%%
y11=filter(h,1,DATA_tot_1);% 1st subframe of STACO-OFDM signal after passing
through channel
y21=filter(h,1,DATA_tot_2);% 1st subframe of STACO-OFDM signal after passing
through channel
ps1=(norm( y11)^2)/length( y11);% electrical power
ps2=(norm( y21)^2)/length( y21);% electrical power
ps=ps1+ps2;% electrical power
%%%%%%%%%%%%%%%%%%%%%%%%%%%%%%%%%%%%%%%%%%%%%%
SNR1=ebNo_aco+10*log10(5)+10*log10(se_total/se1)-10*log10(2);% effective
SNR of STACO-OFDM
SNR_lin = 10^(SNR1/10); %effective SNR of STACO-OFDM to linear scale
Esym1=sum(abs(y11).^2)/length(y11); %Calculate actual symbol energy
Esym2=sum(abs(y21).^2)/length(y21); %Calculate actual symbol energy
N01=Esym1/ SNR_lin;%noise variance
N02=Esym2/ SNR_lin;%noise variance
    noiseSigma1 = sqrt(N01);%Standard deviation for AWGN Noise
    noiseSigma2 = sqrt(N02);%Standard deviation for AWGN Noise
    no_se=randn(1,length(y11)+length(y21));
    n1 = sqrt(1024/1056)*noiseSigma1*randn(1,length(y11));%noise samples on 1st subframe
    n2 = sqrt(1024/1056)* noiseSigma2*randn(1,length(y21));%noise samples on 2nd subframe
```

```
rx_aco_new1=(y11+n1);%adding AWGN  samples on 1st subframe
rx_aco_new2=(y21+n2);%adding AWGN  samples on 2nd subframe
%%%%%%%%%%%%%%%%%%%%%%%%%%%%%%%%%%%%%%%%%%%%%
pn1=(norm( n1)^2)/length( n1);% noise power
pn2=(norm( n2)^2)/length( n2);% noise power
pn=pn1+pn2;% noise power
H=Y1./(((abs(Y1)).^2)+pn./ps);% equivalent channel effect for equalization of 1st stratum
H11=Y11./(((abs(Y11)).^2)+pn./ps); % ch. Effect for equalization of 2nd stratum
H111=Y111./(((abs(Y111)).^2)+pn./ps); % ch. Effect for equalization of 3rd stratum
%sucessive demodulation for STACO-OFDM information recovery
%IST STRATUM INFO RECOVERY
RX1=rx_aco_new1(33:1056); %removing CP from 1st subframe
RX2=rx_aco_new2(33:1056); %removing CP from 2nd subframe
rx4_aco55= RX1(1:end)- RX2(1:end); %higher strata interference cancelation
rx4_aco55555=(beta1)*(rx4_aco55); %removing the scaling factor
zero_table_aco11_new=zeros(1,N_aco1);
zero_table_aco11_new(1:1:1024)=rx4_aco55555;
J_J4_aco=fft(zero_table_aco11_new'); %FFT
J_J4_aco11= J_J4_aco.*(H');% equalization
f_aco=   J_J4_aco11(1:2:N_aco1);
p_aco=f_aco((2:512),:); %1st half of the data
p_k_aco=2*p_aco; % removing clipping effect
%%%%%%%%%%%%%%
H2_aco=modem.qamdemod(H_aco1);
H2_aco.OutputType='Bit';
H2_aco.SymbolOrder='gray';
demodulate_data_aco=demodulate(H2_aco, p_k_aco);%demodulation of symbols
demodulate_data2_aco=reshape(demodulate_data_aco,1,N_data1);
% remodulating the iformation recovered at 1st stratum
X_aco11=modulate(H_aco1, demodulate_data_aco);%32qam signal
hermitian_symetric_aco11=[0;X_aco11;0;conj(flipud(X_aco11))]; %hrmitian symm
```

```
for 32-qam ACO1
parellel_serial_aco11=reshape( hermitian_symetric_aco11,1,
length( hermitian_symetric_aco11));
zero_table_aco11=zeros(1,N_aco1); %zeros generation
zero_table_aco11(1:2:end)=parellel_serial_aco11; % odd carriers are loaded with zeros
ifft_data_aco11=ifft(zero_table_aco11.'); % IFFT
ifft_data_aco11111=-1.*ifft_data_aco11;  % samples polarity flipping
ifft_data_aco11(1025:end)=ifft_data_aco11111(1025:end); % flipped samples
clipped1_aco11=max(ifft_data_aco11,0); % asymmetrically clipping
clipped_aco11=(1/beta1)*(clipped1_aco11.'); % scaling
Nclipped_aco1_new11= clipped_aco11(1:1024); % 1st subframe
clipped_aco1_new11=[ Nclipped_aco1_new11(993:1024)  Nclipped_aco1_new11(1:end)];
Nclipped_aco1_new22= clipped_aco11(1025:end); % 2nd subframe
clipped_aco1_new22=[ Nclipped_aco1_new22(993:1024)  Nclipped_aco1_new22(1:end)];
yy1=filter(h,1,clipped_aco1_new11); % including channel effect
yy2=filter(h,1,clipped_aco1_new22); % including channel effect
%2nd STRATUM INFO RECOVERY
rx_aco11= rx_aco_new1(1:end)-yy1(1:end); % removing 1st stratum contribution
rx_aco111=rx_aco_new2(1:end)-yy2(1:end); % removing 1st stratum contribution
rx4_aco1=rx_aco11(33:1056)+rx_aco111(33:1056); % adding both subframes
rx4_aco12=(sqrt(2)/2)*rx4_aco1; % scaling for conservation of frame power
rx4_aco13=(beta2)*(rx4_aco12.'); % removing scaling
J_J4_aco1=fft(rx4_aco13); % FFT
JJ_J4_aco1= J_J4_aco1.*(H11');% equalization
JJJ_J4_aco1= JJ_J4_aco1.';
f_aco1= JJJ_J4_aco1(2:2:N_aco2);% removing even carriers
p_aco1=f_aco1((1:256),:); %1st half of the data
p_k_aco1=2*p_aco1; % scaling to remove clipping effect
%%%%%%%%%%%%%%%%%%%%%%%%%%%%%%%%%%%%
H2_aco1=modem.qamdemod(H_aco2);
H2_aco1.OutputType='Bit';
```

```
H2_aco1.SymbolOrder='gray';
demodulate_data_aco1=demodulate(H2_aco1, p_k_aco1);%demodulation of symbols
demodulate_data2_aco1=reshape(demodulate_data_aco1,1,N_data2);
% remodulating the iformation recovered at 2nd stratum
X_aco22=modulate(H_aco2, demodulate_data_aco1);%16-qam signal
hermitian_symetric_aco22=[X_aco22;conj(flipud(X_aco22))]; %hrmitian symm
for 16-qam ACO1
parellel_serial_aco22=reshape( hermitian_symetric_aco22,1,
length( hermitian_symetric_aco22));
zero_table_aco22=zeros(1,N_aco2); %zeros generation
zero_table_aco22(2:2:end)=parellel_serial_aco22; % even carriers are loaded with zeros
%%%%%%%%%%%%%%%%%%%%%%%%%%%%%%%%%%%%%%%%%%%%%%
ifft_data_aco22=ifft(zero_table_aco22.'); % IFFT
clipped1_aco222=max(ifft_data_aco22,0); % asymmetrically clipping
Nclipped_aco222=(1/beta2)*(1/sqrt(2))*(clipped1_aco222.'); % scaling
clipped_aco222=[Nclipped_aco222(993:1024) Nclipped_aco222(1:end)]; % merging
yy3=filter(h,1,clipped_aco222); % including channel effect
%%%%%%%%%%%%%%%%%%%%%%%%%%%%%%%%%%%%%%%%%%%%%%
%3rd STRATUM INFO RECOVERY
rx_aco221_new1=rx_aco11(1:end)-yy3(1:end); % removing 2nd stratum contribution
rx_aco221_new2=rx_aco111-yy3; % removing 2nd stratum contribution
RX3= rx_aco221_new1(33:1056); % CP removing
RX4= rx_aco221_new2(33:1056); % CP removing
rx4_aco2=RX3(1:512)+RX3(513:1024)+RX4(1:512)+RX4(513:1024); % adding copies
rx4_aco22=(1/2)*rx4_aco2; % scaling for conservation of frame power
rx4_aco222=(beta3)*(rx4_aco22.'); % removing scaling factor
J_J4_aco2=fft(rx4_aco222); %FFT
JJ_J4_aco2= J_J4_aco2.*(H111'); % equalization
JJJ_J4_aco2=JJ_J4_aco2.';
f_aco2= JJJ_J4_aco2(2:2:N_aco3);%removing even carriers
p_aco2=f_aco2((1:128),:); %1st half of the data
```

```
    p_k_aco2=2*p_aco2; % scaling to remove clipping effect
%%%%%%%%%%%%%%%%%%%%%%%%
    H2_aco2=modem.qamdemod(H_aco3);
    H2_aco2.OutputType='Bit';
    H2_aco2.SymbolOrder='gray';
    demodulate_data_aco2=demodulate(H2_aco2, p_k_aco2);%demodulation of symbols
    demodulate_data2_aco2=reshape(demodulate_data_aco2,1,N_data3);
%%%%%%%%%%%%%%%%%%%%%%%%%%%%%%%%%%%%%%%%%%%%
    [nErr1 bErr1(aa_1,k)]=symerr( generate_data_aco1,demodulate_data_aco);
    [nErr2 bErr2(aa_1,k)]=symerr( generate_data_aco2,demodulate_data_aco1);
    [nErr3 bErr3(aa_1,k)]=symerr( generate_data_aco3,demodulate_data_aco2);
%%%%%%%%%%%%%%%%%%%%%%%%%%%%%%%%%%%%%%%%%%%%
    [Y(aa_1,k)]=nErr1+nErr2+nErr3;
    X=length(generate_data_aco1)+length(generate_data_aco2)+length(generate_data_aco3);
    end
    end
   Z=mean(Y')/X; % BER of STACO-OFDM scheme
   EB6=EbNo_aco;
   width = 5;     % Width in inches
   height = 3.5;    % Height in inches
   alw = 0.75;    % AxesLineWidth
   fsz = 11;      % Fontsize
   lw = 2;      % LineWidth
   msz = 8;       % MarkerSize
  figure(1)
  pos = get(gcf, 'Position');
  set(gcf, 'Position', [pos(1) pos(2) width*100, height*100]); %<- Set size
  set(gca, 'FontSize', fsz, 'LineWidth', alw); %<- Set properties
  semilogy(EB6,Z,'bo-','linewidth',2);grid on;hold on; % plotting the BER
  set(gca,'GridLineStyle','--')
  xlim([0 40])
```

```
ylim([0.00001 1])
xlabel('E_b(elec)/N_o')
ylabel('BER')
end
```